Review

Metal Organic Polygons and Polyhedra: Instabilities and Remedies

Soumen K. Samanta

School of Chemistry, University of Bristol, Cantock's Close, Bristol BS8 1TS, UK; soumen.samanta@bristol.ac.uk

Abstract: The field of coordination chemistry has undergone rapid transformation from preparation of monometallic complexes to multimetallic complexes. So far numerous multimetallic coordination complexes have been synthesized. Multimetallic coordination complexes with well-defined architectures are often called as metal organic polygons and polyhedra (MOPs). In recent past, MOPs have received tremendous attention due to their potential applicability in various emerging fields. However, the field of coordination chemistry of MOPs often suffer set back due to the instability of coordination complexes particularly in aqueous environment-mostly by aqueous solvent and atmospheric moisture. Accordingly, the fate of the field does not rely only on the water solubilities of newly synthesized MOPs but very much dependent on their stabilities both in solution and solid state. The present review discusses several methodologies to prepare MOPs and investigates their stabilities under various circumstances. Considering the potential applicability of MOPs in sustainable way, several methodologies (remedies) to enhance the stabilities of MOPs are discussed here.

1. Introduction

Metal organic materials are thriving class of materials that are produced from the self-assembly of multitopic organic linkers and metal ions with suitable coordination numbers [1–12]. Combination of varieties of metal ions and organic building blocks led to the synthesis of numerous self-assembled materials including coordination polymers (CPs) [13–15], porous crystalline coordination polymers popularly known as metal organic frameworks (MOFs) [16–20] and metal organic polyhedra (MOPs) [4,7,9,21]. Introduction of coordination polymers in the twentieth century followed by the discovery of porous coordination polymer in last two decades established metal-coordination driven self-assembly method as powerful strategy to prepare novel materials. Development of synthetic strategy to produce crystalline porous materials and advancement of crystallographic method to determine the solid-state structures have significantly impacted the field of coordination chemistry. Metal organic polygons and polyhedra (MOPs) separately introduced first by Fujita [21] and subsequently by Yaghi [22] and Zaworotko [23] include wide ranges of metallo-supramolecular structures that dates back to its first discovery in 1990s with significant contributions from Raymond [9,24], Stang [4,5,25–27], Nitschke [11,28,29], Zhou [30,31] and many others [32–37]. MOPs are emerging class of discrete metallo-supramolecular materials, assembled from organic linkers and metal-based secondary building units (SBUs), and have found to be suitable for applications such as catalysis, sensing, gas adsorption, biomedical application and membranes [38–48].

Nevertheless, the chemical, thermal and hydrothermal stabilities of MOPs have been perceived as problematic particularly when compared with industrially relevant other metal organic materials like zeolites and emerging class of metal organic frameworks [6,42,49–54]. Many water-stable and thermally-stable MOFs find themselves useful for important industrially relevant applications like gas separation [55], ion-exchange [56], water desalination [57]. Pioneering works of Yaghi (Figure 1), Zaworotko and Zhou independently

led to the preparation of carboxylate-based MOPs isolated as solid materials in order to develop novel porous materials [3,16,19,30]. Depending on the applications sought, different functional stabilities of the supramolecular materials are needed. Hydrolytic and thermal stabilities are useful for the industrial applications including gas adsorption, ion-exchange, water desalination etc. and carboxylate-based MOPs often exhibit fragile nature to decompose into fragments upon their exposure to heat, water or other stimuli including other chemicals making them less suitable for solution-based applications. Parallel to the carboxylate-based MOPs, pyridine (N-donor)—based MOPs were prepared in abundance utilizing various methodologies by Fujita, Raymond, Stang, Nitschke and many others. In general, N-donor ligands tend to form more stable metal organic complexes as they form stronger bonds with respective metal ions and thus become more relevant for MOPs to be useful for both solid and solution-based applications. Unlike carboxylate-based MOPs which were extensively used for gas adsorption studies, MOPs containing N-donor ligands have seldom studied in solid state, rather they were extensively investigated for solution-based chemistry. Accordingly, preparation of MOPs with exceptional thermal and hydrothermal stabilities is one of the major thrust in the field of metal-coordination chemistry.
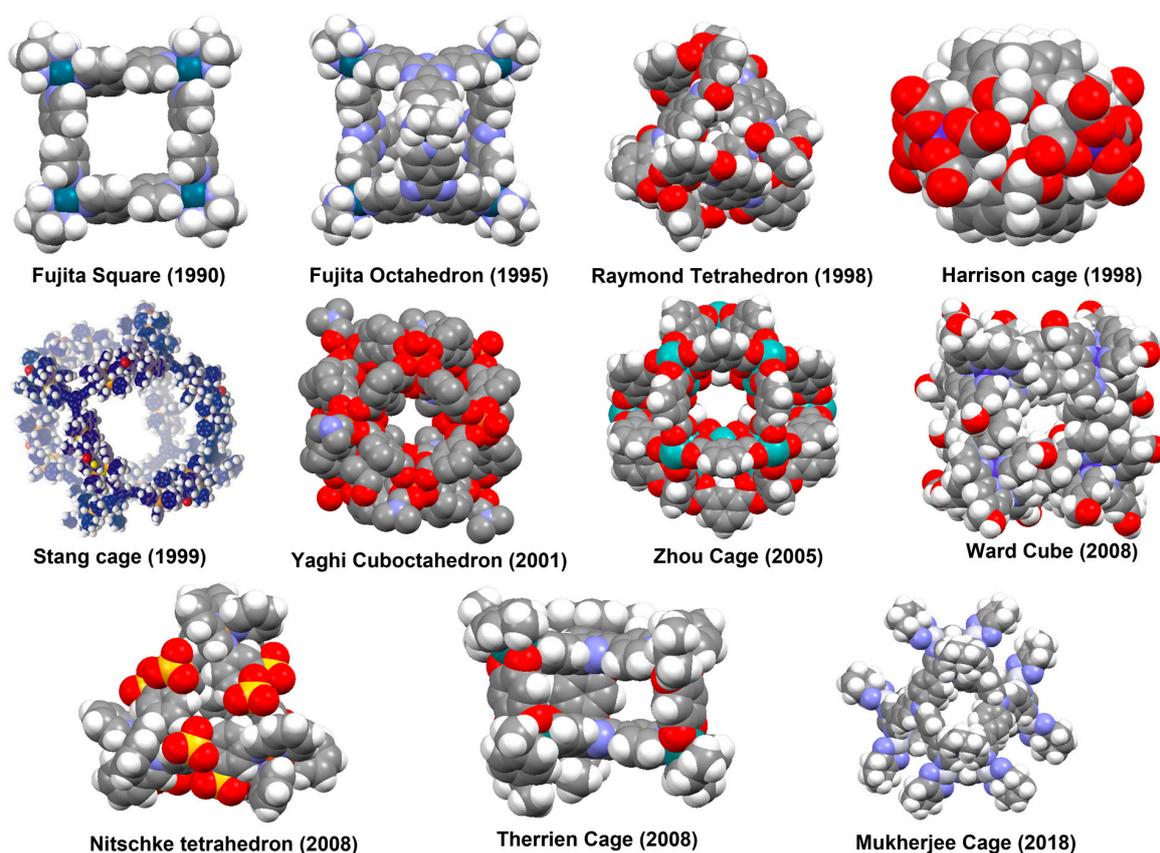
Figure 1. Representative examples of metal organic polygons and polyhedra (MOPs) that appeared in literature since early 1990s until recently, prepared using metal coordination chemistry from various donor-based ligands. In the parenthesis is reported the time when they appeared in literature. Pictures are reproduced by permissions from Refs. [22,27,37,58–65]. Copyright 1990, 1998, 2001, 2005, 2008, 2018 from American Chemical Society. Copyright 1995, 1999 from Nature Publishing Group. Copyright 1998, 2008 from Wiley-VCH.

Focus given in this review is on the synthetic strategies to prepare discrete MOPs, on their relative thermal and hydrothermal stabilities, and on several developing strategies in order to render water-stable and thermally-stable MOPs. Metal organic polygons and polyhedra (MOPs) were prepared from various organic linkers and metal ions with the

abundance of two classes of MOPs namely-carboxylate-based MOPs and pyridine-based MOPs being the most popular. Despite various classifications reported in literature to categorize MOPs, metal organic polygons and polyhedra (MOPs) can broadly be classified into three groups based on their composition—(1) N-donor ligands coordinated to the metal ions, (2) O-donor ligands coordinated to the metal ions and (3) ligands containing mixed donor atoms coordinated to the metal ions. Yaghi and coworkers first developed the blueprint to prepare carboxylate-based MOPs including the geometric requirements for carboxylate linkers and SBUs. Enhanced relative stabilities of N-donor based MOPs over O-donor based MOPs render themselves more relevant for excellent solution-based chemistry whereas O-donor based MOPs particularly carboxylate-based MOPs are found to be suitable for exploring solid state applications of materials. Several phenolate linker-based MOPs have also been reported but they have mostly been studied in solution phase. In addition to achieving the enhanced stability of MOPs, synthesis of carboxylate-based MOPs with high surface areas is one of the major challenges because in most cases their potential continues to be compromised by the various issues, most likely by their relative stabilities. We choose to discuss about the stability issues (Figure 2) of metal organic polygons and polyhedra (MOPs) in this review and several remedies taken into consideration (Figure 3) so far to enhance their relative stabilities. The approaches adopted to enhance their stabilities can be implemented further in future to render stable MOPs tailored to suitable applications. Readers are advised to keep in mind that the title of the present article uses the term "Metal Organic" which identifies itself with modern theme of coordination chemistry that describes discrete structures bearing weak metal ligand interactions as metal organic materials. Also, this review excludes the examples of MOPs featuring traditional metal-carbon bonds. To the best of the knowledge, this is one of the first review article discusses on the stability issues of all kinds of MOPs, with another report by Ghosh and coworkers exclusively on the stabilizing strategies of carboxylate-based MOPs [66].
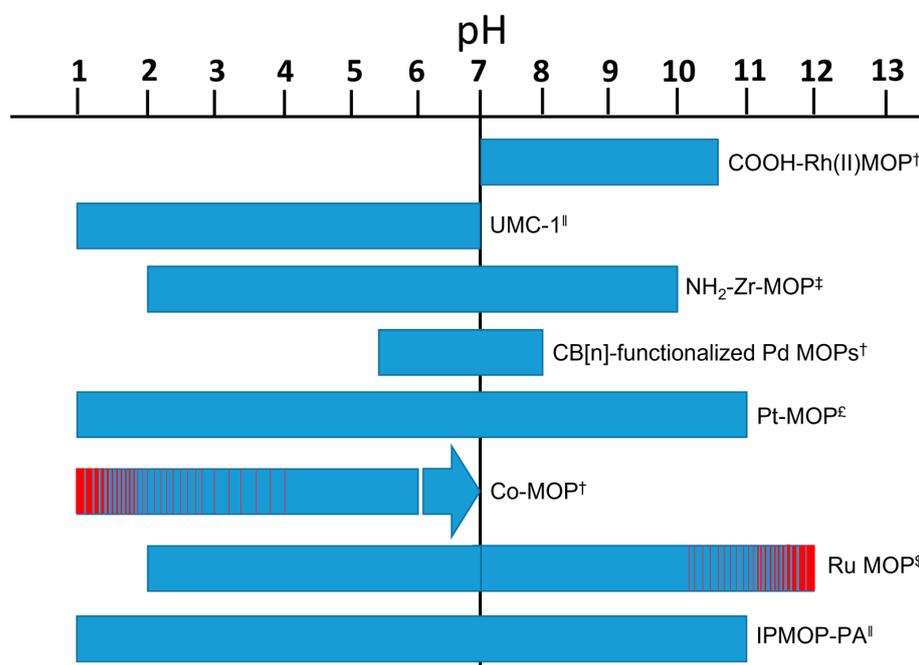
Figure 2. Chemical stabilities of some representative MOPs over the pH range based on literature data. Bar length indicates the pH range that the MOPs remain stable. Arrow represents that the MOP can withstand beyond the pH limit. The red bar indicates the pH ranges that MOPs start to disintegrate. Stabilities are determined by several methods like NMR (†), ESI (‡), powder X-ray diffraction (‖) and fluorescence microscopy ($), apart from those marked with £ representing the methods to determine stabilities are not reported.

2. Strategies to Prepare Stable MOPs

Metal organic polygons and polyhedra (MOPs) that withstand aqueous environment are utmost important in the field of coordination chemistry. MOPs that are not only water soluble but stable towards thermal, aqueous and chemical environments are significantly challenging to prepare. The major concerns for the chemical stability of MOPs have been largely related to water and water-vapour coming from the atmospheric moisture. The chemical weak points of MOPs are the nodes i.e., metal-linker bonds which produces either protonated linkers or hydroxide-ligated nodes. Basic solution accelerates the formation of hydroxide-ligated nodes and the acidic solution produces the protonated linkers. Due to the abundance of water and atmospheric moisture in all possible applications like transportation, storage or separation; the hydrolytic stability becomes the decisive property of any materials to measure their relevance towards real-world applications. Accordingly, we focus on the MOPs that are studied towards aqueous environments. In addition to its universal applicability, water is a coordinating solvent and acts as a competitive ligand for metal complexes [67], thereby hindering the cage formations by compromising structural integrities. Therefore, use of metal clusters makes MOPs highly labile in water owing to the nature of weak reversible metal-linker bonds which can then be ascribed to the thermal stability of materials relying on metal linker bond strength and number of linkers connected to metal clusters. Also metal organic frameworks (MOFs) are often tested for thermal stabilities over wide temperature ranges alongside with their aqueous and chemical stabilities [68,69]. Accordingly, preparing MOPs with exceptional kinetic stability (Figure 4) needs careful considerations of choosing metal clusters and organic linkers. Other strategies of circumventing the complications arising from metal-linker bond breakages include employing covalent modification strategies by interlocking self-assembled products to synthesize kinetically inert products which of course is a tedious method due to laborious synthetic demands. Thus, poor stability is one of the major concerns and has considerably limited the scope of MOPs for various potential applications. Several economic and convenient approaches (Figure 3) to prepare MOPs that exhibit good thermal, aqueous and chemical stabilities include: (1) increasing the metal-ligand bond strength, (2) choosing appropriate counter anions with water solubilizing polar substituents or charged functional groups during self-assembly processes, (3) introducing chelating groups in organic linkers, (4) post-functionalization strategies, (5) shielding the labile metal ions from water (or chemical) attack using hydrophobic residues, (6) preventing the aggregation of MOPs by dispersing them on other surfaces or porous matrix and (7) converting MOPs into stable extended frameworks.
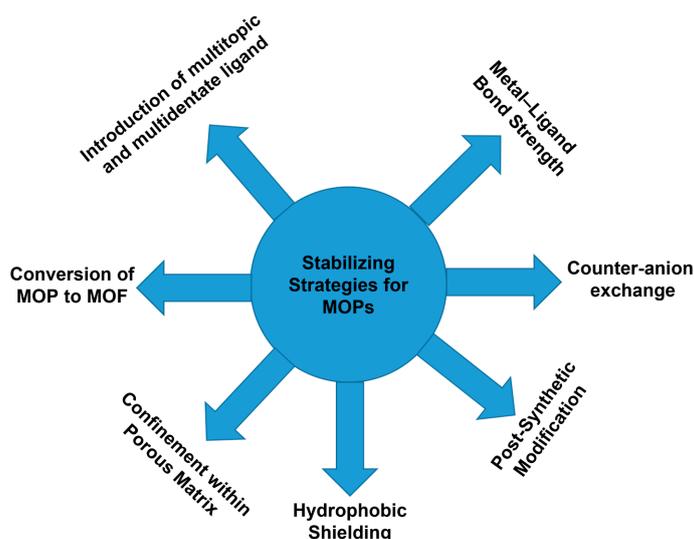

Figure 3. Schematic representation of design principles leading to hydrolytically stable porous MOPs in order to overcome the common instability limitations of MOPs.
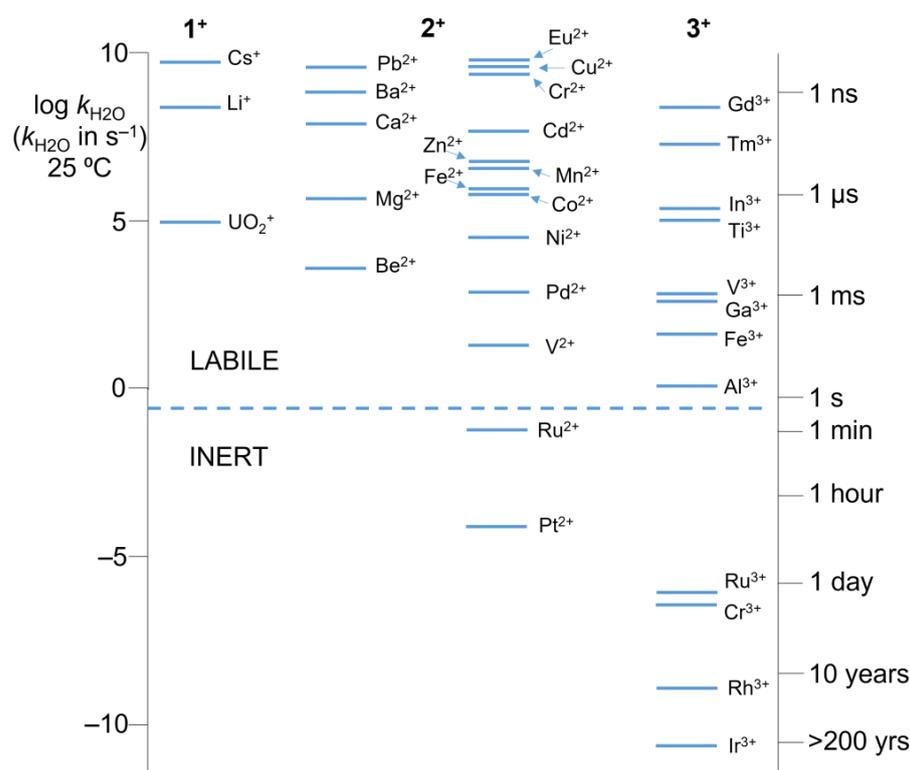
Figure 4. Water exchange rate constants ($\log k_{H2O}$, s^{-1}) and mean lifetime (τ_{H2O}, s) for primary shell water molecules on aqua metal ions at 25 °C. The dotted line represents Taube's inert/labile boundary [70]. Reproduced with permission from Ref. [71]. Copyright 2005 from American Chemical Society.

Self-assembly is defined as the spontaneous formation of higher-order structures constructed from simpler building blocks. Unlike kinetic dominance in covalent synthesis, enthalpy-entropy compensation plays predominate role in rendering higher order structures in a thermodynamically driven process. Accordingly, preparation of higher order structures needs labile moieties in order to assemble them. Use of kinetically inert moieties in a self-assembly process often ends up into undesired oligomeric materials. Use of labile moieties allows the self-corrections to occur during the self-assembly under thermodynamic conditions [71]. However, the benefit is often traded-off by the long-term instability of higher-order metal organic structures, particularly during their usages for various applications. Common strategies to create MOPs that exhibit excellent stability is to use kinetically "inert" metal ions or metal clusters during the self-assembly, whereas other method includes the use of pre-synthesized kinetically locked components constructed and subsequently use them to render higher-order structures. For alkali, alkaline earth and lanthanide (with filled d orbitals) metal ions; metal-ligand bonding is largely electrostatic (or ionic) in nature as the hard bases form the strongest complexes with the metal ions located up in the column in the periodic table. For example, Cs^+ and Eu^{2+} formed the least stable aquo complex with mean lifetime ($\tau_{H2O} = 10^{-10}$ s) in the sub nanosecond range (Figure 4). As the ligand field effects are almost absent, chelate or macrocyclic ligands are often needed for achieving higher affinity of coordinating ligands towards respective metal ions. On the contrary, transition metal ions afforded thermodynamically stable metal complexes with monodentate ligands due to large gain in ligand field stabilization energy (LFSE). LFSE gain increases across the row in the periodic table going from left to right due to increasing population of lower energy *d*-orbitals. Exceptions are shown by Cr^{2+} and Cu^{2+} metal ions as the electronic configuration of Cr^{2+} (d^4, t_{2g}^4) and Cu^{2+} (d^9, t_{2g}^6, e_g^3) make them suitable candidate to exhibit Jahn-Teller distortions, where the initially assumed octahedron geometry undergoes distortion leading to strengthening the four equitorial metal-ligand bonds at the expense of two axially elongated metal-ligand bonds, resulting

in high gain in LFSE. For first row transition metal ions, higher affinity constants are also observed for chelate and macrocyclic metal complexes compared with monodentate ligand-coordinated metal complexes mostly due to achieving higher entropic gain. However, stability constant of metal complexes should not be necessarily confused with their kinetic inertness as the overall higher thermodynamic stability sometimes can be overwhelming. For example, both Cu^{2+} and Cr^{2+} aquo complexes exhibited similar water exchange rates like Cs^+ metal ion as Jahn-Teller effect makes the axially located metal ions more labile. Other transition metal aquo complexes are reasonably inert with mean lifetime (τ_{H2O}) from millisecond to nanosecond. With main group alkali metal ions, the lability increases from Li^+ to Cs^+ due to decrease in charge density and increase in coordination number of metal ions. The alkaline earth metal ions showed similar pattern as the lability increases on moving from Be^{2+} to Ba^{2+}. Filled d^{10} orbitals also put Zn^{2+}, Cd^{2+} and Hg^{2+} at the higher end of the lability scale due to low to moderate surface charge density with increase in ionic radii as the group is descended. Generally, second and third row d-block elements form kinetically more inert complexes with higher degree of covalency in metal-ligand bonding due to better orbital overlap between metal ions and organic ligands. Aquo complex of Pt^{2+} metal ion is considerably inert with mean lifetime (τ_{H2O}) about an hour compared to Pd^{2+} aquo complex. Similar to palladium, ruthenium (Ru^{2+}) and rhodium (Rh^{2+}) aquo complexes showed similar lability with mean lifetime (τ_{H2O}) of several seconds. Iridium (Ir^{3+}) forms extremely inert complex with water with mean lifetime > 200 yrs resulting from high gain in LFSE due to smaller ionic radius and high charge density of Ir^{3+} metal ion. Smaller ionic radii and higher charge density make Ru^{3+}, Cr^{3+} and Rh^{3+} aquo complexes extremely inert with mean lifetime (τ_{H2O}) from several days to several years. Hard/soft bases in combination with hard/soft metal ions based on Pearson's hard/soft-acid/base principle are thus expected to render stable metal-ligand complexes.

As mentioned earlier that chelate ligands form stronger complexes with metal ions, therefore degree of chelation and ligand topicity can be considered systematically to prepare robust metal-ligand complexes. Introducing chelating ligands around metal centers can offer more denser connections and render better stability to the complexes. Ligand topicity (tetratopic > tritopic > ditopic) also plays important role in stabilizing the multi-metallic complexes as the denser connections can make them thermodynamically more stable compared with less denser counterparts. For example, Fujita and coworkers demonstrated that ligand exchange rate ($k_{obs} = 1.9 \times 10^{-7}$ s^{-1}) remains significantly slower in a cuboctahedron MOP comprised of 48 Pd(II)-pyridine interactions in cooperative fashion compared with monodentate model complex, [Pd(py)$_4$] (OTf)$_2$ (py = pyridine) [72]. Li and coworkers reported the preparation of increasingly stable supramolecular structures by enhancing the metal ligand interactions in sphere-in-sphere structure compared with ring-in-ring structure [73]. Although choosing appropriate metal ions and organic linkers primarily contributed to synthesize stable MOPs, other factors often play decisive roles in determining their relative stabilities. Post-synthetic methods can be employed to prepare stable MOPs compared with pristine MOPs as the attaching functional moieties on the outer surface entailing the prevention of the metal ions from water or other chemical attacks. For example, Zhou and coworkers showed that the stability of dicopper paddlewheel-based carboxylate MOP can be further enhanced by putting polyethylene glycol on the outer surface of the MOP in post-synthetic fashion [74]. Decorating the hydrophobic shields around the metal centers would be another way to prepare stable MOPs as in an interesting example Ghosh and coworkers demonstrated that greater shielding around metal centers could enhance the stability of MOPs [75]. Scientists also adopted the procedure to synthesize MOPs via counter-anion exchange to make water soluble and stable MOPs that are otherwise difficult to bring in water. Nitschke and coworkers reported the preparation of water soluble and stable MOP by counter-anion exchange method, otherwise impossible to achieve [76].

MOPs are attractive materials considering their availabilities in various topologies, functionalities, solution processabilities and recylabilities. However, compared with MOFs, metal organic polygons and polyhedra are less studied as solid porous materials mainly due to their reduced stabilities. Disadvantages MOPs have in the solid state are not only the chemical or hydrolytic instabilities but also lack of suitable strong supramolecular interactions that hold MOPs in the solid state after removal of solvents (known as activation) for external guest molecules to enter the pores. Metal organic frameworks are interconnected 3D networks which are mostly held together by directional metal-ligand bonds to render well-organized pores. Use of rigid organic linkers often renders MOFs stable even after activation. Lack of strong directional metal-ligand interactions between individual MOPs made them more fragile in solid state as they are susceptible to collapse following activation and tend to aggregate. Methods adopted to retain their porosity in solid state following activation include (1) immobilizing the MOPs on solid support or on porous matrix and (2) converting them into extended frameworks using organic linkers. Study showed that the solid-state performance of MOPs significantly enhanced following their immobilizations on solid surfaces or after their conversion into extended three-dimensional metal organic frameworks (MOFs). For example, Zhou and coworkers reported the enhanced gas storage performance of carboxylate-based MOPs following their immobilization on mesoporous silica nanopores SBS-15 [77].

3. MOPs Containing O-Donor Ligands

Strong directional metal-ligand interactions enable rational designing of discrete structures which become less obvious when other noncovalent interactions like H-bonds, π-π, dipole-dipole and Van der Waals interactions [78,79] are at play. MOPs with varied shapes and topologies were prepared by choosing appropriate metal ions and rigid organic linkers. Variety of organic ligands in combination with wide range of metal ions led to the synthesis of novel metal organic materials with emerging functionalities. Well-defined coordination geometries of transition metal ions make them suitable candidates for the preparation of MOPs with desired shapes and topologies. Extensive works on coordination polymers establishes the carboxylate-based dinuclear paddlewheel complexes, $M_2(COO)_4$ as novel secondary building units (SBUs) which were then used in combination with various carboxylate-based multitopic rigid or flexible linkers in order to prepare coordination polymers and porous coordination polymers. Extensive works on coordination polymers eventually led to the evolution of giant field of crystalline porous solid materials [13–15]. Dinuclear paddlewheel complex, $M_2(COO)_4$ uses two metal ions which are interconnected by four carboxylate groups at the equatorial position of each metal center. Some dinuclear metal complex like $Mo_2(COO)_4$ exhibits metal-metal quadruple bond between metal centers [80]. In last two decades, dinuclear paddlewheel complexes $M_2(COO)_4$ were emerged as prime candidates for the preparation of carboxylate-based MOPs. Designing of such MOPs are significantly different from the MOPs prepared from other metal ions. Initial reports on the preparation of self-assembled carboxylate-based MOPs were independently documented by the groups of Yaghi [22], Zaworotko [23] and Zhao [30]. Yaghi and coworkers had demonstrated the synthesis of porous MOPs constructed from copper-based SBU and ditopic carboxylate linkers (Figure 5). Use of copper(II) acetate, $Cu_2(COO)_4$ paddlewheel cluster as rigid SBU with linear linker 1,4-benzene dicarboxylate (BDC)—a source of O-donor ligand produces metal organic frameworks with permanent porosity [81]. Analogous benzene-1,3-dicarboxylate (*m*-BDC) linker with 120° bite angle and dicopper paddlewheel SBU produces truncated-cuboctahedron containing 12-paddlewheels linked with 24 *m*-BDC linkers. The polyhedron (MOP 1) was characterized as $Cu_{24}(m\text{-BDC})_{24}(DMF)_{14}(H_2O)_{10}$ with open metal sites axially coordinated by solvent molecules suitable for post-functionalization both at the inner cavity and outer surface of MOP using external ligands. Dicopper secondary building units are connected to four identical linkers in identical fashion to form a planar vertex arrangement, often called as augmentation giving rise to augmented-cuboctahedron with an average diameter of 15 Å

and a volume of 1766 Å^3 [22]. Parallel to this report, Zaworotko and coworkers demonstrated that upon addition of 2,6-dimethylpyridine to the mixture of a methanolic solution of 5-OH-BDC and $Cu(NO_3)_2$ spontaneously produces $Cu_{24}(m\text{-BDC})_{24}(DMSO)_{12}(MeOH)_{12}$ (MOP 2) as rhombihexahedron. Polar hydroxy groups located at the outer surface make MOP 2 highly soluble and stable in polar solvents compared to the pristine MOP 1 [58]. Subsequently, great varieties of MOPs were synthesized by putting various substituents at the 5-position of 1,3-benzene dicarboxylic acid. Bromo and amine-functionalized BDCs gave large-sized rhombicuboctahedron MOPs that are isoreticular to MOP 1 with lower tetragonal symmetry for amine-functionalized MOP compared to bromo-functionalized MOP [82].

Independently, Zhou and coworkers had demonstrated the synthesis of carboxylate-based cuboctahedron MOPs by reacting dimolybdenum and dicopper paddlewheel clusters with rigid organic linkers 5-^{t}Bu-BDC (BBDC) and m-BDC with 120° bent angle [80]. The coordination assemblies, $Mo_{24}(BDC)_{24}$ and $[Mo_{24}(BBDC)_{24}](py)_{12}$ afforded anticuboctahedron and cuboctahedron geometries, respectively depending on the manner two halves of the paddlewheel clusters are aligned. Each pyridine molecule is axially coordinated to the outer metal center of each Mo-Mo paddlewheel pair. Interestingly coordination assemblies of $Cu_{24}(BBDC)_{24}(S)_{24}$ and $Cu_{24}(BDC)_{24}(S)_{24}$ afforded only cuboctahedron clusters with enclosed voids of ~15 Å diameter. Similarly, other variants of MOP 1 were synthesized by various groups including Yaghi, Tonigold, Larsen, Zhou and others [82–87]. For example, sulfonated nanoball was synthesized by Zaworotko and coworkers with molecular formula $[Cu_2(5\text{-}SO_3\text{-BDC})_2(4\text{-methoxypyridine})_{0.5}(CH_3OH)(H_2O)_{1.5-x}]_{12}$ [88]. Other variants of MOP 1 include the synthesis of aliphatic chain, alkene and alkyne-functionalized MOPs using dicopper paddlewheel as SBUs with isoreticular structural features compared with pristine MOP 1 [74,82,85,86]. Attaching hydrophobic units imparted higher solubility as observed for MOPs functionalized with long aliphatic and 2-(2-hydroxyethoxy)ethoxy chains [84].

Use of angular ditopic ligands other than prototypical benzene dicarboxylic acid (BDC) allows the expansion of the library of carboxylate-based MOPs. For example, 2,7-naphthalenedicarboxylic acid (2,7-NDC) and 2,7-biphenylenedicarboxylic acid (2,7-BPEDC) were successfully utilized to prepare copper-based MOPs $[Cu_{24}(2,7\text{-NDC})_{24}(DEF)_8(H_2O)_{16}]$ and $[Cu_{24}(2,7\text{-BPDC})_{24}(NMP)_{12}(H_2O)_{12}]$, respectively with same topology as MOP 1 [82,89,90]. Both structures are isoreticular in nature. Angular ditopic linkers containing heteroatoms were also used to prepare diverse and novel class of MOPs. 2,2′:5,2″-terthiophene-5,5″-dicarboxylic acid (H_2TTDC) and 9H-carbazole-3,6-dicarboxylic acid ($H_2$9H-3,6-CDC) linkers with bite angle very close to 90° gave copper-based MOPs $[Cu_{12}(TTDC)_{12}(NMP)_6(H_2O)_6]$ and $[Cu_{12}(9H\text{-}3,6\text{-CDC})_{12}(DMA)_6(H_2O)_6]$, although the general formulas are different from the conventional copper-based MOPs constructed from 120° angular linkers [91,92]. Interestingly, methodical probing allows the angle-driven self-assembly approaches to prepare MOP architectures with varied topologies. Tuning the bite angles ($0° \leq \theta < 180°$) between two carboxylic acid reaction centers and the size of the linkers facilitated the designing of specific polyhedra structures. Most commonly observed bite angles are 0°, 60°, 90° and 120°. Dicopper and dimolybdenum (containing quadruply bonded Mo-Mo) paddlewheel metal clusters in combination with dicarboxylate linkers with variable lengths and varied bridging angles (between 0° and 120°) gave diverse class of carboxylate-based MOPs.
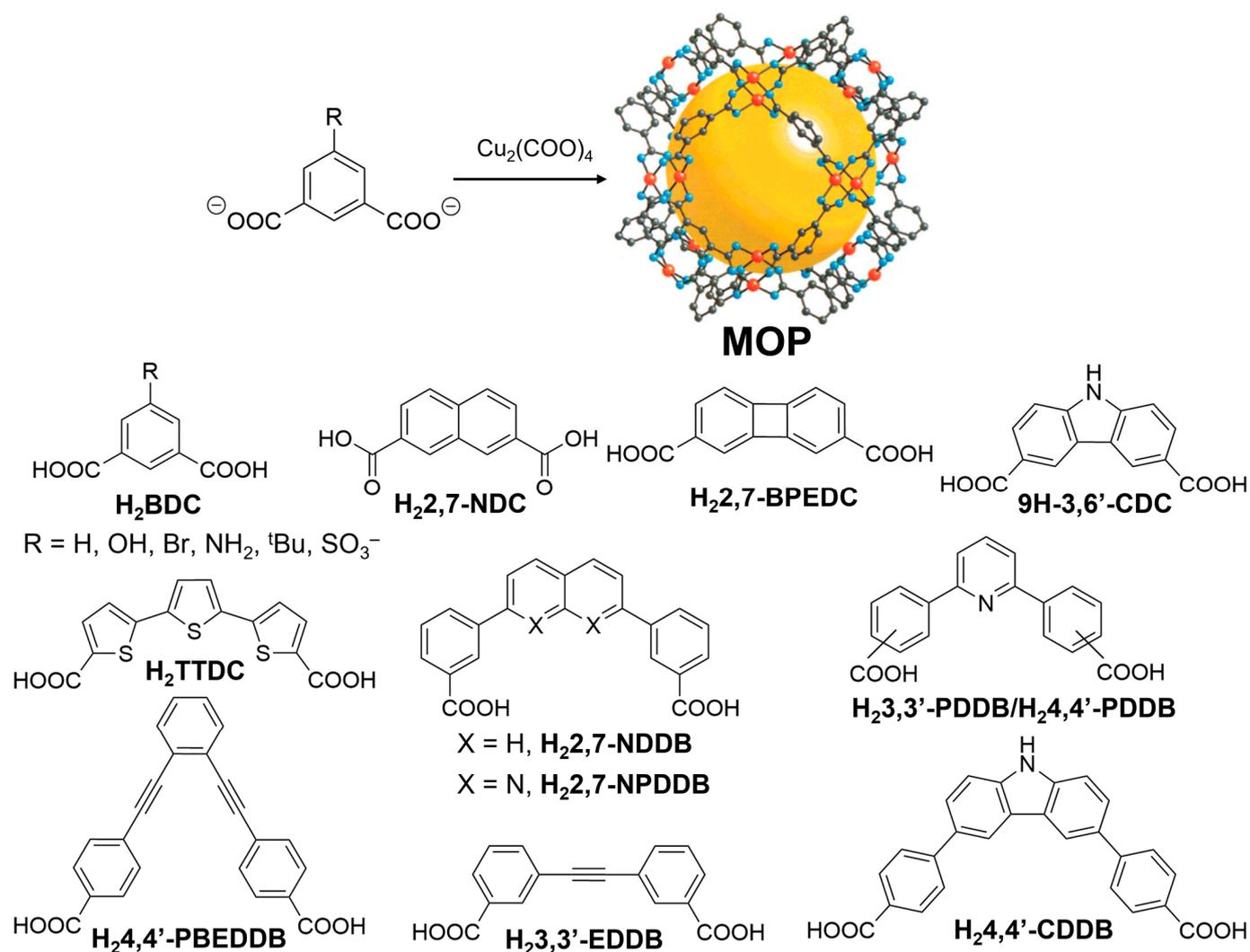
Figure 5. (**Top**) General designing of metal-carboxylate self-assembled MOP prepared from 5-substituted benzene 1,3-dicarboxylate and dimetallic paddlewheel cluster. (**Bottom**) Several ditopic carboxylic acid linkers used to prepare diverse class of metal-organic polyhedra (MOPs). Reprinted by permission from Ref. [22]. Copyright 2001 from American Chemical Society.

Parallel arrangements of carboxylic acid groups in $H_2(2,7\text{-NDDB})$ and $H_2(2,7\text{-NPDDB})$ with the bridging angle of $0°$ gave isostructural large tetragonal MOPs $[Cu_2(2,7\text{-NDDB})_2(DMA)_2]_2$, $[Cu_2(2,7\text{-NPDDB})_2(DMA)_2]_2$ and $[Mo_2(2,7\text{-NPDDB})_2(DMA)_2]_2$ with four bridging ligands surrounding two paddlewheel dicopper/dimolybdenum metal clusters [93]. Similarly, ligands $3,3'\text{-PDDB}$ and $3,3'\text{-PBEDDB}$ gave lantern-type isostructural MOPs with molecular formulas $[Mo_2(3,3'\text{-PDDB})_2(S)_2]_2$ and $[Mo_2(3,3'\text{-PBEDDB})_2(NMP)_2]_2$ [94]. Octahedron structures were derived when dicarboxylic acid linkers of $90°$ bend angles are used. Examples of Mo-Mo paddlewheel cluster-based octahedron structures include $[Mo_2(9H\text{-}3,6\text{-CDC})_2(DMPU)]_6$ and $[Mo_2(4,4\text{-CDDB})_2(S)_{7/6}]_6$, where DMPU represents 1,3-dimethyl-3,4,5,6-tetrahydro-2(1H)-pyrimidinone [94]. Organic linkers with $120°$ bridging angles gave cuboctahedron and anticuboctahedron MOP as discussed earlier when BDC (vide supra) and their derivatives linkers were used [80]. Linkers with $60°$ bridging angles produce geometrical structures similar to trigonal cages which include the example of $[Mo_2(3,3'\text{-EDDB})_2(S)_2]_3$, $[Mo_2(4,4'\text{-PBEDDB})_2(S)]_3$ and $[Mo_2(4,5\text{-}(MeO)_2\text{-}4,4'\text{-PBEDDB})_2(S)_2]_3$ (S represents solvent molecules) [94].

Till date numerous reports have been documented on the preparation of diverse class of MOPs using O-donor ligands. However, their aqueous instabilities have significantly eluded their utilities for the real-world applications as the stability of weak metal-ligand interactions becoming the crucial factor for determining the hydrolytic stability of coordination complexes and MOPs. Amongst several available dimetallic paddlewheel clusters, copper-based carboxylate MOPs were abundantly synthesized and studied. Labile metal coordination sites of copper-based carboxylate MOPs enables the metal centers to interact post-synthetically with smaller guest molecules or co-ligands in order to solubilize the molecular architectures. However, MOPs constructed from dicopper paddlewheel clusters and carboxylate linkers have several pitfalls—they often fall apart in aqueous media and transform into 3D network in presence of excess ligands, however mostly they remain stable in organic solvents. Tonigold and Volkmer had studied the relative stabilities of MOPs constructed from 5-(2-(2-hydroxyethoxy)ethoxy)benzene-1,3-dicarboxylic acid and Cu(II) ions in comparison with dicopper paddlewheel complex, $Cu_2(COO)_4$ which undergoes easy decomposition in aqueous solution and other polar solvents [84]. Study suggested the relative thermodynamic stability of Cu-based MOP compared with $Cu_2(COO)_4$ paddlewheel complex due to combined effect of chelate and positive cooperativity arising from the interplay between multiple metal ions and organic linkers. Therefore, enhancing the (aqueous)-stability of Cu-based MOPs is crucial for further extension of the technology to be applicable for real-world benefits. Accordingly, several methodologies adopted to stabilize MOPs include post-functionalization method, hydrophobic shielding of metal ions, immobilization of MOPs on other surfaces, building extended frameworks from MOPs etc. Post-synthetic modification (PSM) strategy is found to be a legitimate route for the construction of hydrolytically stable metal-coordination structures including MOPs and MOFs [95]. Extensive investigations have been carried out on PSM amendment of MOFs [95–98] and very few reports are known hitherto on PSM of MOPs as they seldom retain their structural integrities after post-functionalization. Zhou and coworkers reported the synthesis of alkyne-functionalized MOP 3 constructed from dicopper paddlewheel complex and 5-substitutted-1,3-benzene dicarboxylic acid [74]. Given the liability of dicopper paddlewheel complex in aqueous environment, the hydrolytic stability of alkyne-functionalized MOP 3 was tested in water following PSM amendments (Figure 6A). Alkyne-substituted MOP was reacted with azide-terminated polyethylene glycols (PEG) using click chemistry to create MOP 4. Following PSM amendment, MOP 4 was found to be remain water soluble and stable. Presence of long polymeric shells at the outer surface of MOP and presumably the intermolecular aggregation of functionalized MOPs prevented water molecules from attacking the dicopper paddlewheel clusters rendering them water stable in order to be useful for drug transport. Controlled release of 5-fluorouracil, an anticancer drug which was loaded inside the cavity of MOP 4, was observed over a period of 24 h demonstrating the ability of Cu-based MOPs to be applicable for drug delivery applications. Paramagnetic behaviours, aqueous availabilities and stabilities of PEG-functionalized copper(II)-based MOPs make them suitable candidate to be useful as contrast agents. Akin to covalent modifications, noncovalent post-synthetic modification was also carried out on dicopper paddlewheel cluster-based MOPs and the amendment was done successfully leading to the development of new emergent materials. Huo and coworkers demonstrated that noncovalent post-synthetic amendment can be successfully done on prototypical MOP-SO$_3$ structure which is successfully constructed from 5-sulfonate-1,3-benzenedicarboxylic acid and dicopper paddlewheel cluster [99]. By virtue of 24 negative charges sticking out of MOP surface, sulfonated MOP becomes better water soluble and can be surface-functionalized with surfactants like dimethyldistearyl ammonium chloride via ionic self-assembly (Figure 6B). Structural integrity of MOP was fully preserved following the electrostatic interaction-based surfactant functionalization, which therefore excludes all the possibilities of disassembly during synthetic amendments enabling them to take part in the preparation of ordered honeycomb architecture at the air/water interface. Two dimensional hexagonally ordered pore array with average pore size of 3.5 µm was realized from scanning electron microscopy

(SEM) images. The aggregates of surfactant encapsulated MOP nanocages are ~20–30 nm in diameter and the discrete particles are about 3 nm in diameter. Hydrophobic surfactants decorated on the MOP surface significantly reduces the chances of MOP to be exposed to water/air environment, thereby greatly enhances humidity-resistance. In a recent report, Sun and coworkers demonstrated that photopolymerization can significantly enhance the hydro-stability, dispersity and processability of a prototypical copper-based MOP 5 [100]. MOP 5 constructed from dicopper paddlewheel and amino-isophthalic acid linker was used as a precursor in a reaction with methacrylic anhydride to produce methacrylic-functionalized MOP 6. UV irradiation of methacrylic-functionalized MOP 6 in presence of butyl methacrylate as crosslinking agent afforded photopolymerized MOP-BMA (MOP 7). The hydrophobic polymer segment renders humidity resistance to cross-linked MOP-BMA. In comparison with pristine MOP which degraded upon exposure to the humid condition over a period of 6 h, MOP-BMA remains stable over a period of 24 h. While MOPs in the polymer matrix are observed with high dispersity and thermal stability compared with the pristine MOPs, processability of the material is of particular importance from the perspective of practical applications. Crosslinked MOP exhibits better reusability in comparison with precursor crystalline MOPs demonstrating the viability of post-synthetic modification strategy for better usage of Cu-based MOPs.

A more generalized way to prepare stable MOPs is to shield the labile metal centers from water/chemical-attack. Anchoring hydrophobic functional groups on the outer surface of MOPs would turn the MOPs more water-resistant [101] and thus should be considered as more generalized and straightforward approach to prepare stable MOPs irrespective of the metal ions and linkers used during the synthesis. Yaghi and coworkers had synthesized dicopper paddlewheel-based carboxylate MOPs functionalized with dodecoxyalkyl chains [85]. Kim and coworkers demonstrated the ability of dodecoxyalkyl-functionalized MOPs to act as synthetic ion channel for transporting proton and alkali-metal ions across lipid membranes [102]. The prospect of potential applications of highly stabilized MOPs makes them more appealing for studying their systematic preparation procedures. In a recent report, Ghosh and coworkers had studied the inertness of copper-based MOPs toward water by systematically putting hydrophobic moieties around the metal centers [75] and had synthesized series of chemically ultrastable copper-based carboxylate MOPs (Figure 7). Four neutral spherical MOPs with general formula $[Cu_{12}(L_x)_{12}(H_2O)_{12}]$ (L_x: NDI core-based amino acid variant) were synthesized on a large scale by solvothermal method from dicopper paddlewheel cluster and naphthalene diimide linkers appended with amino acid variants—alanine, valine, isoleucine and phenyl alanine. Eight triangular windows and 24-alkyl groups are appended to each cage structures. Chemical stabilities of those MOPs were investigated under both acidic and basic conditions as well as under several oxidizing and reducing conditions. Smaller alkyl chains on the outer surface render MOPs unstable in water when compared with bulkier alkyl groups-functionalized MOPs. MOPs substituted with isoleucine and valine variants show moderate aqueous stability in comparison with phenyl alanine modified MOP which exhibits ultrastability under a wide range of pH values, in strong oxidizing and reducing media over a period of several days. Such exceptional stability can be attributed to the dense hydrophobic shielding of dicopper paddlewheel metal clusters preventing water molecules and other chemicals to undergo chemical ligation at the labile metal centers. Contact angle measurement revealed that hydrophobic (WCA ≈ 74°) to superhydrophobic surface (WCA ≈ 155°) properties can be achieved for copper-based carboxylate MOPs by simply fine-tuning the alkyl-side chains on the outer surface of MOPs.
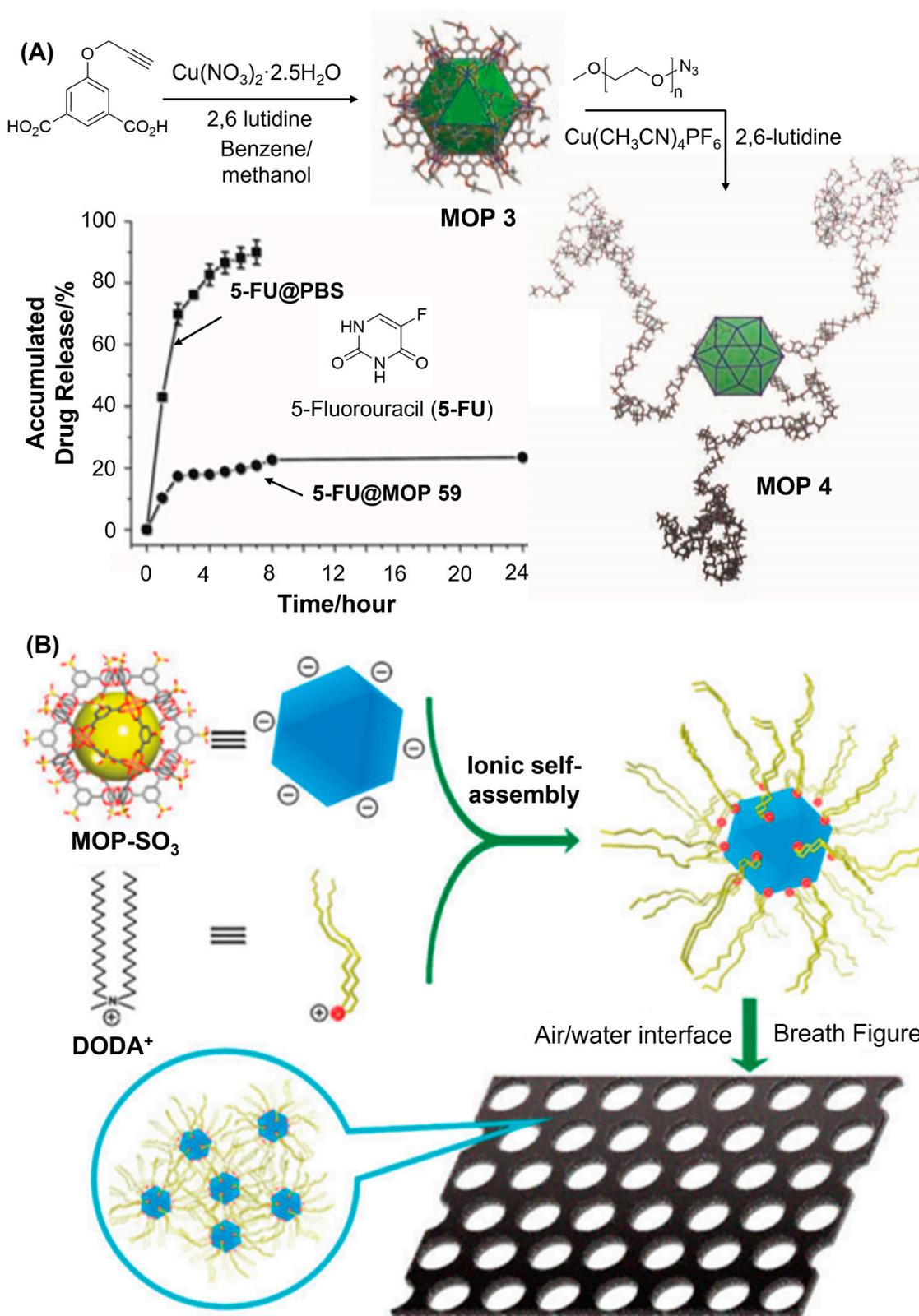
Figure 6. (**A**) Synthesis of copper (II) containing cuboctahedron MOP 3 and its post-synthetic modification with PEG to give water-soluble and stable MOP 4, and its role in controlled release of 5-fluorouracil (5-FU) drug. (**B**) Illustration of surface functionalized MOP-SO$_3$ via ionic self-assembly (ISA) and their ordered honeycomb architectures at the air/water interface. Reprinted by permission from Refs. [74,99]. Copyright 2011 from Wiley-VCH and copyright 2012 from Royal Society of Chemistry.
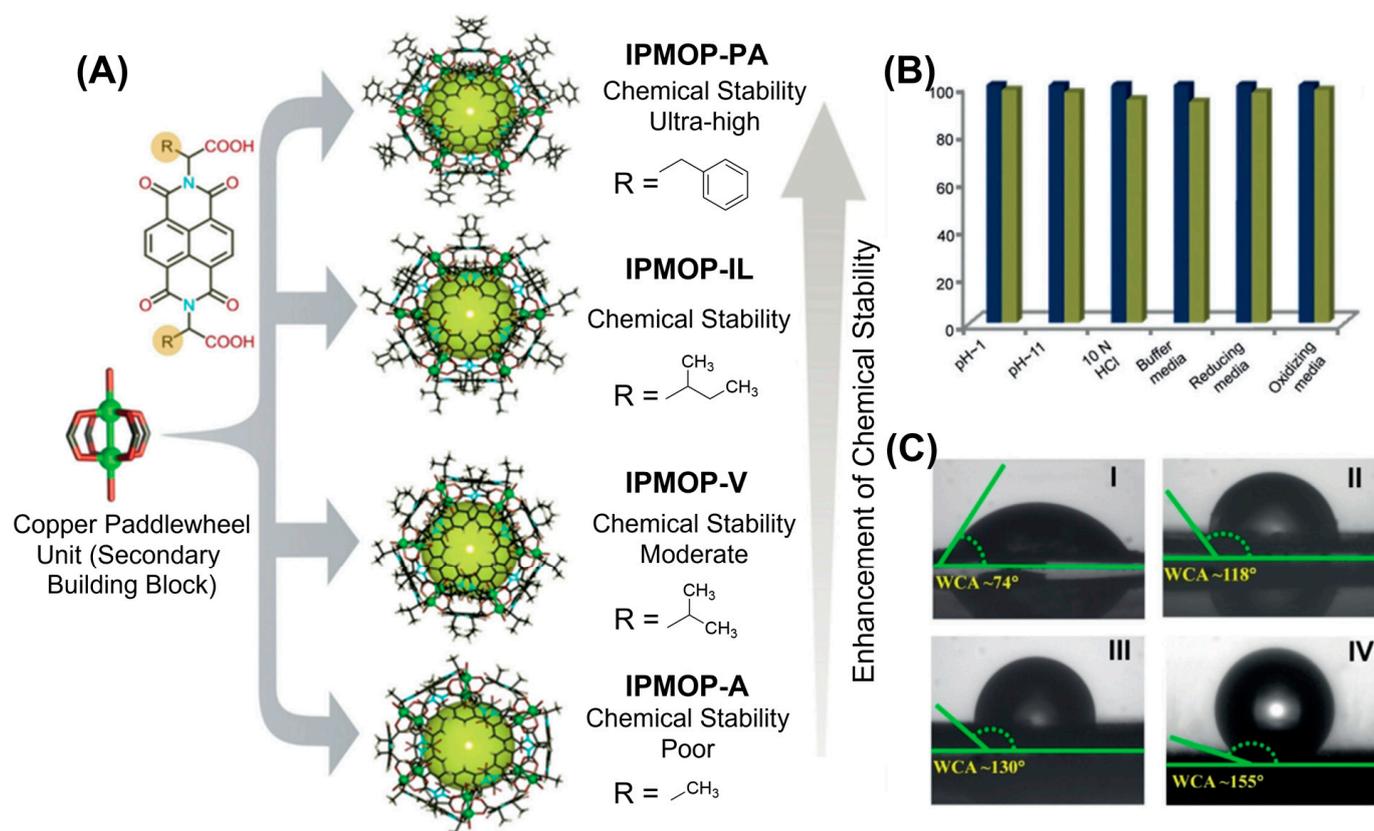
Figure 7. (**A**) Synthetic strategy for IPMOPs and their corresponding crystal structures following the systematic enhancement of their chemical stability (from bottom to top). (**B**) Bar diagram representing the reproducibility of the treatment of IPMOP-PA under various harsh conditions. Navy blue: before treatment of crystal, dark yellow: after crystal treatment. (**C**) Water droplet placed on pelletized IPMOPs, showing water contact angles (WCAs) of (I) $\approx 74°$, (II) $\approx 118°$, (III) $\approx 130°$ and (IV) $\approx 155°$ for IPMOP-A, IPMOP-V, IPMOP-IL and IPMOP-PA, respectively. Reprinted by permission from Ref. [75]. Copyright 2019 from Wiley-VCH.

Protecting labile metal ions from water-attack via hydrophobic shielding and/or post-synthetic amendment are definitely the viable strategies to prepare stable MOPs. However, ideal strategy would be to enhance the inertness of metal-ligand interactions by increasing metal-ligand bond strengths. For example, high-valent metal ions with high charge density and small ionic radii form stronger bonds with carboxylate linkers rendering the metal-ligand bonds less susceptible (Figures 8–13) to aqueous instabilities. In general, Ti^{4+}, Zr^{4+}, Hf^{4+}, Cr^{3+}, Ga^{3+}, Al^{3+} and other metal ions with high charge density and carboxylate ligands are considered to be hard acid and hard base, respectively and they form metal-ligand bonds stronger than Cu-O bond [103]. Wide varieties of metal organic frameworks were reported using first row transition metal ions starting from Cr^{2+} to Zn^{2+}. Interestingly great varieties of MOPs which are amenable for the incorporation of M_2 paddlewheel metal clusters other than dicopper paddlewheel as secondary building units are created in order to tune their porosities and stabilities. In the first-row transition metal ions of the periodic table, Cr^{2+} metal complexes experience lesser Jahn-Teller distortion effect compared with Cu^{2+} metal complexes, therefore higher kinetic stability of Cr complexes is anticipated. Among M_2 paddlewheel units, dichromium paddlewheel cluster, $Cr_2(COO)_4$ forms well-known coordination polymers with carboxylate linkers. Zhou and coworkers had first reported the synthesis of Cr(II)-based MOP (MOP-8) by reacting $Cr_2(OAc)_4$ with several isophthalate ligands and the BET surface area was measured to be 1000 m^2/g, one of the highest reported surface area among MOP-based systems [104].

Cr-based MOP 8 was found to be isostructural with the corresponding Cu/Mo-based MOP 8 with each dichromium unit, Cr_2 assembled with four carboxylate linkers originating from four different isophthalate linkers and 24 ligands coordinated to 12 units of Cr_2 units serving as vertices to form cuboctahedron cage. Gas adsorption study revealed better N_2 uptake behaviour of Cr(II)-MOPs at higher temperature compared with analogous Cu(II)-MOPs. High dissociation energy (513 kJ/mol) of Cr-O bond makes Cr(II)-MOPs thermally more stable as shown by their thermogravimetric analysis. Cu(II)-MOPs showed step-by-step increase in N_2 uptake upto 200 °C and lower uptake was observed beyond 200 °C. Interestingly, Cr(II)-MOPs showed negligible uptake until the activation temperature of 160 °C is achieved and finally N_2 uptake reached to 387 cm^3/g upon activation at 200 °C demonstrating the good maintenance of porosities of chromium-based materials following activation. Higher coordination bond strength between the coordinating solvent molecules and chromium metal centers makes the activation temperature higher for gas uptake. Cr(II)-MOPs are susceptible to arial oxidations and produces Cr(III)-MOPs following the oxidation of Cr^{2+} metal ions to high valence Cr^{3+} metal ions (Figure 8A). Unlike Cu(II)-MOPs which are unstable in air, strong Cr^{3+}-O coordination bond makes oxidized chromium-MOPs exceptionally stable to preserve their porous structures in the solid state to exhibit good H_2 uptake properties even after leaving the materials for one month in air. Bloch and coworkers had demonstrated that carbazole containing MOPs which are part of metal organic frameworks like DUT-49 [105] and PCN-82 [106] showed excellent methane and hydrogen storage capacities, can be synthesized independently to study their gas adsorption properties (Figure 8B). Accordingly, chromium(II)-based octahedron cage, $Cr_{12}(cdc)_{12} \bullet nDMF$ (MOP-9) was synthesized by reacting anhydrous $Cr_2(OAc)_4$ with carbazole dicarboxylic acid (H_2cdc) in dimethylformamide-methanol mixture under air-free condition [107]. TGA analysis revealed the excess of 60% solvent accessible void in $Cr_{12}(cdc)_{12}$ crystals and initial solvent exchange triggered structural rearrangement. $Cr_{12}(cdc)_{12}$ exhibits a BET surface area of 1235 m^2/g upon activation at 70 °C, one of the highest surface area reported for molecular metal organic materials. Analogous isostructural MOPs, $Mo_{12}(cdc)_{12}$ and $Cu_{12}(cdc)_{12}$ exhibited BET surface areas of 1108 m^2/g and 657 m^2/g, respectively which are much lower compared with chromium-based MOPs. Similar BET surface area trends were observed from gravimetric uptake analysis for methane storage with capacities of 148, 135, 81 cm^3/g for $Cr_{12}(cdc)_{12}$, $Cu_{12}(cdc)_{12}$ and $Mo_{12}(cdc)_{12}$, respectively (Table 1). Nevertheless, surface areas shown by these molecular materials fall short of the record values displayed by porous metal organic frameworks like DUT-49 [108] and PCN-81 [106] in order to be useful for high-pressure gas storage application. Achieving permanent porosity requires activation of MOPs which remains challenging mostly due to collapse of the extended structures and thus very much dependent on activation conditions [109]. Bloch and coworkers had reported the synthesis of chromium(II)-based MOPs using benezene-1,3-dicarboxylic acid ligand which is also known to produce MOPs in combination with other metal ions like copper (II) and molybdenum (II) [110]. Interestingly, ^{t}Bu-substituted chromium(II)-MOP (Cr-^{t}Bu-bdc) was found to be significantly thermally stable with optimal activation temperature of 75 °C in comparsion with Cr-OH-bdc MOP with having the Langmuir surface area of 187 m^2/g. Under this condition, Cr-^{t}Bu-bdc MOP showed BET surface area of 1796 m^2/g which is the highest surface area reported for metal organic polyhedra. Importantly, the materials retained significant surface area of 1588 m^2/g even after heating upto 175 °C.
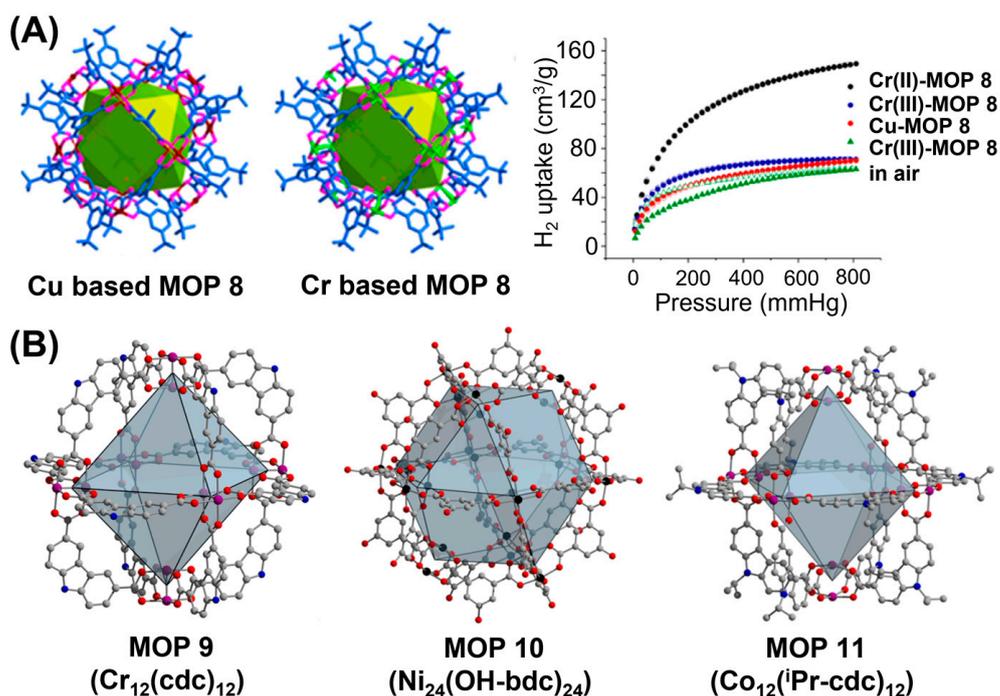
Figure 8. (**A**) Crystal structures of Cu^{II}-based MOP 8 and Cr^{II}-based MOP 8. H$_2$ adsorption isotherms of Cr(II)-MOP 8, Cr(III)-MOP 8, Cu(II)-MOP 8 and Cr(III)-MOP 8 kept in air for 1 month. (**B**) Crystal structures of MOP 9 (Cr$_{12}$(cdc)$_{12}$), MOP 10 (Ni$_{24}$(OH-bdc)$_{24}$) and MOP 11 (Co$_{12}$(^{i}Pr-cdc)$_{12}$) are shown. Reprinted by permission from Refs. [104,107,111]. Copyright 2017, 2018 from American Chemical Society.
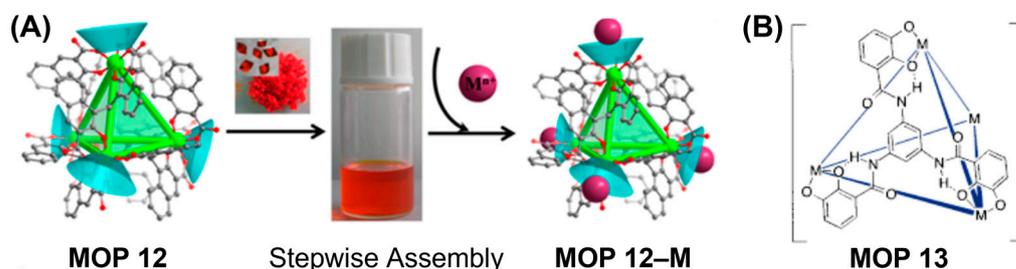
Figure 9. (**A**) Assembly of the tetrahedron MOP 12 with calixarene-like coordination-active vertices for potential metal ion trapping. (**B**) Titanium-based tetrahedron metal cluster MOP 13. Reprinted by permission from Refs. [59,112]. Copyright 1998 from Wiley-VCH and copyright 2017 from American Chemical Society.

Table 1. Methane storage properties of MOP 9 (M$_{12}$(cdc)$_{12}$, M = Cu, Cr, Mo) cages in comparison to PCN-81 [a].

Materials	BET Surface Area m^2/g	35 bar Capacity cm^3/g [cm^3/cm^3]	65 bar Capacity cm^3/g [cm^3/cm^3]
Cu$_{12}$(cdc)$_{12}$	657	81.3 [69.4]	111.8 [95.4]
Cr$_{12}$(cdc)$_{12}$	1235	147.5 [112.1]	193.9 [147.8]
Mo$_{12}$(cdc)$_{12}$	1108	135.0 [111.5]	181.1 [150.0]
PCN-81	4050	305.3 [146.8]	448.7 [215.8]

[a] All values are total uptake.

Other first row transition metal ions like nickel, cobalt, iron, zinc were also successfully utilized to prepare porous coordination cages in order to tune their porosities and stabilities. Introduction of paddlewheel clusters from variable metal ions led to the synthesis of diverse class of coordination cages. Recently, Bloch et al. had reported the preparation of coordination cages using cobalt(II) and nickel(II) metal ions [111]. Zinc(II)-containing paddlewheel units lack metal-metal bonding. Instability of square-planar Zn^{2+} complexes make them particularly challenging to retain the porosities of Zn-based MOPs and MOFs after removal of coordinated solvent molecules which results in degradation of porous materials. Reaction between 5-hydroxy-isophthalic acid and nickel(II) acetate yielded $Ni_{24}(OH\text{-}bdc)_{24}$ cuboctahedron cage in high yield with average Ni-Ni distance in the paddlewheel of 2.65 Å comparable to Cu-Cu distance in $Cu_{24}(OH\text{-}bdc)_{24}$ (Figure 8B) but significantly longer than quadruply bonded Mo-Mo distance in $Mo_{24}(OH\text{-}bdc)_{24}$. Moreover, topological variants of MOPs can be synthesized by tuning the bridging angles between carboxylic acid groups. Reaction of 9-isopropylcarbazoledicarboxylic ($^{i}Pr\text{-}cdc$) acid with $NiOAc_2 \bullet 4H_2O$ or $CoCl_2 \bullet 6H_2O$ afforded octahedron coordination cages $Ni_{12}(^{i}Pr\text{-}cdc)_{12}$ and $Co_{12}(^{i}Pr\text{-}cdc)_{12}$, respectively with having six bimetallic paddlewheel units in each coordination cage. All three MOPs maintain their crystallinities after solvent exchanges and their three-dimensional structural packing result in potentially accessible channels within their structures following activation. Structural rearrangements due to lack of three-dimensional inter-cage interactions result in significant loss in porosity in $Ni_{24}(OH\text{-}bdc)_{24}$ MOP upon activation. Interestingly, carbazole-based materials exhibited excellent thermal stability under evacuation to retain their porosities upto activation temperature of 200 °C. Therefore, precise ligand functionalization with judiciously chosen metal ions can potentially be the best combination to optimize the porosities and stabilities of metal organic polyhedra (MOPs).

Analogous to other first row transition metal ions, titanium metal particularly high valent Ti^{4+} metal ion can be used to prepare stable metal organic polyhedra. Compared with other metal ions, Ti-based metal organic polyhedra are very rare in literature. Zhang and coworkers had demonstrated the synthesis of water soluble and ultrastable Ti-based tetrahedron [112]. Solvothermal assembly of $Ti(^{i}OPr)_4$ or $TiCl_4$ with embonic acid gave rise to anionic tetrahedral Ti_4L_6 cage (MOP 12) in orthorhombic (PTC-101) or cubic (PTC-102) arrangements (Figure 9A). Each Ti-center is adopted to distorted octahedron coordination geometry chelated by three carboxyl-phenol groups with uncoordinated oxygen atoms pointing outwards. Solubility and ultra-stability of Ti_4L_6 cage in water is confirmed by electrospray ionization mass spectrometry affording stepwise assembly function with other metal ions. The crystals of PTC-101 and PTC-102 can be easily dissolved in water. Unusual mixed valency of $Ti^{3+/4+}$ was observed in the Ti_4L_6 cage as identified by electron spin resonance and X-ray photoelectron spectroscopy analysis. Visible-light induced homogeneous photo-decomposition of acid blue 93 and alkali blue 4B were successfully achieved by these cages. Raymond and coworkers had expanded the synthesis of Ti-based metal coordination cage using catecholate-based organic linkers which satisfy the coordination sphere of tetravalent titanium (Ti^{IV}) metal ions by having three coordinating chelating groups (Figure 9B). Reaction of three-fold symmetric tris-catecholate based ligand with the methanolic solution of $[Ti(O_nBu)_4]$ afforded the formation of tetrahedral cluster of stoichiometry (MOP 13) Raymond and coworkers had further demonstrated that other hard trivalent or tetravalent transition and main group metal ions e.g., Ga^{III}, Fe^{III}, Al^{III}, Ge^{IV}, Sn^{IV} can be successfully combined with catecholate ligands to prepare coordination complexes of high thermodynamic stabilities and enough labilities to ensure clean formation of the tetrahedral clusters [59,113,114]. Higher stability for the tetravalent Ti^{IV} and Ge^{IV}-based hosts can be anticipated from slower guest exchange rate compared with trivalent Ga^{III}, Fe^{III}, Al^{III} hosts as the crystal field effects remain insignificant for metal ions with similar ionic radii, the lability depends on the charge density of the metal ions with more highly charged metal ions having slower water exchange rate [115]. In contrast, guest exchange in hosts having more inert metal-ligand bonds is as facile as the guest exchange

in hosts with more labile metal-ligand bonds, rather distortion of host structure is sufficient for the passage of guests and certainly does not require metal-ligand bonds rupture within the hosts.
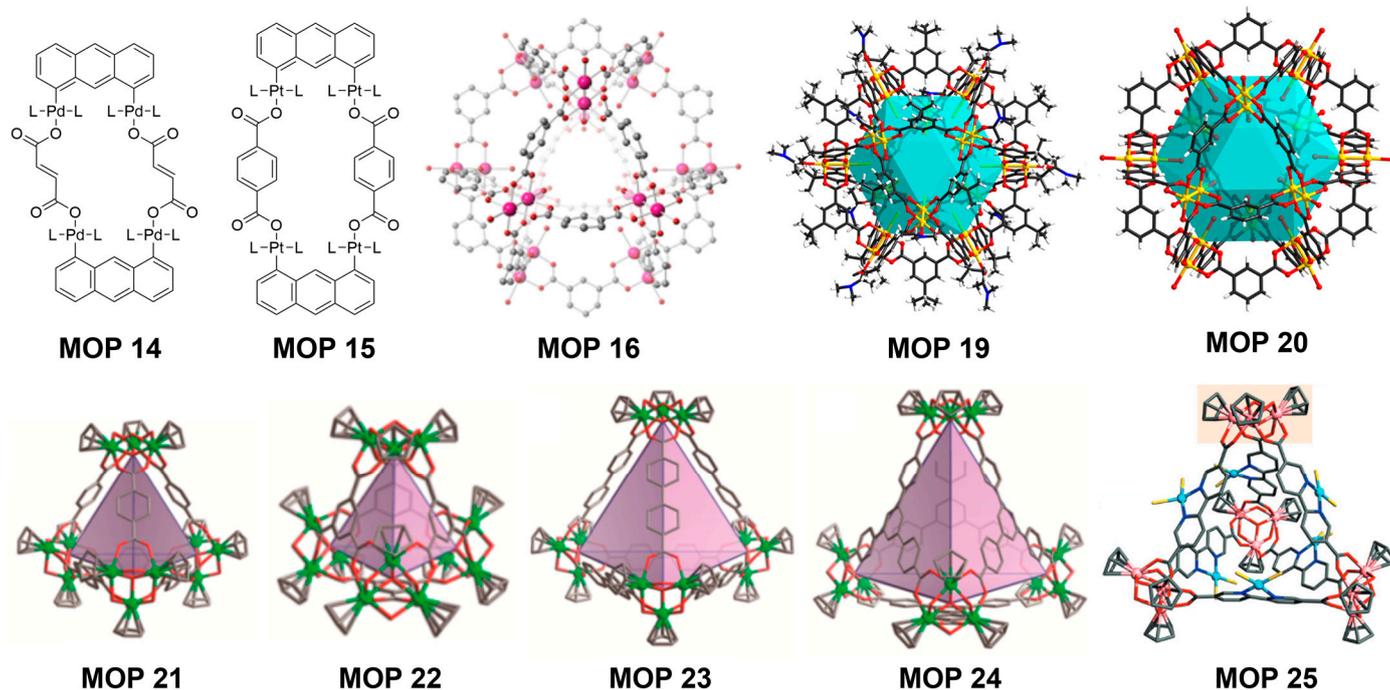

Figure 10. O-donor based MOPs prepared using second row transition metal ions. Chemical structures of Pd-based MOP 14 and MOP 15. Crystal structures of Rh-based anticubooctahedron MOP 16 and Ru-based two cuboctahedron cages, MOP 19 and MOP 20. Crystal structures of Zr^{IV}-based tetrahedron MOP 21, MOP 22, MOP 23 and MOP 24 are shown. MOP 25 is the crystal structure of Zr-bpydc-CuCl$_2$. Reprinted by permission from Refs. [116–121]. Copyright 2009 from Royal Society of Chemistry. Copyright 2003, 2013, 2016 from American Chemical Society. Copyright 2016 from Wiley-VCH. Copyright 2015 from Elsevier.

Compared with first row transition metal ions, second row transition metal ions tend to form relatively stable complexes. Examples include dirhodium paddlewheel motifs which are particularly interesting for the preparation of stable carboxylate-based MOPs due to their high chemical stabilities, but the relative inertness of their equatorially-oriented carboxylate groups makes it very challenging to prepare the MOPs via ligand-exchange reactions. Similarly, it was believed that MOPs bearing Pt-O or Pd-O bonds would be unstable due to hard-soft combination. Mukherjee and coworkers had reported the synthesis of neutral molecular rectangular MOP driven by Pd-O interaction [116]. Dipalladium(II)-based organometallic clip containing anthracene unit in combination with disodium fumarate salt afforded molecular rectangular MOP 14 driven by the electrostatic interaction between the anionic fumarate and Pd(II) metal ion (Figure 10). Utilizing Pt-O interaction, Stang and coworkers had reported the synthesis of MOP 15 (Figure 10) from phenanthrene-based diplatinum molecular clip and dicarboxylate linkers [117,122]. Linear ditopic carboxylate linker gave triangular MOP whereas angular ditopic carboxylate linker produced rhomboidal MOP. Kitagawa and coworkers had demonstrated the synthesis of rhodium-based metal-organic cuboctahedra MOP 16 (Figure 10) with molecular formula [Rh$_2$(bdc)$_2$(S)$_2$]$_{12}$•(S); S = Solvent molecules [118]. Relative stability of rhodium-based MOP 16 was assessed in comparison with isostructural Cu(II)-analogue. Interestingly, copper(II)-based MOP showed very limited nitrogen uptake following activation at 323 K indicating the copper(II) analogue becoming nonporous after solvent removal. Dirhodium-based MOP can be successfully activated upon heating at 368 K and showed nitrogen adsorption capacity of 130 cm^3/g at relatively low pressure (P/P$_0$ = 0.1) confirming the presence of

microporous cavities inside dirhodium-based MOP. Rhodium-paddlewheel motif provides rigidity to the molecular backbone and imparts high thermal and chemical stabilities. Maspoch and coworkers had reported the role of strategic use of protecting groups in the synthesis of Rh(II)-based MOPs with previously inaccessible functionalities [123]. Synthesis of both carboxylic and amine-functionalized MOPs need careful designing of protection and deprotection strategies in order to prevent the formation of undesired coordination polymers facilitated by strong affinities of Rh(II)-paddlewheels towards carboxylic acids and N-donor groups (Figure 11A). Protection of one of the three carboxylic acid groups of 1,3,5-benzenetricarboxylic acid by 2-(trimethylsilyl)ethanol followed by the treatment with $Rh_2(OAc)_2$ under solvothermal condition gave COOTSE-RhMOP in cuboctahedron geometry consisting of 12 dirhodium paddlewheel units and 24 protected carboxylic acid linkers. Successful deprotection strategy led to the formation of carboxylic acid functionalized Rh(II)-MOP (MOP 17) demonstrating the ability of Rh(II)-MOP to withstand post-synthetic modification. Interestingly, deprotected Rh(II)-MOP was found to maintain the structural porosity compared with protected MOP as revealed from their increased gas uptake capacities which can be attributed to the removal of bulky protecting groups having beneficial effects on the porous properties of the materials [124,125]. COOH-Rh(II)MOP can be dissolved in water at near physiological pH and did not show any signs of degradation even after leaving in aqueous solution for 7 days demonstrating exceptional chemical stability of Rh(II)-based MOP. Similarly, amine-functionalized Rh(II)-MOP (MOP 18) was successfully synthesized by BOC-protecting the amine group of 5-aminoisophthalic acid linker. Owing to the strong processability, deprotection of NBoc-Rh(II)MOP either by thermolysis or by treatment with trifluoroacetic acid (TFA) gave the amine-functionalized Rh(II)-MOP which becomes more porous than the protected starting materials. Interestingly, NH_2-functionalized Rh(II)-MOP exhibits better gas uptake behaviour compared with Cu(II) analogue [126].
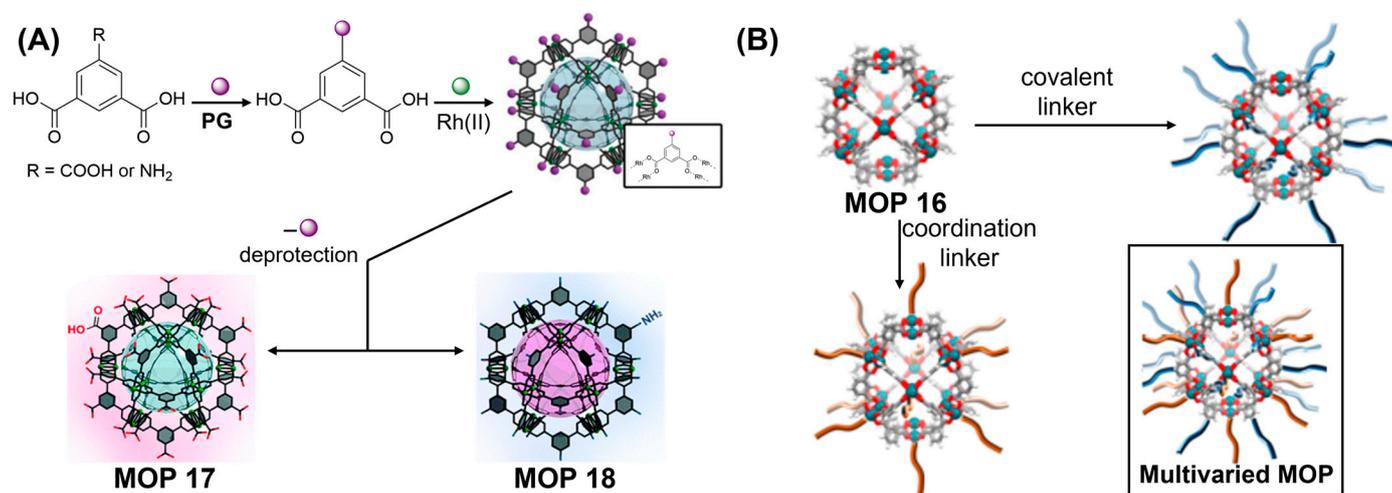
Figure 11. (**A**) Scheme of protecting group strategy to synthesize COOH-tagged cuboctahedron Rh(II)-based MOP 17 and NH_2-tagged Rh(II)-based MOP 18. (**B**) Post-synthetic covalent and coordination modification of cuboctahedron MOP 16. (Inset) Illustration of a cuboctahedron Rh-MOP functionalized on the 12 dirhodium paddlewheels through coordination chemistry (in orange) and on the 24 organic linkers through covalent chemistry (in blue). Reprinted by permission from Refs. [123,127]. Copyright 2019 from Royal Society of Chemistry and copyright 2019 from American Chemical Society.

It has been challenging to implement post-synthetic functionalization on MOPs due to their chemical instabilities. However, stable MOPs synthesized using inert metal-carboxylate bonds like Rh-O however remain amenable for post-functionalization. Maspoch and coworkers had demonstrated the post-synthetic covalent and noncovalent functionalization methods on Rh(II)-based MOPs [127]. Two robust octahedral Rh(II)-based MOP 16 with varied solvents, $[Rh_2(bdc)_2(H_2O)_2]_{12}$ and $[Rh_2(OH-bdc)_2(H_2O)(DMA)]_{12}$ were selected for post-functionalization mainly due to their chemical robustness and presence of intrinsic micropores. Carboxylate-based Rh-Rh paddlewheel clusters are mostly inert at their equatorial sites however they remain highly reactive at their axial sites. Given these affinities, ligand-exchange reaction at the axial sites of metal centers would enable surface functionalization of Rh(II)-MOPs using N-donor ligands like 4-tertiarybutyl pyridine (*tert*Py) which can axially coordinate to the outer metal centers of all Rh_2 paddlewheel units giving rise to surface-functionalized Rh-MOP with chemical formula of $[Rh_2(bdc)_2(tertPy)(H_2O)]_{12}$. Covalent functionalization was carried out by activating the hydroxyl groups of organic linkers pointing outwards of the Rh(II)-MOP. Sodium hydroxide was reacted with acyl chloride or acid anhydrides. Orthogonal reactivities of Rh-Rh paddlewheels and the organic linkers therefore yielded doubly-functionalized Rh-MOPs featuring 36 new functional molecules. Although, post-functionalization at the outer surface induces surface area reduction compared with pristine materials, post-functionalized Rh(II)-MOPs importantly maintain their intrinsic microporosities in the solid state.

Designing of supramolecular polymers from metal organic polyhedra (MOPs) with permanent microporosities is very challenging as the requirement of crystallinity impedes the materials processing and often amorphous materials end up being nonporous. Furukawa and coworkers had reported novel strategy to prepare amorphous supramolecular polymeric materials with controlled microporosities [128]. Porous Rh-based carboxylate MOP 16 ($[Rh_2(bdc)_2]_{12}$, bdc = benzene-1,3-dicarboxylic acid) was allowed to react with ditopic imidazole linker 1,4-bis(imidazole-1-ylmethyl)benzene (bix) at the labile axial position of each Rh metal centers to yield cross-linked supramolecular polymers. By controlling the self-assembly pathways, macroscopic morphologies of supramolecular polymers can be successfully fine-tuned from spherical colloidal particles to colloidal gels with increasing hierarchical porosities. Gas adsorption experiments which were performed on colloidal polymeric particles and aerogels demonstrated that the intrinsic porosities of the monomers were not only preserved during the supramolecular polymerization, but also supramolecular polymeric materials outperformed the CO_2 uptake of the porous monomers. This can be attributed to the presence of micro and macropores in supramolecular polymers compared with monomeric Rh(II)-MOP 16 which undergoes aggregation in the solid state. Better gas uptake behaviour of aerogels over polymeric particles further emphasizes the influences of macroscopic morphologies on the gas adsorption properties.

Other second row transition metal ions like ruthenium also forms inert metal-ligand complexes and therefore are expected to produce robust and stable MOPs. Dinuclear Ru_2^{n+} paddlewheel clusters with oxidation states ranging from +4 to +6 were reacted with various carboxylate-based organic linkers to produce metal organic composites. Zhou and coworkers first reported the synthesis of metal organic polyhedra constructed (Figure 10) from dinuclear ruthenium paddlewheels [119]. Reaction of H_2CDC (9H-3,6-carbazoledicarboxylic acid), H_2BBDC (5-tert-butyl-1,3-benzenedicarboxylic acid) and H_2BDC (1,3-benzenedicarboxylic acid) with Ru_2^{n+} [n = 4 for $Ru_2(OAc)_4$ and n = 5 for $Ru_2(OAc)_4Cl$] under solvothermal condition gave two octahedron cages $[Ru_2(CDC)_2Cl]_6$ and $[Ru_2(CDC)_2]_6$ and two cuboctahedron cages $[Ru_2(BBDC)_2Cl]_{12}$ (MOP 19) and $[Ru_2(BDC)_2]_{12}$ (MOP 20).

Among other metal-ligand bonds, the Zr-O coordination bond is exceptionally strong with the bond dissociation energy upto 766 kJ/mol. Zr^{4+} and carboxylate linkers are hard acid and hard base, respectively; and MOPs constructed from zirconium metal ion and carboxylate linkers are thus expected to be robust and stable. Liu and coworkers had first reported the synthesis of four Zr^{IV}-based carboxylate MOPs—MOP 21, MOP 22, MOP 23 and MOP 24 with molecular formulas $\{[Cp_3Zr_3\mu_3\text{-}O(\mu_2\text{-}OH)_3]_4(BDC)_6\}Cl_4\bullet nS$, $\{[Cp_3Zr_3\mu_3\text{-}O(\mu_2\text{-}OH)_3]_4(BTC)_4\}Cl_4\bullet 4DMF\bullet nS$, $\{[Cp_3Zr_3\mu_3\text{-}O(\mu_2\text{-}OH)_3]_4(BPDC)_6\}\bullet Cl_4\bullet nS$, and $\{[Cp_3Zr_3\mu_3\text{-}OH)_3]_4(BTB)_4\}\bullet Cl_4\bullet nS$ (Cp = cyclopentadienyl, bdc = benzene-1,4-dicarboxylate, btc = benezene-1,3,5-tricarboxylate, bpdc = 4,4′-biphenyldicarboxylate, H_3btb = 4,4′,4″-benzene-1,3,5-triyltris (benzoic acid) and S represents free solvent molecules), respectively [120]. All four cages have tetrahedral geometries and they are isostructural in nature. Trinuclear zirconocene cluster appears to be a 3-connected secondary building unit having pyramidal geometry with carboxylate ligands oriented to one face and the μ-OH groups oriented to the other, in which the C_2 axes in carboxylate ligands forms an angle of about 60°. Hong and coworkers had reported the synthesis of hetero-metal decorated Zr^{IV}-based carboxylate tetrahedral MOP 25, Zr-bpydc-MCl_2 (M = Pd^{2+} or Cu^{2+}, H_2bpydc = 2,2-bipyridine-5,5-dicarboxylic acid) [121]. Effective use of hard/soft—acid/base principle allows the orthogonal self-assembly of Zr-bpydc-$CuCl_2$ cage via three different strategies—postsynthetic metallation, a stepwise metallo-ligand approach and one-pot reaction. Preparation of stable porous materials with permanent porosities and good solution processabilities is exceedingly challenging. Chen and coworkers had reported the preparation of Zr-based MOP 26, $[Cp_3Zr_3(\mu_3\text{-}O)(\mu_2\text{-}OH)_3]_8(D\text{-cam})_{12}\cdot Cl_8\cdot nS$ (D-cam = D-camphoric acid, S = free solvent molecule) which possesses both intrinsic and extrinsic porosities (Figure 12A) [129]. MOP-based supramolecular framework maintains their original structure after activation and exhibits permanent porosity with moderately high surface area of 1201 m^2/g as demonstrated by gas adsorption isotherm. Each single vertex of the cage was held together with other three vertices from three different cages using O-H•••Cl•••H-O hydrogen bonds with 24 of those H-bonds of one cage linked with the surrounding cages. Charge-assisted H-bonding interaction enables cubic cages to form porous hydrogen-bonded metal organic framework. Yuan and coworkers had demonstrated that the porosity and stability of Zr-MOP based hydrogen-bonded framework depends on the degree and strength of the charge-assisted H-bonding interactions [130]. Two previously reported zirconium MOPs with molecular formula $\{[Cp_3Zr_3(\mu_3\text{-}O)(\mu_2\text{-}OH)_3(bdc)_{1.5}]^+\bullet 4(DMF)_4Cl^-\}_4\bullet 31DMF\bullet 90H_2O$ (bdc = 1,4-benzenedicarboxylic acid) and $\{[Cp_3Zr_3(\mu_3\text{-}O)(\mu_2\text{-}OH)_3(btc)]^+\bullet 4(DMF)_2Cl^-\}_2\bullet 26DMF\bullet 35H_2O$ (btc = 1,3,5-benzenetricarboxylic acid) when treated with different solvent like dimethyl amine, two new hydrogen-bonded frameworks $\{[Cp_3Zr_3(\mu_3\text{-}O)(\mu_2\text{-}OH)_3(bdc)_{1.5}]^+\ 4(Me_2NH_2)^+\ 2Cl^{-6}\}\bullet 35H_2O$ and $\{[Cp_3Zr_3(\mu_3\text{-}O)(\mu_2\text{-}OH)_3(btc)]^+\bullet 4(Me_2NH_2)^{2+}Cl^{-6}\}\bullet 24H_2O$ are formed. Compared with two pristine MOPs, newly formed MOPs not only exhibit higher ratio of O-H•••Cl^- bond, but also contain stronger bridging H-bonding interactions which results in enhanced porosity and robustness of the framework in guest-free state. PXRD analysis after gas adsorption reveals that crystallinity of newly formed MOPs are well maintained while the pristine MOPs collapse to amorphous materials indicating lower N_2 uptake for pristine MOPs owing to the existence of the intrinsic pores with collapsed interstitial cavities. Higher N_2 uptake was observed for newly formed MOPs which can be attributed to the existence of well-maintained intrinsic and extrinsic pores following activation.
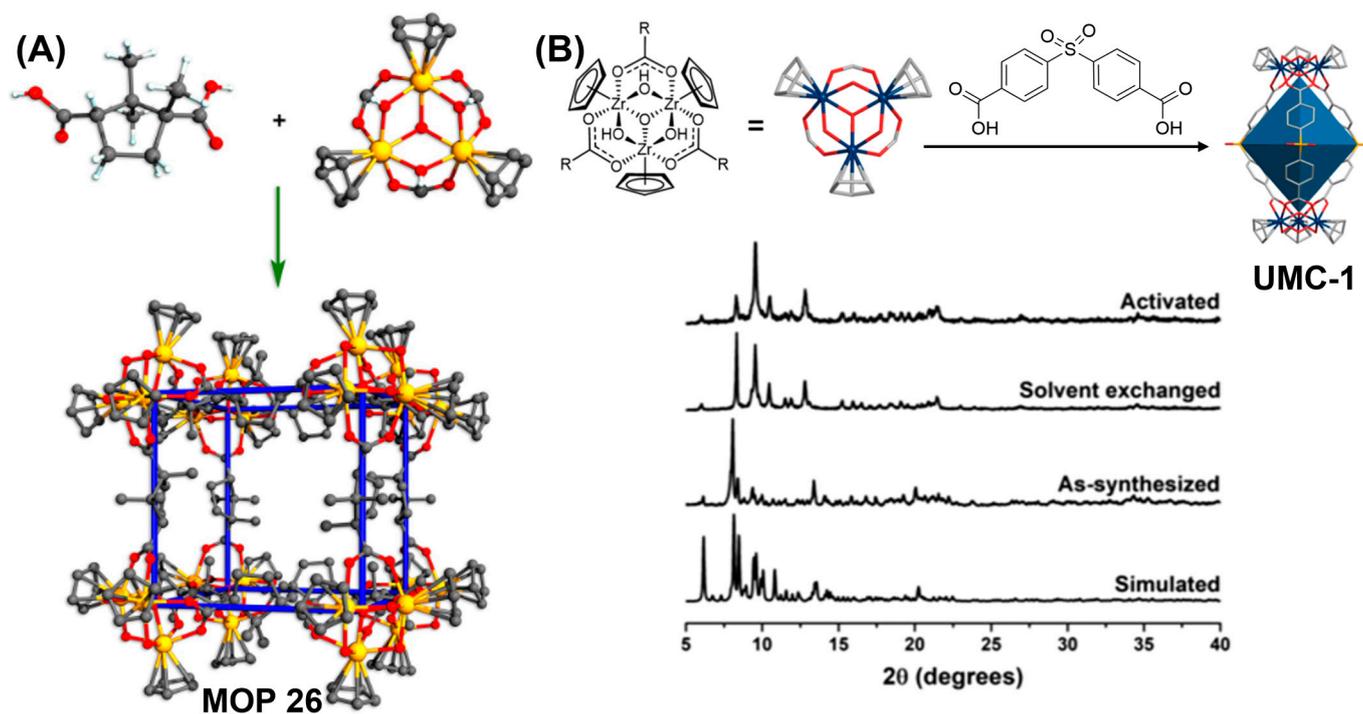
Figure 12. (**A**) Self-assembly of cubic cage [Cp$_3$Zr$_3$μ$_3$-O(μ$_2$-OH)$_3$]$_8$(D-cam)$_{12}$ from D-camphoric acid and Cp$_3$Zr$_3$O(OH)$_3$. (**B**) Synthesis of UMC-1. Simulated and experimental powder X-ray diffraction patterns of UMC-1 when activated. Afterward, the crystallinity of UMC-1 was preserved. Reprinted by permission from Refs. [129,131]. Copyright 2017 from Wiley-VCH and copyright 2018 from American Chemical Society.

Choe and coworkers had reported the synthesis of porous Zr-based coordination cages with synergistic binding centers for CO_2 molecules [131]. Major challenges to enhance gas adsorption behaviour include: (1) strengthening intercage interactions for enhanced permanent porosity and (2) decorating MOPs with strong ligand binding centers for CO_2 adsorption. Zr(IV)-based M$_6$L$_3$ cage UMC-1: {[Cp$_3$Zr$_3$O(μ$_2$-OH)$_3$]$_2$(SDB)$_3$}·Cl$_2$ (H$_2$SDB: 4,4′-sulfonyldibenzoic acid; Cp: cyclopentadienyl) was accordingly prepared from trinuclear Zr cluster and banana-shaped organic linker. The SO_2 group in the organic linker facilitates the intercage interactions providing strong binding centers for CO_2. Powder X-ray diffraction pattern reveals that UMC-1 retains both intrinsic and extrinsic porosities which can be attributed to proper maintaining of the intercage interactions even after activation (Figure 12B). Interestingly, UMC-1 remains stable under aqueous acidic solution (pH = 1) to neutral pH = 7 after prolonged exposure for 24 h. Exceptional hydrolytic stability of UMC-1 can be attributed to the strong Zr-O bond strength. Interestingly, another variant of Zr-based MOP, UMC-2 which features the absence of SO_2 group has the same molecular geometry as UMC-1 but different packing pattern. UMC-2 becomes amorphous following activation. Unsurprisingly, UMC-2 with no porosity has significantly lower CO_2 adsorption capacity compared with UMC-1 but has better CO_2 uptake selectivity over N_2 adsorption due to the availability of synergistic carbon dioxide binding centers at the organic linkers. Given the solution processability and aqueous stability, UMC-1 represents a model material for carbon separation application based on its high adsorption selectivity. Zhang and coworkers had reported the synthesis of Zr-based carboxylate MOP with molecular formula of [Cp$_3$Zr$_3$(μ$_3$-O)(μ$_2$-OH)$_3$]$_2$L$_3$•4Na•4H$_2$O constructed from cationic SBUs of Cp$_3$Zr$_3$(μ$_3$-O)(μ$_2$-OH)$_3$ and broken linear organic ligand Na$_2$H$_2$L containing two sulfonate groups [132]. Multiple charge-assisted H-bonding interactions between μ$_2$-OH and SO_3^- groups decorated on the MOP surface and electrostatic interactions between cationic vertexes and anionic SO_3^- groups significantly consolidated the porous frameworks in

order to maintain their porosity after desolvation, heating to 150 °C and immersion in water, strong acid or weak base solution as revealed by unaltered PXRD profiles after each treatment. Superior stability of Zr-based MOP further prompted its potential applicability towards gas adsorption which reveals the CO_2-selective capture profile over N_2 making them suitable for CO_2 separation from flue gas mixtures. Sulfonate functionalities render MOP highly proton conductive (1.14×10^{-3} Scm^{-1}) and humid (98% relative humidity).

Furthermore, exceptional aqueous and thermal stabilities of Zr-based carboxylate MOPs make them amenable for post-synthetic modifications [133]. For post-synthetic modification, Choe and coworkers had chosen amine-functionalized Zr-based tetrahedron MOP 27 as prototypical MOP with molecular formula $[Cp_3Zr_3(\mu_2\text{-O})(\mu_3\text{-OH})_3]_4[BDC\text{-}NH_2]_6[(C_2H_5)_2NH_2]_2Cl_6$ constructed from trinuclear zirconium cluster and 2-amine-1,4-dicarboxylic acid linker [134]. Good solution processibility of Zr-based MOP was also demonstrated by exceptional aqueous stability. Retention and/or enhancement of permanent porosity of carboxylate-based MOPs following post-synthetic polymerization is particularly challenging task. NH_2-functionalized Zr-based MOP 27 was covalently crosslinked using flexible acyl chloride linkers by utilizing the condensation reaction to form cross-linked MOPs without significant structural changes of Zr-based MOP. Microporosities of tetrahedron MOPs in cross-linked material are well maintained based on gas adsorption study. This crosslinking strategy can be used for advanced applications like synthesis of polymeric membranes and molecular separations. Guo and coworkers had demonstrated successful utilization of covalently cross-linked MOPs for the preparation of interfacial microstructure with enhanced water permeance and attractive separation performance [135]. Permanent pores inherited from amine-functionalized Zr-based MOP 27 and network pore originated from rigid cross linkers (e.g., trimesoyl chloride) enable cross-linked MOPs to exhibit better separation efficiency by letting through monovalent and divalent salt ions and rejecting larger dye molecules. Therefore, strong Zr-O metal-ligand interaction enables scientists to prepare aqueous and thermostable MOPs useful for performing various applications like gas storage and separation. In a recent report, Zhao and coworkers systematically studied the aqueous stabilities of several Zr-based MOP 27 (Figure 13A) over wide range of pH [136]. Amine-functionalized Zr-MOP 27 (NH_2-ZrT-1) and three others Zr-MOPs (ZrT-1, ZrT-3 and ZrT-4) with no amine groups but with different organic linkers (1,4-benzenedicarboxylic acid, 1,1′-dicarboxylic acid-4,4′-biphenyl and 1,3,5-tris(4-phenylcarboxylic acid)benzene) were chosen for the study. All four Zr-MOPs exhibited exceptional stabilities under neutral, acidic and weakly basic aqueous environments (pH = 2.2 to pH = 9.8). Exceptional stability also allows NH_2ZrT-1 MOP 27 to undergo covalent post-assembly modification (PAM) without any sign of decomposition of the MOP. Mannich reaction was carried out to study the process-tracing and was conducted using formaldehyde in methanol/water solvent mixtures at 25 °C. ^{1}H NMR and ESI-TOF-MS were successfully utilized to monitor the sequential nature of PAM processes by recording the reaction course at various time intervals.

In an another report, Zhao, Yuan and coworkers demonstrated the heterogeneous post-assembly modification strategy (Figure 13B) in order to prepare supramolecular frameworks [137]. Exceptionally stable zirconium-based MOP was used to prepare metal organic frameworks (MOFs) amenable for further post-functionalization, which is otherwise impossible to achieve using other synthetic approaches starting from post-functionalized organic ligands mainly due to the reactivities and instabilities of the linkers during the coordination-driven self-assembly process. It was envisaged that 2-acrylamidoterephthalic acid and trinuclear zirconium cluster would give rise to tetrahedron ZrT-1-AA MOP 28 bearing acrylamido group. Although 2-aminoterephthalate was successfully post-functionalized with acryolyl chloride to prepare 2-acrylamidoterephthalic acid, subsequent self-assembly reaction remained unsuccessful. Under aqueous hydrochloric acid condition 2-acrylamidoterephthalic acid undergoes partial hydrolysis to release 2-aminoterephthalic acid, certain portion of the post-functionalized ligand also transforms into 2-(bicyclo[2.2.1]-hept-5-ene-2-carboxamido)terephthalic acid via the Diels–Alder (D–A) reaction by react-

ing with the in situ formed cyclopentadiene from zirconium metal clusters. Also, the synthesis of ZrT-1-AA MOP 28 was unsuccessful via homogeneous post-synthetic modification of ZrT-1-NH$_2$ MOP 27 which was prepared via self-assembly from 2-amino-1,4-benzenedicarboxylic acid and trinuclear zirconium metal cluster. Homogeneous postsynthetic modification proceeded with low efficiency in methanol partly due to the alcoholysis of acrolyl chloride with methanol. Accordingly, ZrT-1-AA MOP 28 was synthesized via heterogeneous PAM from the bulk ZrT-1-NH$_2$ MOP 27 crystals. The amino motifs in the ZrT-1-NH$_2$-based crystalline supramolecular frameworks remain accessible due to framework's interpenetrated porosity. Cubic ZrT-1-NH$_2$ crystals following solvent exchange were treated with acryloyl chloride in hexane for one day to give ZrT-1-AA. PAM of MOFs was studied via ESI-TOF-MS. With the increase of reaction time, the peaks gradually shifted toward higher m/z ratio as more amino groups of ZrT-1-NH$_2$ were functionalized. Furthermore, ZrT-1-AA is crosslinked into shaped materials by using poly(ethylene glycol) diacrylate binder. The relative proportion of the binder determines the flexibility, shape, amount of loaded MOPs in the materials and prevents the leakage of MOPs from the composite materials. Shaped materials exhibited moderate CO$_2$ uptake compared with as-synthesized ZrT-1-AA which is amorphous powder demonstrating the applicability of large-scale fabrication of functional MOPs for practical applications.
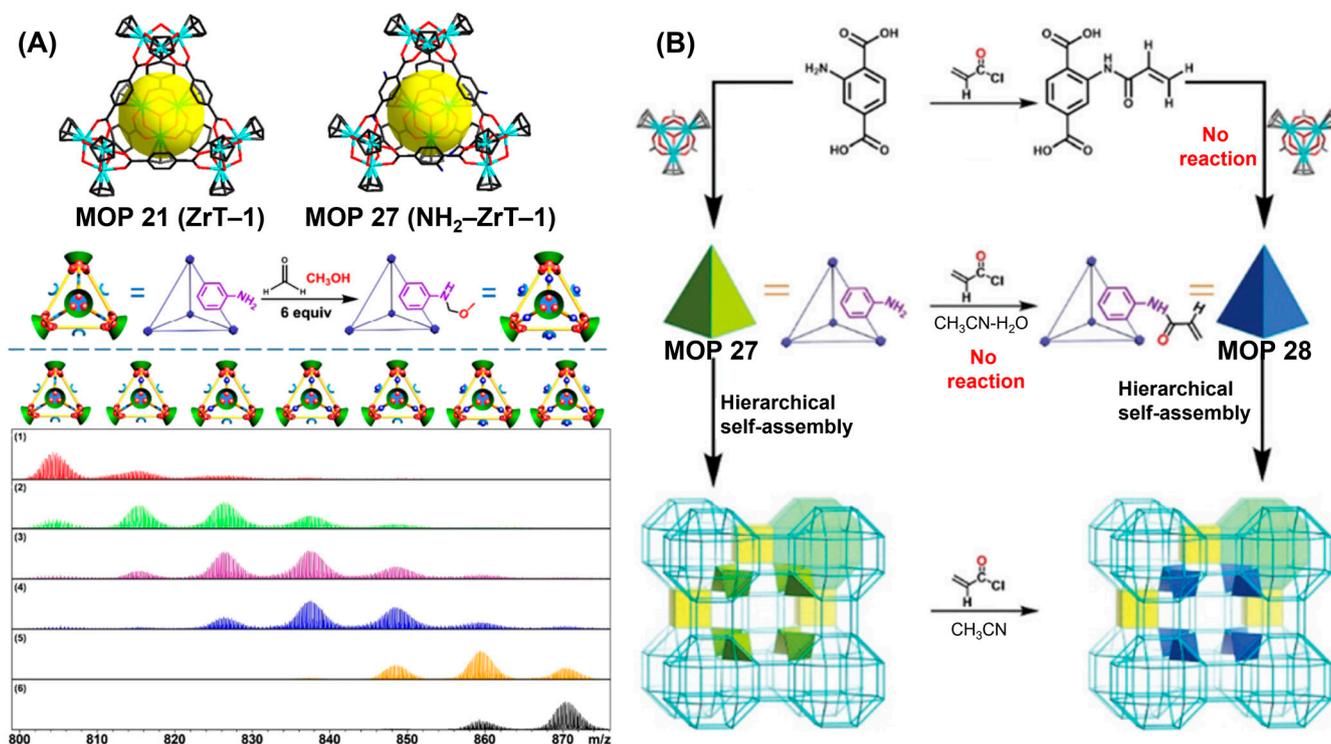
Figure 13. (**A**) Crystal structure of Zr-based MOP 21 and MOP 27. Schematic representation of post-assembly modification of MOP 27 upto six available sites in each cage. ESI-TOF MS spectra of MOP 27 in acetonitrile/water over a wide pH range. (**B**) Transformation of MOP 27 into MOP 28 via heterogeneous PAM in the supramolecular framework. Reprinted by permission from Refs. [136,137]. Copyright from 2018 from American Chemical Society and copyright 2021 from Royal Society of Chemistry.

Various other strategies to enhance the stabilities and porosities of MOPs include mixed functionality strategy to give mixed-composition products, but not necessarily mixed-composition starting materials or reaction solutions may yield mixed-composition products. Accordingly, mixed-metal, mixed-ligand and mixed-metal counter anion strategies have been reported for the synthesis of mixed functionality MOPs [138–140]. Hong and coworkers had first demonstrated the synthesis of high nuclearity heterometallic calixarene-

based carboxylate MOP 29 with chemical composition of $Na_4Ni_{24}Ln_4L_3$ (L = dicarboxylate linkers) constructed from large mixed-metal clusters $Na_2Ni_{12}Ln_2$ (Ln = Dy and Tb) and linear dicarboxylate linkers [141]. Based on gas adsorption studies, good permanent porosity was shown by all heterometallic metal organic polyhedra (HMOP). Doonan and coworkers had reported the synthesis of heterobimetallic metal-organic polyhedra MOP 31 constructed from heterometallic paddlewheel nodes using Pd(II) metal ion along with other transition metal ions like Cu(II), Ni(II), Zn(II) and 5-tert-butyl-1,3-benzenedicarboxylate organic linker [140]. Interestingly, the Pd(II) metal ions are preferentially aligned toward the inner surface of the cuboctahedron MOP and first row metal ions are predominantly positioned on the cage periphery. Activation produces MOPs with coordinatively unsaturated metal sites decorated on the external surface for proposed interaction with gas molecules in the solid state, with H_2-adsorption enthalpies in excess of -12 kJ mol^{-1} for NiPd-bimetallic MOP.

Mixed-ligand strategies worked out beautifully to prepare carboxylate-based MOPs. MOPs prepared from different types of linkers can assume different topologies and feature multiple functionalities as well. Combination of angular ditopic ligands with dissimilar bend angles are particularly intriguing. Following this approach, Zhou and coworkers had demonstrated the synthesis of metal organic polyhedra featuring mixed functionalities [138]. Combination of ditopic carboxylic acid linkers, 9H-carbazole-3,6-dicarboxylate (9H-3,6′-CDC) with 90° bend angle and 4,4′-pyridine-2,6-diyldibenzoate (H_2pddb) with 120° bend angle with dicopper paddlewheel metal cluster generates hendecahedra MOP 32 with odd numbers of faces (eleven) and odd numbers of vertices (nine). In contrast, ditopic linker with 90° bend angle and dicopper paddlewheel form an octahedron MOP 33 and linker with 120° bend angle yields a cuboctahedron MOP 34 (Figure 14B). Preliminary gas adsorption studies revealed type I sorption behaviour indicative of a microporous material with Langmuir surface area of 372 m^2/g which is relatively low compared with calculated accessible surface area. Sample became almost amorphous following activation as revealed by powder X-ray diffraction (PXRD) which is attributed to the blockage of the cavity due to the positional rearrangement of molecular structure. Hong and coworkers had demonstrated the synthesis of mixed-ligand carboxylate MOP 35 with molecular formula $[Co_{24}(BTC4A)_6(\mu_4\text{-Cl})_6(1,4\text{-BDC})_{12}] \bullet 6$Hdma (Hdma = 1,4-dimethylamine cation) via [6 + 12] condensation of cationic tetranuclear-metal building blocks generated in situ from p-*tert*-butylthiacalix[4]arene and 1,4-benzenedicarboxylic acid organic linker [142]. Permanent porosity was determined by the gas adsorption isotherm of activated sample showing pseudo-type I isotherm typical of materials with permanent microporosity. In another report, Zhou and coworkers had reported the bridging-ligand-substitution strategy to successfully prepare mixed-ligand MOPs via the interconversion of MOPs prepared from various angular ditopic carboxylic linkers [89]. Mixed-ligand quasi-spherical structure MOP 36 $[Cu_{24}(5\text{-}^tBu\text{-BDC})_{12}(2,7\text{-NDC})_{12}(S)_{24}]$ and distorted octahedron MOP 37 $[Cu_{12}(5\text{-}^tBu\text{-BDC})_6(3,3′\text{-EDDB})_6(S)_{12}]$ were synthesized by ligand substitution reaction of octahedron MOP (prepared from 5-^{t}Bu-BDC and dicopper paddlewheel) using $H_2(2,7\text{-NDC})$ and $H_2(3,3′\text{-EDDB})$ ligands with bend angles of 120° and 60°, respectively (Figure 14C). Synthesis of mixed-ligand cages were favoured either thermodynamically or kinetically in bridging-ligand-substitution reactions. Solubility of MOPs and substituting ligands in the appropriate solvent mixtures are pre-requisite for bridging-ligand-substitution strategies. Sulfonate and hydroxyl-functionalized dicopper paddlewheel-based MOPs were successfully converted into carbazole-based MOPs using carbazole dicarboxylic acid ligands before finally converting them into 1,4-benzenedicarboxylic acid-based MOP using 1,4-benzenedicarboxylic acid as substituting ligand. Bridging linkers with different properties enable the synthesis of new metal organic polyhedra with distinct topologies (like size, shape) and functionalities.
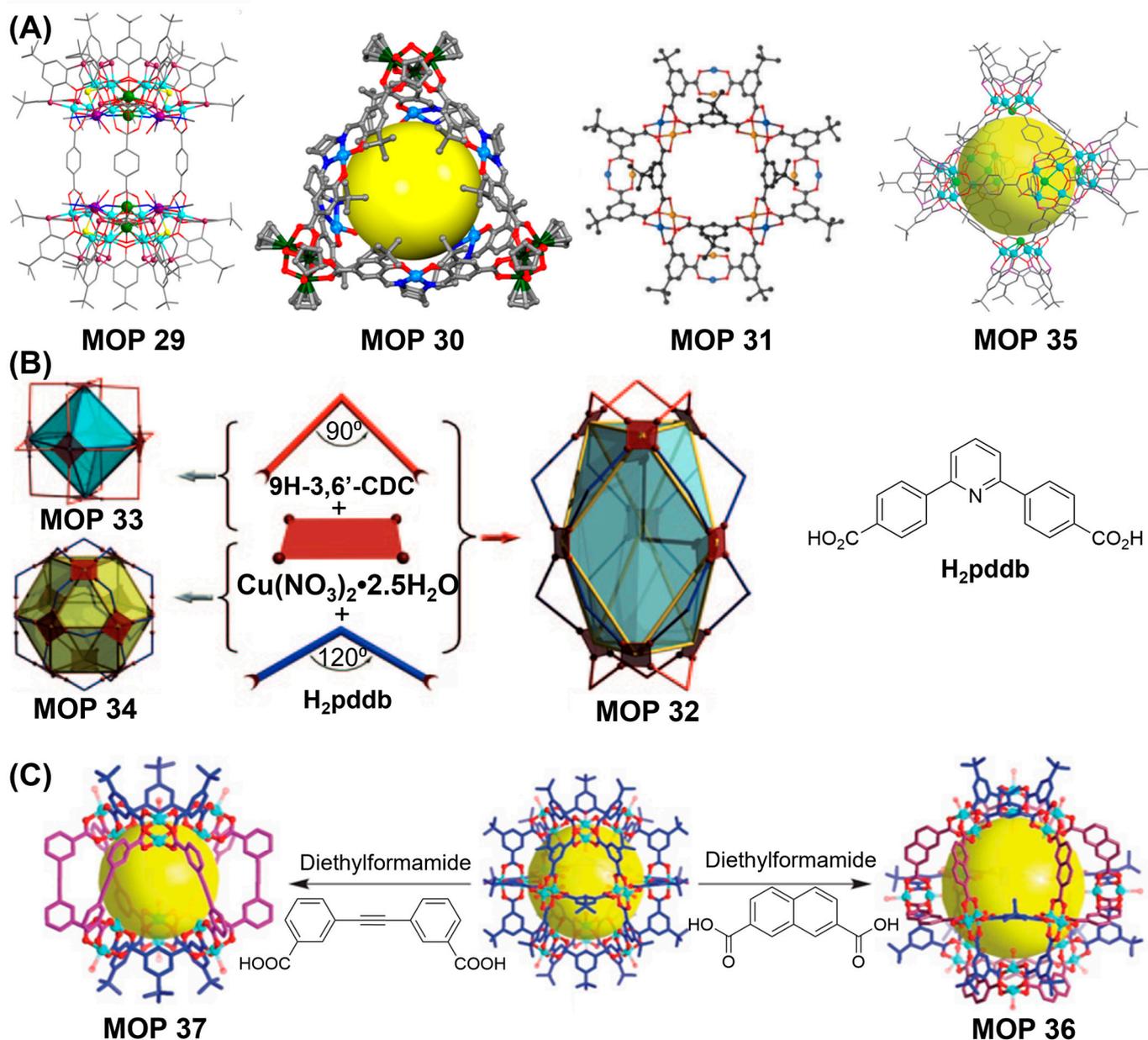
Figure 14. (**A**) Crystal structures of metal organic polyhedra—MOP 29, MOP 30, MOP 31, MOP 35 prepared using mixed-metal and mixed-ligand strategies. (**B**) The self-assembly of three metal-organic polyhedra MOP 32, MOP 33 and MOP 34 with ditopic angular linkers and four-connected square nodes are reported. (**C**) Mixed ligand MOP 36 and MOP 37 were prepared via ligand-exchange strategy. Reprinted by permission from Refs. [89,138,140–143]. Copyright 2009 from Wiley-VCH. Copyright 2012 and 2016 from Royal Society of Chemistry. Copyright 2015 and 2018 from American Chemical Society. Copyright 2010 from Nature Publishing Group.

Calix[4]arenes are versatile macrocyclic synthetic container compounds which have been highlighted for use as building blocks for the preparation of cage compounds with various metal ions in combination with other carboxylic acid linkers [144]. Self-assembled calixarene-based tetranuclear cluster complexes are prepared from quadruply deprotonated *p*-tert-butylsulfonylcalix[4]arene, transition metal ions like Mn(II), Co(II), Ni(II) etc. and acetate anions where four sulfonyl oxygen atoms and four phenoxo atoms are coordinated to four metal ions that are further attached to four acetate groups and one μ_4-hydroxo oxygen atom (Figure 15A). Subsequently, calixarene-based

tetranuclear metal cluster and tricarboxylate ligand gave Co(II) and Ni(II) polyhedra with molecular formula as $[M_4(\mu_4\text{-}H_2O)(BTC4A)]_6(1,3,5\text{-}BTC)_8$; M = Co(II) and Ni(II). Interestingly, Ni(II)-based MOP 38 was found to be remarkably robust and chemically stable upto 400 °C as revealed by thermogravimetric analysis (TGA) and has permanent porosity as shown by gas adsorption studies [145]. Zhang and coworkers had reported the synthesis of Co(II)-based four octahedron MOPs by allowing ternary acids 1,3,5-benzenetricarboxylic acid (H_3BTC) or $4,4',4''$-benzene-1,3,5-triyl-tribenzoic acid (H_3BTB) to react with *p*-tert-butylthiacalix[4]arene (H_4TC4A) or p-phenylthiacalix[4]arene (H_4PTC4A) in [6+8] solvothermal condensation reactions [146]. Six cobalt-calix[4]arene clusters with octahedron arrangement are bridged together by eight BTC or BTB linker [147] giving rise to MOP 39-42 $\{[Co_4(TC4A)Cl]_6(BTB)_8\}^{6-}$, $\{[Co_4(TC4A)Cl]_6(BTC)_8\}^{6-}$, $\{[Co_4(PTC4A)Cl]_6(BTB)_8\}^{6-}$, and $\{[Co_4(PTC4A)Cl]_6(BTC)_8\}^{6-}$ (Figure 15B) with periphery diameters of up to 4.7 nm, internal voids of up to 1.7 nm and with exceptionally high thermal stabilities. Wang and coworkers had demonstrated the synthesis of type II calix[4]arene-based metal organic polyhedra assembled from divalent metal ions Ni(II) or Co(II), sulfonylcalix[4]arenes and linear 1,4-benzenedicarboxylic acid linker [148]. The octahedron geometry arranges six calix[4]-arene-based metal clusters at each vertices bridged together by twelve 1,4-benzenedicarboxylic acid linkers spanning across the edges of the octahedron. While guest-binding behaviour is determined by individual cages, the solid-state binding phenomena is dependent on the spatial organization of MOP. At solid-liquid interface, Co(II) MOP adsorbs 5 equiv. of methylene blue (MB) from the aqueous solution at much faster rate compared with Ni(II) MOP demonstrating their hydrolytic stabilities. At solid-gas interface, Ni(II) MOP shows better performance towards gas adsorption studies compared with Co(II) MOP, however the gas adsorption capacities of both MOPs are significantly lower which can be attributed to the partial collapse of the solid state packing of the MOPs after solvent evacuation.

Bloch and coworkers had demonstrated a novel strategy to prepare porous ionic cages with mixed functionalities and tunable properties where both counterions (cation and anion) are intrinsically porous in nature [139]. Prerequisite conditions suitable for the preparation of doubly porous cages include having the requisite charges, permanent porosities, high stabilities and solubilities in various solvents or solvent mixtures in order to be compatible with solvent metathesis. Prototypical cuboctahedron sulfonate-functionalized copper paddlewheel-based MOP $[Cu_{24}(SO_3\text{-}bdc)_{24}]^{24-}$ was selected as anionic MOP and highly stable zirconium-based MOP $[Zr(\mu_3\text{-}O)_4(\mu_2\text{-}OH)_{12}(Cp)_{12}(Me_2\text{-}bdc)_6]Cl_4$ was targeted as cationic MOP particularly for their permanent porosities and their abilities to withstand post-synthetic modifications. Combination of methanolic solution of copper-based MOP and zirconium MOP yielded nearly instantaneous precipitation of light-blue insoluble porous salt (Figure 15C) with proposed molecular formula of $[Zr_{12}(\mu_3\text{-}O)_4(\mu_2\text{-}OH)_{12}(Cp)_{12}(Me_2\text{-}bdc)_6]_6[Cu_{24}(SO_3\text{-}bdc)_{24}]$. Comparatively, porous salt has CO_2 and N_2 accessible BET surface area of 252 m^2/g and 496 m^2/g, respectively much higher than those of constituent MOPs. The resulting doubly porous salt displays the spectroscopic signature of the parent cages representing a new and powerful method for the synthesis of porous solid with tailored functionality.
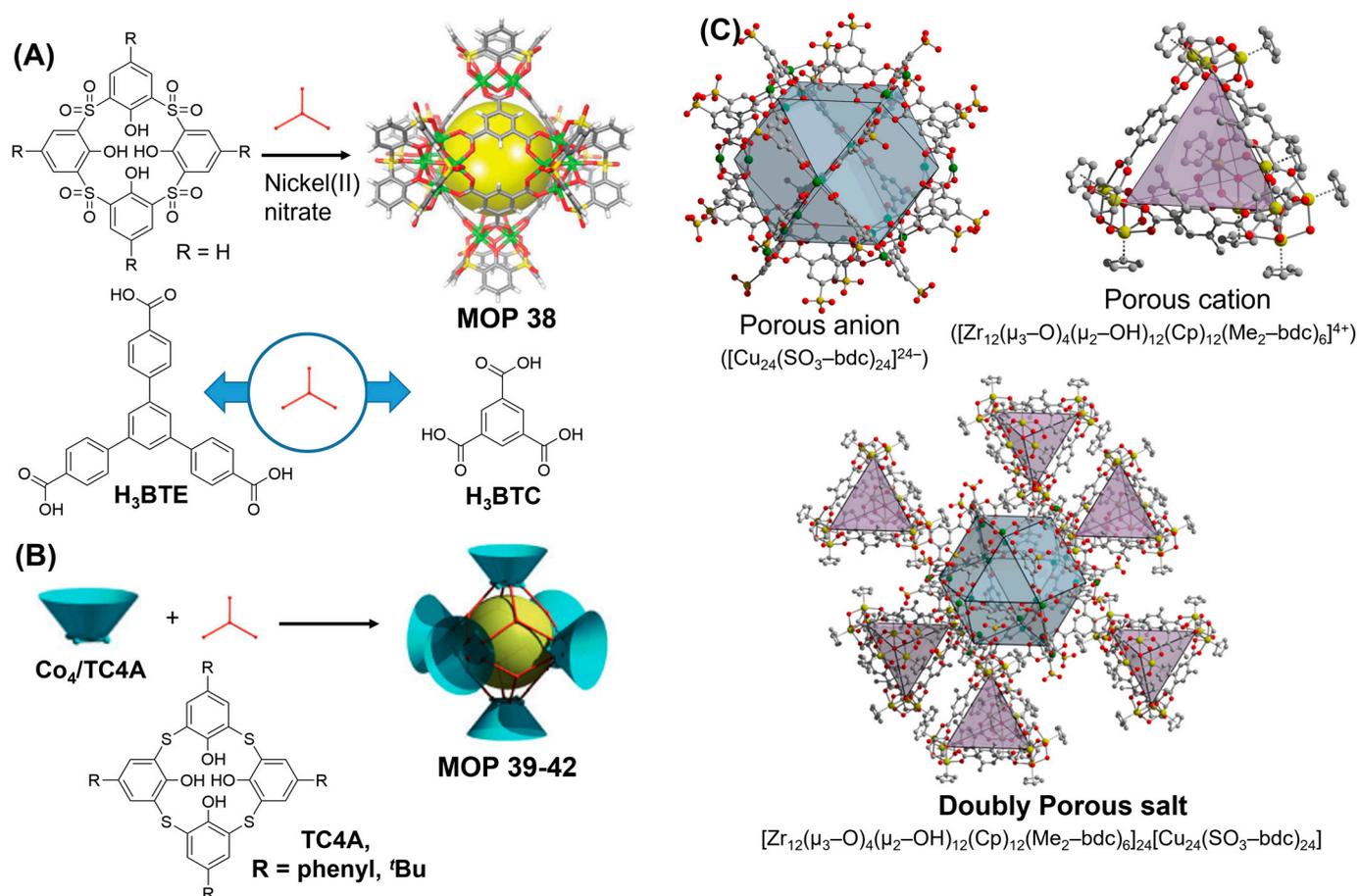
Figure 15. (**A**) Design principle for the assembly of virus-like metal-organic supercontainers via binding of tetranuclear *p*-tert-butylsulfonylcalix-[4]arene complex with H_3BTE and H_3BTC. (**B**) The nanocoordination octahedra formed by Co_4/TC4A shuttlecock-like SBUs and tritopic linkers, where TC4A may be p-tert-butylthiacalix[4]arene/p-phenylthiacalix[4]arene. Copyright 2009 Wiley-VCH Verlag GmbH & Co. KGaA, Weinheim for $([Co_4(TC4A)Cl]_6(BTC/BTB)_8)^{6-}$. (**C**) Charged MOPs used for the preparation of a doubly porous salt where the charge-balancing cations for the cuboctahedron MOP $[Cu_{24}(SO_3\text{-bdc})_{24}]^{24-}$ and anions for the tetrahedron MOP $[Zr_{12}(\mu_3\text{-O})_4(\mu_2\text{-OH})_{12}(Cp)_{12}(Me_2\text{-bdc})_6]^{4+}$. A portion of the crystal structure of the doubly porous salt $[Zr_{12}(\mu_3\text{-O})_4(\mu_2\text{-OH})_{12}(Cp)_{12}(Me_2\text{-bdc})_6]_2[Cu_{24}(SO_3\text{-bdc})_{24}]$. Reprinted by permission from Refs. [139,145–147]. Copyright 2012 and 2020 from American Chemical Society. Copyright 2012 from Royal Society of Chemistry. Copyright 2012 from Wiley-VCH.

In addition to the chemical and hydrolytic stabilities, maintaining porosities of MOPs in the solid state is crucial for their usages towards various potential applications. Carboxylate-based MOPs are particularly attractive for maintaining their micro- and meso-porosities in their crystalline states. Nevertheless, lack of intercage stabilization interaction increases the chances of random rearrangements of MOPs in the solid state and thus they tend to aggregate upon activation. Aggregation causes the blockage of active sites and pore apertures of individual MOPs by the adjacent cages which results in compromising their guest uptake performances severely. Various strategies to circumvent the undesired aggregation of MOPs include the dispersion of MOPs in a porous matrix and the preparation of metal organic frameworks (MOFs) using MOPs as building units to retain their uniformities and porosities. Porous materials with large cavities can successfully accommodate MOPs and their small apertures can prevent leaching or aggregation. Zhou and coworkers had reported that MOPs performance can significantly be enhanced following their dispersion inside mesoporous silica nanopores of SBS–15 [77]. Three dicopper paddlewheel-based

carboxylate MOPs with general formula of $[Cu_{24}(L_x)_{24}S_{24}]$ (S = solvent molecules) were prepared with varied substituents (^{t}butyl, hydroxy and sulfonate) at the 5-position of the 1,3-benzenedicarboxylic acid linker (Figure 16A). Compared with other two MOPs, sulfonated-functionalized MOPs are well dispersed inside the porous matrix of SBA-15. Sulfonated-MOP loaded SBA-15 samples (M3S-0.2, M3S-0.4 and M3S-0.6) were prepared with varying mass fraction (0.2, 0.4 and 0.6) of MOPs in the samples. N_2 absorption-desorption isotherms showed the hysteresis loop, characteristics feature of SBA-15 porous matrix, which closes at relative pressure of 0.7. For MOP-loaded silica, the hysteresis loop can remain open upto relative pressure of 0.5 and the hysteresis performance significantly enhances with increasing MOPs content in mesoporous silica. TGA analysis revealed that thermal stability of MOPs can be significantly enhanced due to their confinement within silica nanopores compared with pristine MOPs. H_2 uptake ability of MOP-loaded silica was significantly enhanced compared with bulk MOPs. Lower MOPs content-loaded silica renders MOPs more well-dispersed within mesoporous silica compared with higher MOPs content-loaded silica. Superior H_2-sorption behaviour was observed for lower MOPs content-loaded silica nanopore due to lack of MOP aggregation within silica nanopores enabling the MOPs maintaining their porosities and open apertures for guest uptake. In an interesting report, Li and coworkers had demonstrated the synthesis of sulfonated-functionalized dicopper paddlewheel-based carboxylate MOP within the mesoporous silica SBA-16 by utilizing double-solvent strategy [149]. Mesoporous silica with inner cavity size of ~6 nm and pore entrance of ~2 nm was employed to host MOP molecules with average diameter of 3 nm (Figure 16B). Interfacial tension drives the precursors containing hydrophilic solution into the hydrophilic cavity of silica nanopore avoiding unnecessary aggregation of MOPs onto the outer surface of pores. Addition of methanolic solution containing precursors and inducer 2,6-lutidine to hexane solution of silica allows methanolic solution to enter the pore via capillary action to prepare isolated MOP molecules within SBA-16 pore. MOP encapsulated SBA-16 showed better sorption behaviour for CO_2 and C_3H_6 compared to bulk MOPs confirming the presence of accessible MOP cavity sites in the mesoporous matrix due to higher dispersities. Not only higher catalytic efficiency was shown by MOPs confined within silica nanopores towards ring-opening reaction of styrene oxide compared with bulk MOPs, also better reusability upto four cycles were demonstrated for the catalytic reaction. Silica-confined MOPs have maintained their structural integrities even after exposing to the humid atmosphere for 7 days, bare are MOPs degraded severely within 24 h demonstrating the ability of silica surfaces to stabilize MOPs. Rao and coworkers had demonstrated a novel strategy to stabilize dicopper paddlewheel-based carboxylate MOPs on the graphene and single-walled carbon nanotube surfaces [150]. Discrete MOPs are covalently attached to the surfaces by reacting carboxylic acid-functionalized graphene/SWNT with the hydroxy groups decorated on the MOP surfaces through ester bonds (Figure 16C). Noncovalent interactions between the Cu units of MOPs and carboxylates on graphene/SWNT, and additional π-π interactions contributed to MOP stabilization. Interestingly, higher catalytic efficiencies were shown by composites MOPGr-2 and MOPNT-2 toward conversion of propylene oxide to propylene carbonate compared to bulk MOPs demonstrating the better preservation of MOPs upon depositing them on graphene/SWNT surfaces. Kitagawa, Choe and coworkers had reported the synthesis of sulfonate-functionalized dicopper paddlewheel-based carboxylate MOP inside a porous metal organic framework host (PCN-77) [151]. Higher proton conductivity and water-vapour capture performance were shown by encapsulated MOPs. Authors claimed that amounts of MOPs inside metal organic frameworks control the volumes of meso- and micropores of the composite materials, opening up the possibilities of hybrid materials for other potential applications like solid-state electrolysis and heterogeneous catalysis.
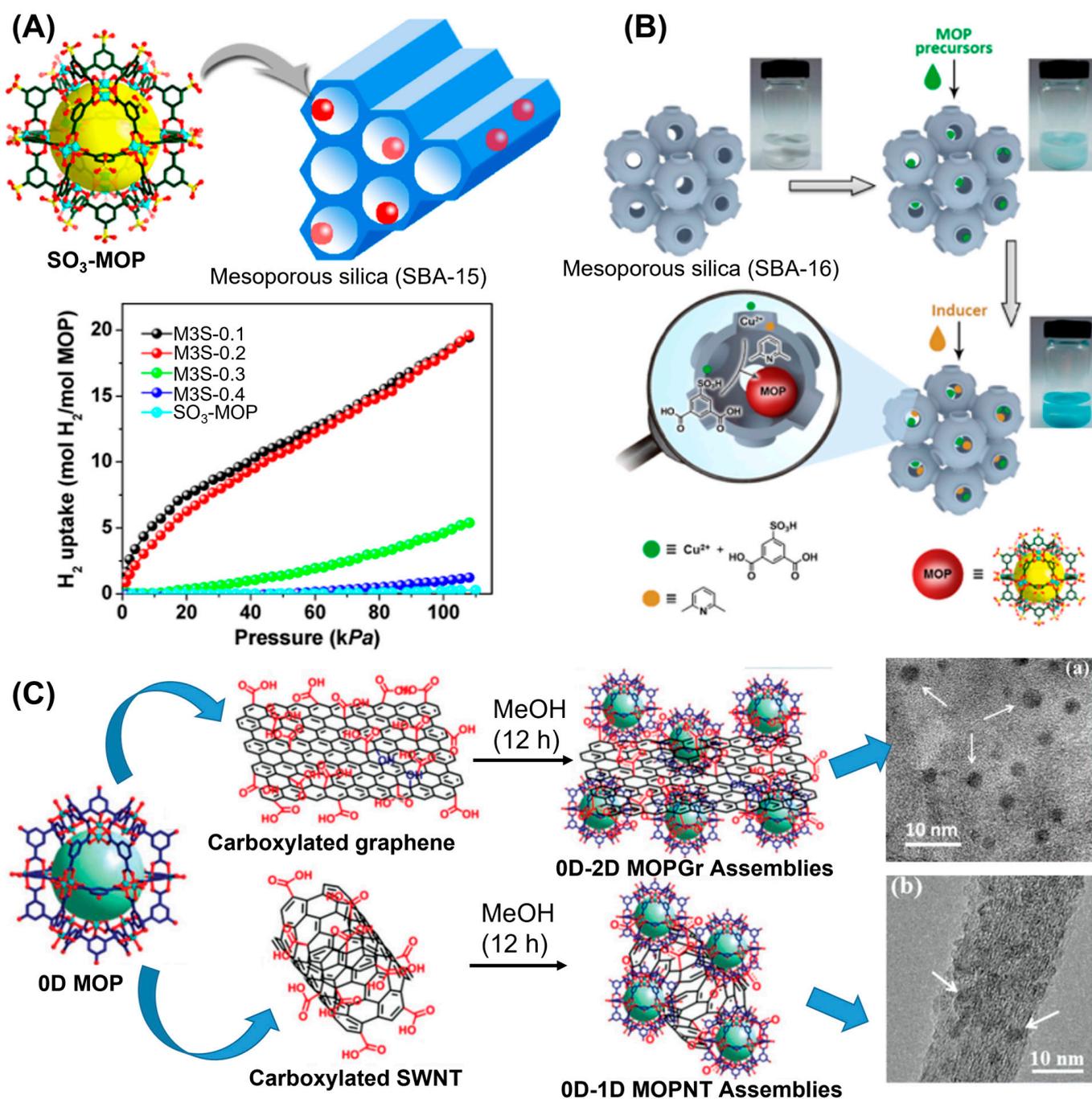
Figure 16. (**A**) Illustration of dispersion of sulfonated MOP in silica nanopores. H_2 adsorption capacities of M3S and SO_3-MOP samples at 77 K are shown. The adsorption capacities of M3S samples (mol of H_2/mol of MOP) were calculated by subtracting the uptake of the SBA-15 support from the measured uptake. (**B**) Schematic representation of the synthesis of MOP-SO_3H in mesoporous silica cavities (SBA-16) by using a double-solvent strategy. Dispersion of SBA-16 in hydrophobic n-hexane. Addition of a hydrophilic solution of MOP precursors in methanol (metal ions and ligands) followed by addition of the inducer (base) for MOPs formation. (**C**) Schematic representation of the synthesis of MOPGr and MOPNT assemblies. Reprinted by permission from Refs. [77,149,150]. Copyright 2012 and 2016 from American Chemical Society. Copyright 2017 from Royal Society of Chemistry.

Discrete metal-carboxylate polyhedra are used as building blocks to design porous coordination frameworks, which can also be employed to stabilize metal organic polyhedra that are otherwise unstable hydrolytically or chemically, and often undergo spontaneous

aggregation in the solid state after guest removal. Higher thermodynamic stabilities of molecular architectures can therefore be envisaged compared with naked metal ions owing to the prevention of potential attack by solvent molecules or other competing ligands to the metal ions by virtue of strong metal-coordination bond. MOPs interconnected by strong coordination bonds using interconnecting ligands render hydrolytically and chemically stabile MOPs, and subsequently prevented MOP reorganization/aggregation upon guest removal. Therefore, MOPs serving as monomers would definitely facilitate to optimize the shapes, sizes and porosities of the 3D networks by introducing strategic tactics to add new linkers to the MOP solutions. Major challenge to prepare MOP-based extended three-dimensional network is the selection of appropriate MOPs with enhanced solubilities, better stabilities and their abilities to grow into three dimensional networks [152]. Traditional approach is the linking of MOPs by using ditopic and tritopic linkers by replacing axially positioned multiple replaceable solvent molecules attached onto the outer surface of PW metal ions of each MOP. Zhou and coworkers had demonstrated the interconversion between twofold interpenetrated 3D framework (MOF) and molecular octahedron MOP 33 prepared from dicopper-paddlewheel cluster and 9H-carbazole-3,6-dicarboxylate (CDC) with amide (N-H) functional groups (Figure 17A). Amide groups tethered onto each linker form H-bonds with appropriate solvent molecules and therefore improve the solubility of molecular cage [92]. Jahn-Teller distorted axially positioned labile coordinated solvent molecules of octahedron MOP undergo ligand exchange reaction with pyridine or 4,4′-bipyridine molecules leading to the conversion into an extended interpenetrated network ($[Cu_4(9H-3,6-CDC)_4(4,4′-bpy)(H_2O)_2]_3)_n$ with six vertices of each octahedron interlinked with bipyridine ligands and about 76% of solvent accessible area. MOF can be transformed reversibly back into molecular octahedron MOP by dissolving in DEF/py (4:1 *v/v*; py = pyridine) solvent mixture. Furthermore, excess of pyridine rearranges molecular octahedron to a helical 1D chain which is otherwise difficult to achieve. Su and coworkers had demonstrated the synthesis of porous coordination framework prepared from cubohemioctahedron cage $[Cu_2(5-NH_2-mBDC)_2]_{12}•(H_2O)_{24}$ as precursor which was derived from dicopper paddlewheel SBUs and 5-NH$_2$-*m*BDC ligands [153]. Solvothermal reaction between cubohemioctahedron cage and 4,4′-bipyridine in N,N′-dimethylacetamide/ethanol (5:1) solvent mixtures afforded 3D framework of molecular formula $\{\{Cu_{24}(5-NH_2-mBDC)_{24}(bpy)_6(H_2O)_{12}•72DMA\}$ containing both micropore and mesopore cavities (Figure 17B). Intrinsic and extrinsic porosities of MOFs allow the encapsulation (23.76 wt% loading) and release of guest like 5-fluorouracil drug. Approximately 80% of the loaded drug was released within few hours followed by a plateau which is presumably due to the initial MOF-structure degradation as confirmed by PXRD pattern. Majority of drugs are loaded inside the mesoporous cavity of MOFs and the rest are encapsulated within the intrinsic pores of MOPs. Su and coworkers had reported the stepwise synthetic strategy for the construction of three 12-connected MOFs with fcu topologies which are the rare examples of MOFs derived from cubohemioctahedron MOP precursor $[Cu_{24}(5-hip)_{24}]$ (5-hip = 5-hydroxyisophthalic acid) [154]. Three different organic linkers pyrazine, 4,4′-bipyridine and 1,2-di(pyridine-4-yl)ethene afforded three different MOFs with molecular formulas $\{[Cu_{24}(5-hip)_{24}(pz)_6(H_2O)_{12}•64DMF\}$, $\{[Cu_{24}(5-hip)_{24}(bpy)_6(H_2O)_{12}•119DMF\}$, and $\{[Cu_{24}(5-hip)_{24}(bpe)_6(H_2O)_{12}•138DMF\}$). Metal organic framework $\{[Cu_{24}(5-hip)_{24}(bpe)_6(H_2O)_{12}•138DMF\}$) was successfully utilized to adsorb and separate methylene blue and methyl orange dyes from mixture of solution containing rhodamine B. Interestingly, MOFs constructed from MOP building units exhibited better performance towards adsorption of dyes compared with pristine MOP precursors. Klosterman and coworkers had reported the synthesis of 1D coordination polymers at room temperature from copper-based M_4L_4 lantern-type MOP which contains inward-directed free amine functional groups and 4,4′-bpy bridging linker. Unsurprisingly the same coordination polymer was not yielded when the M_4L_4-type MOP precursors are mixed together with 4,4′-bpy bridging ligand in solution [155].
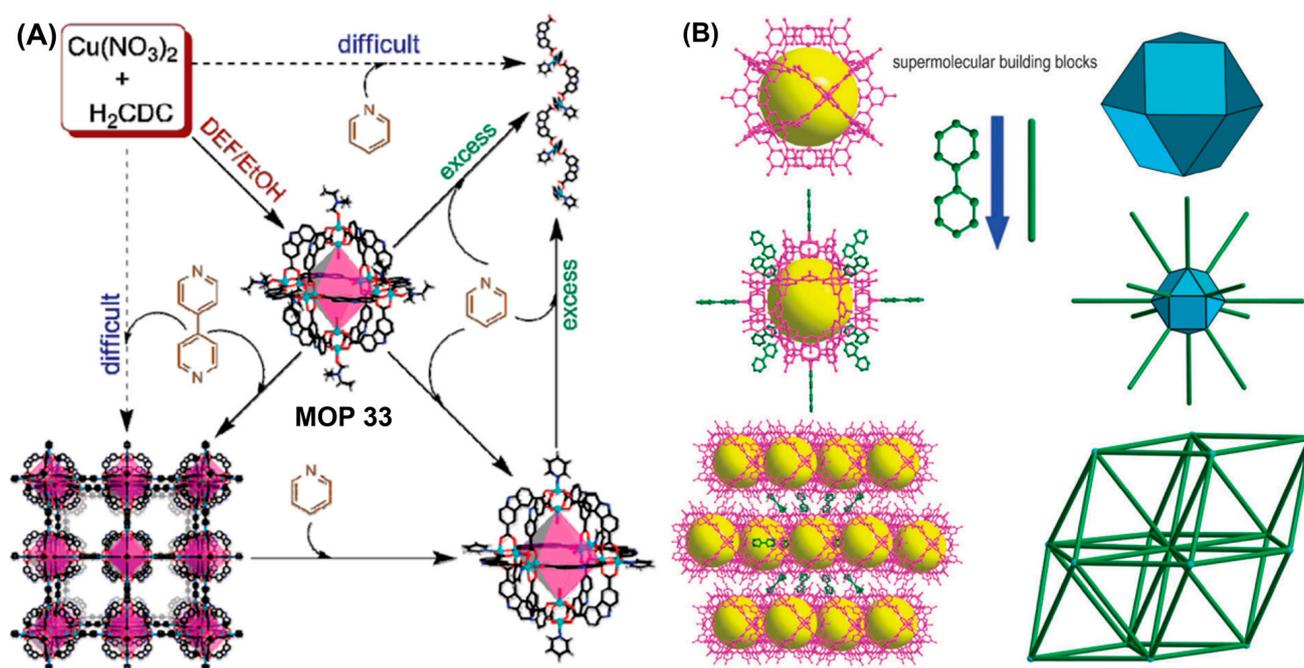
Figure 17. (**A**) Reaction scheme for the modification MOP 33 into pyridine-coordinated MOP, bypyridine-directed MOF, and a continuous 1D chain. (**B**) Extended structures based on NH_2-MOP as a precursor. Schematic diagram showing the appropriate strategy for obtaining MOFs from MOPs. Reprinted by permission from Refs. [92,153]. Copyright 2009 from American Chemical Society and copyright 2011 from Royal Society of Chemistry.

Rigid inter-connected spacers are found to be ideal for maintaining the porosity of metal organic frameworks. Chun, Moon and coworkers had demonstrated the preparation of coordination polymers using flexible linkers as well (Figure 18A). 2,7-naphthalenedicarboxylate (2,7-ndc) and Cu^{2+} afforded cuboctahedron MOP $[Cu_{24}(2,7-ndc)_{24}(DMF)_{10}(H_2O)_{14}]$ with 12 dicopper paddlewheel units [90]. Complete amorphization of octahedron MOP occurs after solvent-exchange and evacuation due to full collapsing of molecular packing. Non-framework coordination polymers were prepared by replacing axially coordinated labile solvent molecules on the outer metal ion of paddlewheel complexes with cross-linkers like ethylenediamine, rigid aromatic linker xylenediamine or long flexible linker diaminoheptane. Compared with pristine MOP, distinct surface features for all three coordination polymers were observed from N_2 adsorption isotherms. Unusual isothermal behaviours were observed for all three coordination polymers. When relatively long linkers connect individual MOP molecules, mesopore volume significantly increases to show large hysteresis loop and much broader pore size distribution which can then be optimized systematically by choosing appropriate MOPs and cross linkers.

Common strategy to prepare MOFs from MOP building units is to attach the cross-linkers to the metal centers of paddlewheel metal clusters of each MOP molecules by replacing the axially-coordinated labile solvent molecules. Use of extended organic linkers can be used further to diversify the synthesis of metal organic frameworks derived from MOP precursors. Eddaoudi and coworkers had reported the synthetic strategy to prepare porous metal organic frameworks by using superbuilding blocks (SBB) [156]. Metal organic truncated cuboctahedron supermolecular building block generated the rhombicuboctahedron tertiary building block in situ was used to prepare a (24-connected)-based MOF. 12 dicopper paddlewheels are joined by 24 molecules of 1,3-BDC linkers with the 5-position of the bend bridging ligand lying exactly on the vertices of the rhombicubooctahedron. Functionalization at the 5-position permits the formation of a rigid triangular molecular building blocks, a 3-connected vertex figure leading to the assembly of a MOF. Solvothermal reaction of 5-

tetrazolylisophthalic acid and $Cu(NO_3)_2 \bullet 2.5\ H_2O$ in dimethylformamide/ethanol afforded (3,24)-connected MOF with molecular formula of $[Cu_6O(TZI)_3(H_2O)_9(NO_3)]_n(H_2O)_{15}$ consisted of truncated cuboctahedron connected to trigonal $Cu_3O(N4CR)_3$ trimers through each tetrazolate (N_4CR) moiety. Higher porosity and larger surface area of the MOF can be achieved by expanding the bifunctional organic linker. Large surface area of 2847 m^2/g for the MOF was estimated using BET method with the largest MOP approaches mesoporous ranges, the smallest MOPs are first to be occupied and the largest are subsequently occupied by guest molecules at high pressure. Zhou and coworkers had demonstrated the synthesis of two dicopper(II) paddlewheel-based porous metal-organic frameworks (PCN-81 and PCN-82) that are sustained with 12-connected nanoscopic octahedra [106]. Solvothermal reaction of tetratopic ligands H_4pbcd and H_4dpbcd with $Cu(NO_3)_2 \bullet 2.5H_2O$ in DMA and DMSO solvent mixture in the presence of HBF_4 acid afforded MOFs: PCN-81 and PCN-82, respectively with general molecular formula of $[Cu_2(ligand)] \bullet 2X$ (X is coordinating solvent). The octahedron building block serves as a 12-connected node to prepare 12-connected network leaving three different types of microporous cages with varied cavity sizes (Figure 18B). Each octahedron MOPs in PCN-82 with internal diameter of 11 Å are constructed from one end of each twelve 90°-angular carbazole-3,6-dicarboxylate moieties and six metal SBUs. MOPs with medium pore diameter (~12.9 Å) are formed by six organic ligands and 12 dicopper paddlewheel as SBUs. Large MOPs with diameter of 18.1 Å are formed by carbazole moiety on the opposite end of each ligand. Surface area measurement revealed that PCN-82 has higher surface area compared with PCN-81 especially for hydrogen, methane and carbon dioxide due to the availabilities of open metal sites and their microporous nature. Freeze-dried PCN-82 maintains the porosity and high crystallinity during PXRD and multi-cycle gas-adsorption measurements.

Solvent-induced noncovalent interactions was successfully utilized as a tool to control the interconversion between discrete and porous chain of MOPs [157]. A "shish-kabob" of MOPs was synthesized by interlinking bulky hydrophobic groups-decorated-MOP either a one-fell-swoop or a step-by-step procedure by varying the dielectric constant of the assembly mixture. Prototypical MOP constructed from 1,3-benzene dicarboxylic acid and dicopper paddlewheel cluster are chosen for the study. A surfactant-like amphiphilic ligand, 5-((triisopropylsilyl)ethnyl) isophthalate ligand along with Cu(II) metal ions in hydrophobic solvent mixture (benzene: methanol = 19:1) afforded a micelle-like cuboctahedron MOP featuring 24 triisopropylsilyl (TIPS) groups attached onto the exterior of MOP (Figure 18C). Interestingly, the same starting materials in a hydrophilic solvent mixtures (DMF: water = 1:2) afforded the same cuboctahedron MOPs with mutual interdigitation of the TIPS group from adjacent MOPs to give a "shish kabob" of cuboctahedron. Distances between two closest Cu(II) metal atoms from two adjacent cages linked through two carboxylate group in a bidentate-bridging mode with Cu-O bond are 2.272 and 2.426 Å. Hydrophobic effect causes the aggregation which leads to the formation of Cu-O bonds between a pair of adjacent MOPs. Such behaviour enables structural interconversion between discrete MOP and a chain of MOPs by switching the dielectric constants of the solvent mixtures. Suspending the 1D chain of MOPs in CH_2Cl_2 led to the dissociation into discrete MOPs presumably due to solvation effect. Furthermore, the discrete MOPs can be successfully transformed into 1D chain MOP by immersing them in DMF-water solvent mixture, confirming the effect of hydrophobicity in order to drive the formation of the ''shish-kabob'' of MOPs. Unsurprisingly, interdigitation and the formation of Cu-O bonds between neighboring MOPs prevent the aggregation in the solid state after activation and lead to maintain the structural integrity of the ''shish-kabob'' of nanocages rendering them more porous compared with discrete MOPs. This dimension augmentation strategy turns out to be a suitable tool for improving and tuning the stabilities and porosities of MOP-based materials (Figure 18D).
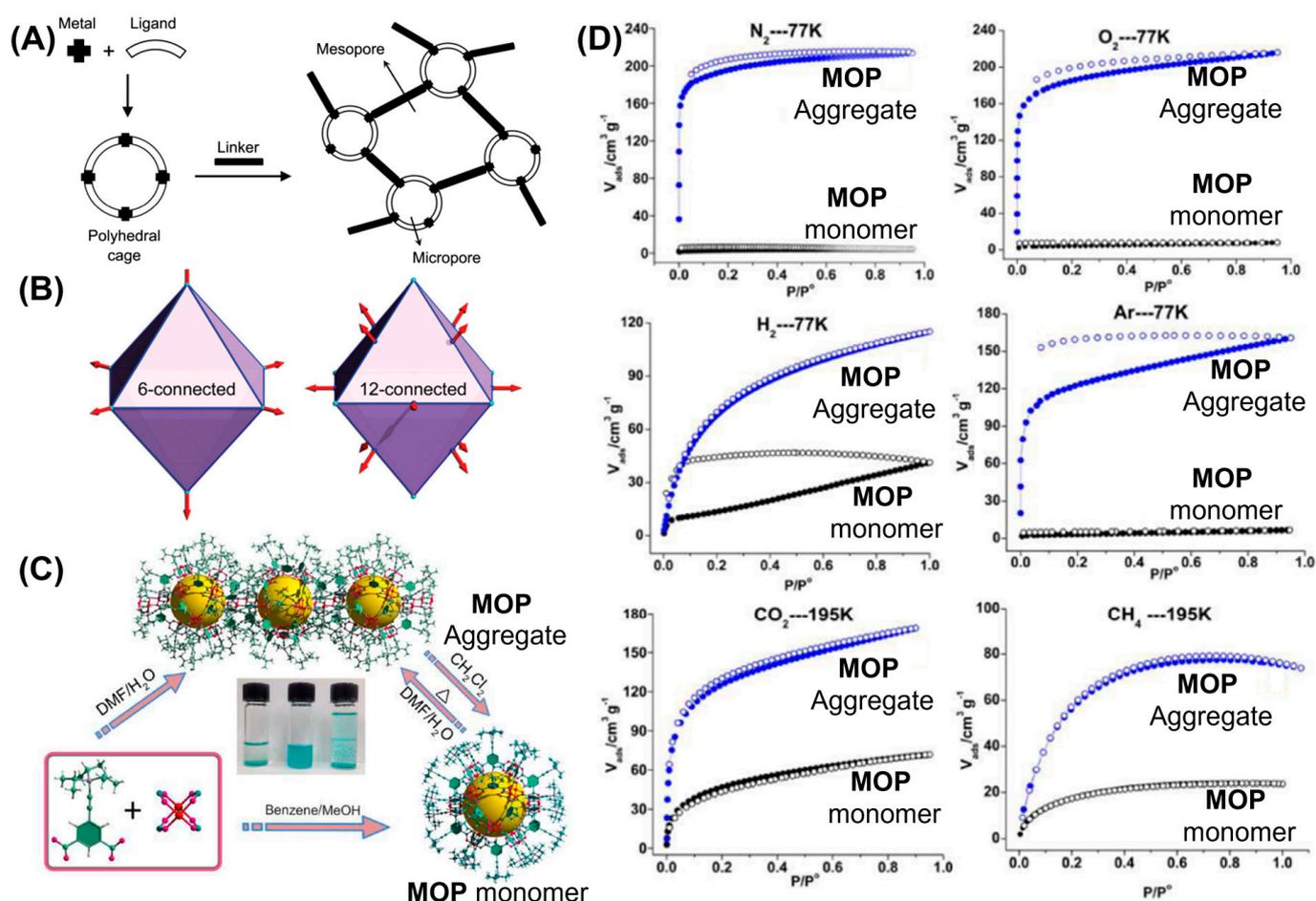
Figure 18. (**A**) Stepwise synthesis of non-framework coordination polymers (CPs) with bimodal porosity, where MOP is used with various diamines (ethylenediamine, xylenediamine, or diaminoheptane) as linkers to obtain a series of non-framework CPs. (**B**) Structural representations of 6-connected and 12-connected octahedron SBBs. (**C**) Interconversion between cuboctahedron MOP and the 1D chain of MOP. (Bottom left) a 5-((triisopropylsilyl)ethynyl)isophthalic acid (TEI) ligand and a dicopper paddlewheel. (Center) MOP monomer synthesized in the mother liquid (left), dissolving chain of 7 in CH_2Cl_2 (middle) leads to the formation of MOP and recrystallization in CH_2Cl_2/DMF (right) yields crystals of MOP. (**D**) The sorption isotherms of N_2, O_2, H_2, Ar at 77 K, CO_2 and CH_4 at 195 K for MOP monomer and MOP aggregate (equilibrium time is 5 s for both MOP monomer and MOP aggregate). Reprinted by permission from Refs. [90,106,157]. Copyright 2011 from Korean Chemical Society. Copyright 2013 from Royal Society of Chemistry. Copyright 2012 from American Chemical Society.

4. MOPs Containing N-Donor Ligands

Second popular class of metal organic polyhedra are made of N-donor ligands. Compared with MOPs derived from O-donor ligands, MOPs synthesized from N-donor ligands and soft metal ions tend to be hydrolytically more stable. Extensive works were done to prepare large body of metal coordination driven supramolecular polygons and polyhedra (MOPs) using N-donor ligands [4,5,8,25,28]. Nevertheless, majority of MOPs have been prepared and studied in organic solvents as the designing of water-soluble and water-stable MOPs has been challenging. It is because not only that water acts as competing solvent but also most of the organic ligands employed in the self-assembly process are poorly water soluble. Additionally the hydrophobic effects engendered by water altered the reaction pathway leading to stacking of organic ligands. Early examples of the synthesis of supramolecular structures using metal-ligand interactions involving N-donor ligands are

reported by Lehn et al. Formation of double-helical metal complexes-the helicates results from the self-organization of oligobipyridine strands around tetrahedrally coordinated Cu$^+$ or Ag$^+$ metal ions [158–161]. Spontaneous self-assembly of hexaazatriphenylene and quaterpyridine with [Cu(MeCN)$_4$]BF$_4$ gave cylindrical inorganic complex with internal cavity [162]. Following this discovery, synthesis of MOP-field experienced a rapid upsurge and the progresses have been documented from various research groups notably Fujita, Stang, Nitschke, Mukherjee, Severin, Schmittel, Shionoya, Ward and many others. Earliest example of N-donor coordinated MOP is reported by Fujita and coworkers followed by the extensive works of Fujita and Stang groups using Pd(II) and Pt(II) metal ions [4,60,61]. Schmittel group have done extensive works on the synthesis of MOPs using transition metal ions like Cu(I), Ag(I) and Zn(II) in order to prepare wide range of N-donor coordinated 2D and 3D metal coordination structures mostly in organic solvents [8]. Heteroleptic approaches were successfully demonstrated and utilized to prepare Cu and Zn-based MOPs by bringing multiple components together. Shiyonoya and coworkers had reported the synthesis of Cu, Ag and Zn-based MOPs [8]. Coronado et al. had reported the preparation of metallo-supramolecular hexagon from the mixture of Cu(II) metal ion and a rigid heteroditopic ligand containing phenanthroline and terpyridine binding units [163]. Zelewsky and co-workers had reported the synthesis of silver metal ion-based interwoven molecular hexagon by employing a pinene-2,2′-bipyridine ligand [164]. Silver based cationic molecular metallacycles were designed using 4-(2-pyridyl)pyrimidine as the organic linker [165]. Dunbar et al. have investigated the effect of anions in anion-templated self-assembly reaction between first row transition metal ions and divergent bis-pyridine ligand [166,167]. Larger anion like [SbF$_6$]$^-$ favoured the formation of molecular pentagon [{Ni$_5$(bptz)$_5$(CH$_3$CN)$_{10}$}SbF$_6$]$^{9+}$ while relatively smaller counter-anions ClO$_4^-$ and BF$_4^-$ gave molecular square [{M$_4$(bptz)$_4$(CH$_3$CN)$_8$}⊂X]$^{7+}$ (M = Ni(II), Zn(II); X = ClO$_4^-$ and BF$_4^-$). Other transition metal ions like iron, cobalt and nickel were also extensively used to prepare various MOPs with most of them soluble in organic solvents demonstrating their good chemical stabilities [168]. Water-stable MOPs ideally should be prepared in water but can also be prepared in organic solvents and be brought into aqueous solution by various approaches like redissolving them in water, performing counterions exchange or attaching water solubilizing groups via presynthetic and postsynthetic modifications, are particularly interesting for their abilities to withstand aqueous environments for real-life applications as the water-contact (mostly from atmospheric moisture) for most of the materials is almost unavoidable. The disadvantages that water-soluble MOPs containing N-donor ligands experience are mostly two-folds: (1) instability of metal-ligand bonds and (2) degradation of organic linkers particularly for those MOPs which utilize dynamic combinatorial chemistry (DCC) to stich organic molecules together. Considering their solution processabilities, solid-state recyclabilities and reusabilities; water-soluble and -stable MOPs containing N-donor ligands are rare in literature. Contrast to solid MOFs, solution-based MOPs can easily deform or de-ligate to enable guest molecules larger than the pore sizes to enter within their cavities. Thus, MOPs involving strong metal-ligand interactions and multi-topic chelating ligands are thus expected to render stable MOPs.

Contrast to MOPs containing O-donor ligands, MOPs containing N-donor ligands have found limited applications in the solid-state, rather they were extensively used to study solution-based properties. Therefore, their aqueous stabilities become indispensable for exploring their properties both in solid and solution state. Majority of MOPs synthesized and studied in organic solvents will not be discussed here as their stabilities have been mostly verified in organic solvents and authors are encouraged to read several excellent review articles available in literature [4,5,8,25]. First row transition metal ions with well-defined coordination geometries were found to be suitable for the preparation of N-donor ligand-coordinated MOPs. Interestingly, kinetic inertness of the first-row transition metal ions obey the following stability order Ni^{II} > Fe^{II} > Co^{II} > Zn^{II} > Cd^{II}. Using first-row transition metal ions, Nitschke and coworkers have done extensive works to prepare N-donor containing MOPs that are water soluble. Nitschke et al. have introduced

new type of water-soluble Fe_4L_6 tetrahedron MOP 43 prepared via subcomponent self-assembly approach which involves the simultaneous formation of dynamic coordinative N→M and covalent C→N bonds in turn leading to the in situ formation of pyridyl imine chelate ligands and their organization around metal ion templates [62]. Subcomponents 2-formylpyridine and 4,4′-diaminobiphenyl-2,2′-disulfonic acid (two sulfonate groups enable water solubility) in combination with Fe(II) metal ion and a base produced water soluble tetrahedron MOP 43 (Figure 19A). MOP exclusively contains iron (II) metal ions in the low-spin state and was found to be stable in aqueous solution owing to the strong binding interaction and mutual stabilization between iron(II) metal ion and the imine ligands. X-ray crystal structure revealed the formation of an anionic tetrahedron with four Fe^{II} vertices and six bis-bidenate ligand edges.

Enantiopure water-soluble MOPs were later synthesized by Nitschke and coworkers, suitable for guest encapsulation and catalysis [169]. Diamino terphenylene subcomponent was functionalized with chiral glycerol groups to prepare enantiopure derivatives, (S,S) and (R,R). Self-assembly reaction of enantiopure derivative either (S,S) or (R,R), 2-formylpyridine and iron(II) sulfate yielded the corresponding chiral $[Fe^{II}_4L_6]_8^+$ MOP ΔΔΔΔ-44 or MOP ΛΛΛΛ-44 in water, respectively (Figure 19B). Compared with previously synthesized terphenyl-edged tetrahedra, the glycerol groups serve not only as water solubilizing agent to render water-soluble MOP but also helps to dictate the handedness of the iron(II) stereocenters despite having the distance between stereochemical elements. MOP ΔΔΔΔ-44 binds to wide range of chiral organic guests demonstrating the ability of enantiopure MOPs for chiral recognition and to catalyze the hydrolysis of the neurotoxic organophosphate dichlorvos. Ward and coworkers had independently reported the synthetic strategies to prepare N-donor containing water-soluble MOP [170]. Self-assembly of cobalt(II) ion with organic linkers containing naphthalene-1,5-diyl spacer with two chelating pyrazolyl-pyridine units led to the formation of cubic MOP 45 $[Co^{II}_8L_{12}]^{16+}$ (Figure 19C). Eight octahedrally organized Co^{II} corners with twelve bridging ligands spanning across the edges are rearranged to prepare the cubic MOP. The attachment of hydroxymethyl substituents to the pyridyl-C_4 sites of each ligand render the MOP 46 water soluble owing to the presence of outward-facing hydroxyl groups. The internal cavity of MOP 46 remains hydrophobic and binds to wide range of guest molecules by exploiting H-bonding interactions with specific sites on the internal surface of the MOPs, nonpolar interactions such as aromatic, van der Waals interactions and solvophobic interactions. Nitschke and coworkers [171] had demonstrated that hydroxymethyl functionalized organic linker when reacted with 2-formylpyridine and $FeSO_4$ in water at 50 °C can render water-soluble $Fe^{II}_4L_6$ tetrahedron MOP 47 with *fac*-stereochemistry at each metal centers (Figure 19D). Prolonged exposure of iron(II) tetrahedron MOP 47 to the aqueous solution led to the isolation of water-soluble $Fe_{10}L_{15}$ prism MOP 48 which recrystallizes from the aqueous buffer. This observation indicates that the tetrahedron and prism are in equilibrium in solution with prism preferentially crystallizes due to lower solubility. Prism with *mer* stereochemistry at each metal center can be separately prepared by mixing the organic subcomponents and $FeSO_4$ at 20 °C in Water-MeOH (1:9) mixture. Interestingly, complete conversion of prism MOP to the tetrahedron MOP was not achieved in water or methanol/water mixture over a period of two months at room temperature until the solution was heated to 50 °C for one week. This observation led to the conclusion that the prism is kinetic product and tetrahedron is the thermodynamic product which was further consolidated by the stability experiments. Prism falls apart in presence of competitive ligand 4-methoxyaniline, however tetrahedron MOP remain intact even after seven days in presence of 20 equiv. of 4-methoxyaniline.
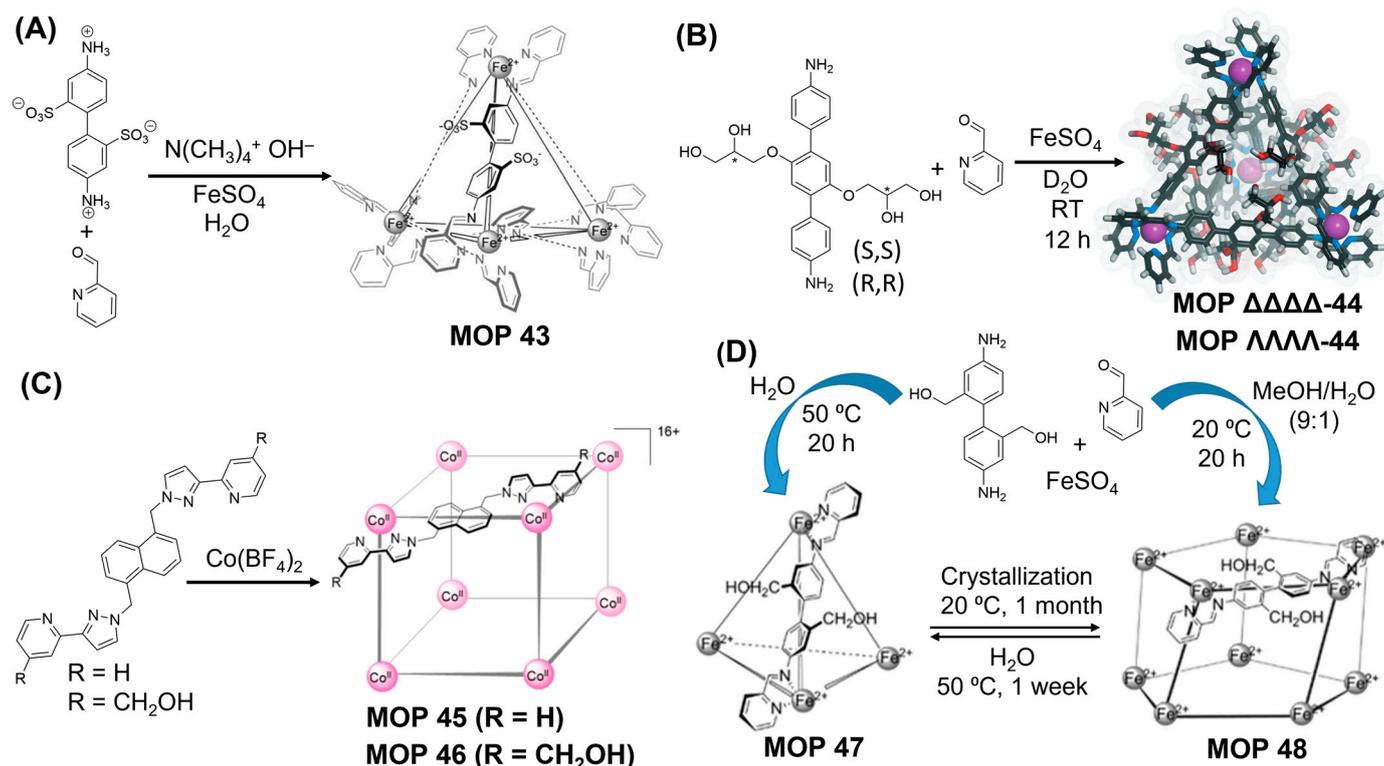
Figure 19. (**A**) Preparation of tetrahedron MOP 43 by aqueous subcomponent self-assembly. (**B**) Enantioselective formation of tetrahedron MOP ΔΔΔΔ-44 and MOP ΛΛΛΛ-44 from enantiopure (S,S/R,R) diamine, 2-formylpyridine and Fe^{II}SO$_4$ by subcomponent self-assembly. (**C**) Preparation of cubic MOP 45 and MOP 46 from the corresponding ligand and Co(BF$_4$)$_2$ salt via self-assembly. (**D**) Subcomponent self-assembly of tetrahedron MOP 47 and prism MOP 48, and their interconversion. Reprinted by permission from Refs. [62,169–171]. Copyright 2008 and 2013 from Wiley-VCH. Copyright 2013 from Royal Society of Chemistry.

Attempt to prepare water-soluble MOPs from highly hydrophobic ligands includes the use of different counter-anions during the self-assembly. Attempt to prepare sulfate counter anion-based MOP from FeSO$_4$ and the corresponding subcomponents in several solvent mixtures remain unsuccessful. Nitschke and coworkers had reported successful anion-exchange strategy to prepare water-soluble MOPs [76] Reaction of four-fold symmetric tetrakis-amine zinc porphyrin and 2-formylpyridine with Fe(OTf)$_2$ afforded cubic MOP 49 with eight octahedrally coordinated Fe^{II} centers located at the corners and six facially-positioned organic ligands (Figure 20). Triflate salt of the corresponding MOP 49 is soluble in organic solvents but remains water-insoluble. Anion metathesis using potassium sulfate or tetrabutylammonium sulfate precipitated out the corresponding sulfate salt of Fe-MOP 49 that becomes water-soluble. Interestingly, no degradation of the sulfate MOP was observed in the concentration range (0.2–15 mM, aqueous solution) at 25 °C over period of several months. Gu and coworkers had reported the synthesis of four different pairs of enantiomers of water-stable tetrahedron MOP [Ni$_4$L$_6$]$^{8+}$ via subcomponent self-assembly of 1,8-di(imidazole-2-carboxaldehyde)octane, aryl-substituted ethylamine and NiCl$_2$•6H$_2$O mixed together in 3:6:2 molar ratio in acetonitrile/diethyl ether solution [172]. Four octahedrally arranged Ni^{II} metal centers are arranged in tetrahedral geometry linked together by six bridging diimidazole ligands spanning across the edges of the tetrahedron MOP. Flexible diimidazole linkers endowed the MOPs with relative water-compatibility. Compared with other transition metal-based tetrahedron MOPs [173], Ni(II)-based MOPs showed better aqueous stability. Chloride salts of each MOP showed better water solubility and remarkable stability with little decomposition over long periods in acidic solution as well as even at a high temperature of 90 °C. High positive charge and suitable size of the

corresponding MOP enable remarkable stabilization of antiparallel G-quadruplex DNA with moderate enantioselectivity.
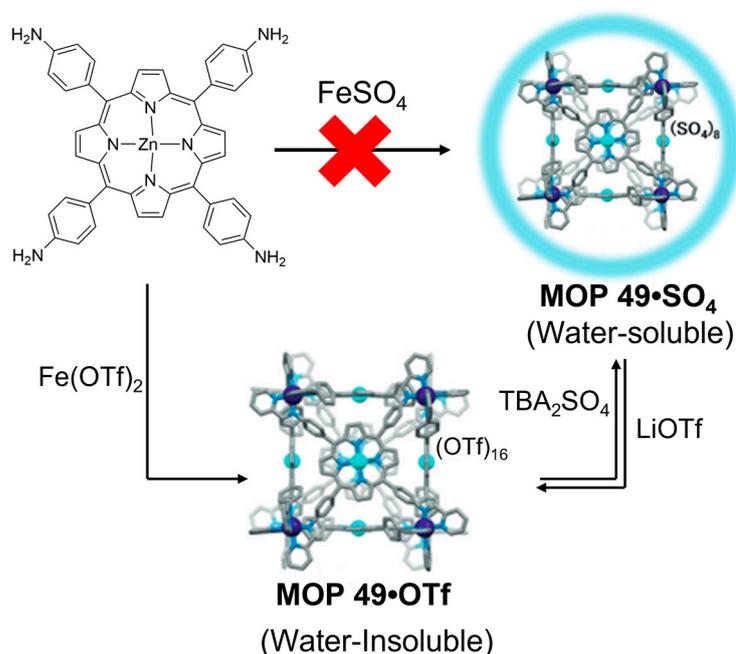

Figure 20. Subcomponent self-assembly of MOP 49•OTf and reversible anion exchange to obtain the water-soluble derivative MOP 49•SO$_4$. Reprinted by permission from Ref. [76]. Copyright 2017 from Wiley-VCH.

Nitschke and coworkers had reported the synthetic strategies to prepare sulfate MOPs using different metal ions (M = Co^{II}, Ni^{II}, Zn^{II} and Cd^{II}) as templates [174] following the strategies either via direct MOP formation from the corresponding metal(II) sulfate and the organic subcomponents or via anion exchange. Subsequently wide variety of MOPs including M$_8$L$_6$ cubes, face-capped M$_4$L$_4$ tetrahedra, edge-linked M$_4$L$_6$ tetrahedra were prepared. Generally hydrophobic counterparts render MOPs water insoluble, however the use of SO$_4^{2-}$ counter anion makes them water-soluble. CoX$_2$ and NiX$_2$ metal salts (X = OTf$^-$, NTf$_2^-$, BF$_4^-$) in combination with di-, tri-, tetratopic organic linkers gave water-insoluble MOPs with various sizes and shapes which become water-soluble following anion metathesis using tetrabutylammonium sulfate salt (Figure 21). Interestingly, their water solubilities and subsequent stabilities are dictated by the three factors: (1) metal-ligand bond strength, (2) degree of chelation and (3) degree of topicity of organic linker. Interestingly Co(II)-based MOPs prepared from linkers containing higher degree of topicity are endowed with enhanced aqueous stabilities. Co(II)-based MOPs made up of ditopic linkers fall apart in water following anion metathesis compared with MOPs constructed from tritopic and tetratopic linkers which remain intact in water. Interestingly Ni(II)-based MOPs showed enhanced stabilities and the corresponding MOPs prepared from ditopic and tritopic ligands can be further utilized to encapsulate hydrophobic guest molecules within their cavities. Use of labile metal ions like Zn(II) or Cd(II) in combination with tritopic and tetratopic organic linkers render the MOPs only soluble in organic solvents as they are easily disassembled in water following anion metathesis. Their aqueous solubilities and stabilities can be enhanced by tuning the degree of chelation. Various bisaldehyde organic linkers in combination with tritopic amine TREN and TRPN when react with MSO$_4$ (M = Zn, Cd) gave water soluble helicates and tetrahedra. Similarly, trisaldehyde in combination with tritopic amines produces water soluble tetrahedron MOPs with enhanced stabilities which can be explained by the higher degree of chelation rendering labile metal-N interactions more resistant to water-attack. Comparative study on the relative stability of cubic MOPs

prepared from transition metal ions (Fe, Co, Ni, Zn, Cd) revealed that the aqueous stabilities (Figure 22) obey the metal-ligand bond strengths in the following order $Ni^{II} > Fe^{II} > Co^{II} > Zn^{II} > Cd^{II}$ as predicted by the Irving-Williams series ($Fe^{II} < Co^{II} < Ni^{II} > Zn^{II}$) [175]. Ni(II), Co(II) and Fe(II)-based MOPs remain stable in water over several months with Ni(II) MOPs being the most stable owing to the lower ionic radius and higher gain in LFSE which is also reflected from the slower rate of aqua ligand exchange. Fe(II)-based MOPs were found to be more stable than Co(II)-based MOPs due to the formation of low spin Fe^{II} complexes compared with high-spin Fe^{II} complex used to prepare the Irving-Williams series. Filled *d*-orbital with no gain in LFSE and large ionic radii of render Zn and Cd MOPs less water stable. Cd(II) MOP was found to be stable in water even less than several minutes while Zn(II) MOP was stable only for 30 min which are in good agreements with ~3–4 order faster water exchange rate compared with most stable Ni(II) aqua complex. This study demonstrated that strong metal-ligand interaction in combination with high degree of chelation and enhanced ligand topicity provided the blueprint to prepare water-soluble and water-stable MOPs.
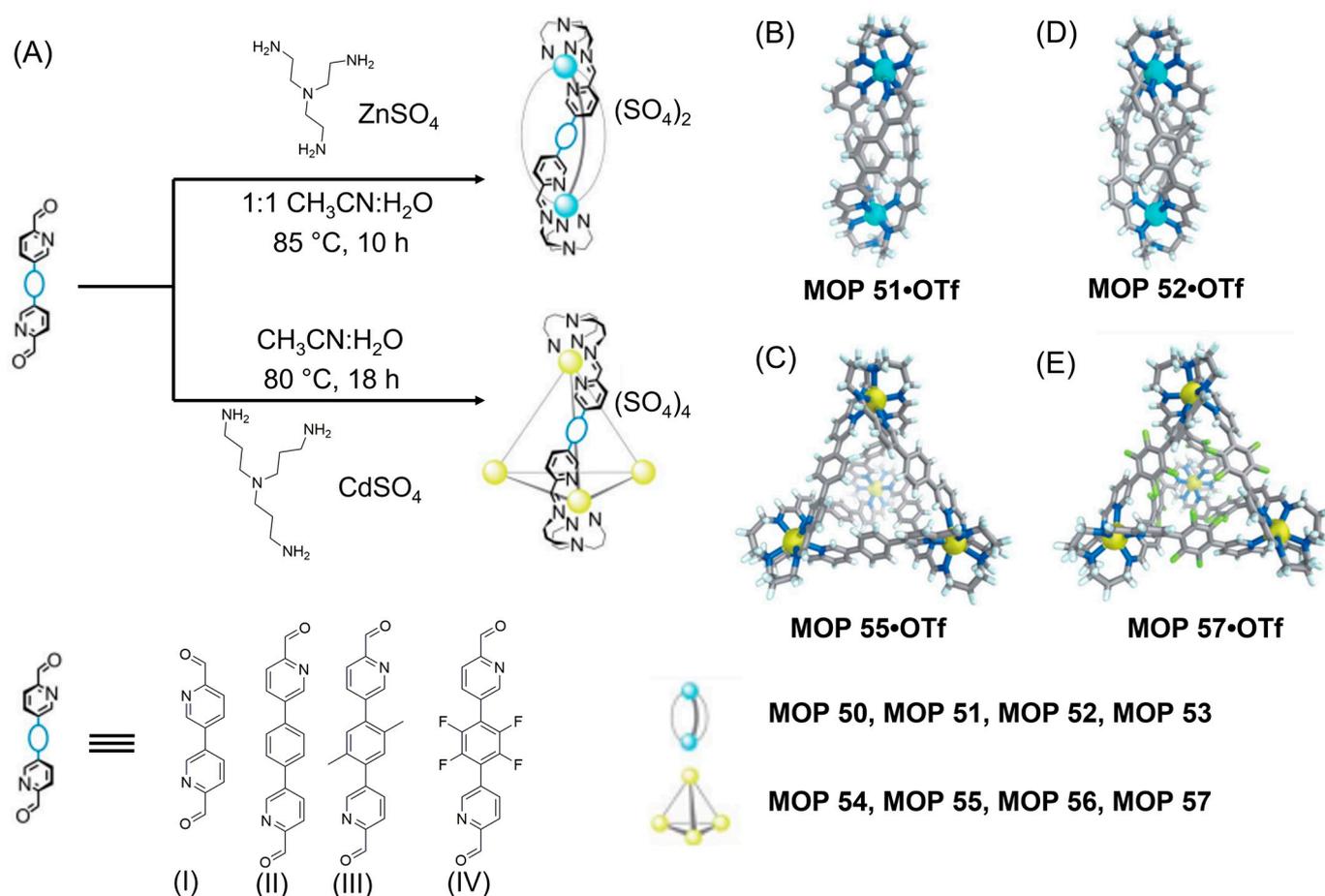
Figure 21. Water-soluble Zn^{II} and Cd^{II}-based architectures. (**A**) Self-assembly of Zn^{II}-helicates and Cd^{II}-tetrahedron from C_2-symmetric subcomponents I–IV and the tritopic amines TREN and TRPN. Structures based upon bis-(pyridine aldehyde): cationic portions of the X-ray structures of (**B**) helicate Zn-MOP 51•OTf and (**C**) tetrahedron Cd-MOP 55•OTf. (**D**) Cationic parts of the X-ray structures of helicate Zn-MOP 52•OTf (based upon aldehyde (III) and (**E**) tetrahedron Cd-MOP 57•OTf (based upon aldehyde (IV). Counterions, solvents and disorder are omitted for clarity. Zn^{II}, Cd^{II} and fluorine atoms are coloured cyan, yellow, and pale green, respectively. Reprinted by permission from Ref. [174]. Copyright from 2019 from Royal Society of Chemistry.
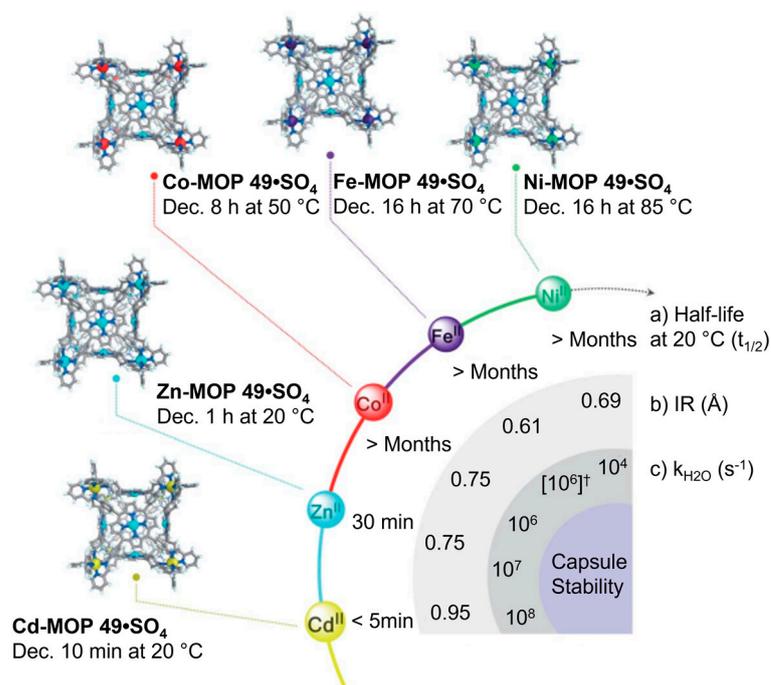
Figure 22. Relative stability of cubes MOP 49•SO_4 in water. Crystal structures (Ni-MOP 49, Fe-MOP 49, and Co-MOP 49) and MM3 models (Zn-MOP 49 and Cd-MOP 49) of cubes with their decomposition conditions are presented. (a) Half-lives ($t_{1/2}$ at 20 °C), (b) ionic radii (IR, Å) and (c) ligand-exchange rates for water (k_{H2O}, s^{-1}) for the different metal ions are displayed for comparison. (†) Although Fe-MOP 49 is low-spin, k_{H2O} for high-spin Fe^{II} is given because $[Fe(H_2O)_6]^{2+}$ is high-spin. Reprinted by permission from Ref. [174]. Copyright from 2019 from Royal Society of Chemistry.

MOPs have found wide applications in separation technology. Parallel to porous solids, porous liquids are beginning to make their footprint in chemical technological applications as well. Porous liquids are described as materials that exist in liquid phase at given temperature range with intrinsic porosity only coming from molecular cavity itself and lack external porosities like conventional liquid. Porous liquid has been classified into three classes [176,177]—type I, type II and type III. Type I porous liquid is a class of porous material existed as neat liquid. Type II and type III porous materials are prepared from porous molecular cage and MOFs, respectively in solvents that are remain inaccessible by the cavity of dissolved materials producing the porous liquids with empty intrinsic pores for guest recognition. Relatively better solution processability of MOPs has given them an edge over MOFs in order to be useful for porous liquid. Nitschke and coworkers had reported that porous liquid can be successfully prepared from N-donors based coordination MOPs [178]. Self-assembly of tritopic pyridine aldehyde linker and para-imidazolyum substituted aniline in the presence with $Zn(NTf_2)_2$ in acetonitrile gave the corresponding tetrahedron MOP 58 which was then used to prepare the corresponding porous ionic liquid using solvent evaporation (Figure 23A). Thermogravimetric analysis revealed that neat liquid MOP 58 showed no significant loss of mass between room temperature and 300 °C. Chlorofluoro hydrocarbons ($CFCl_3$, CF_2Cl_2, CF_3Cl) are long-lived ozone-depleting agents with 1 g of each in the atmosphere being equivalent of several thousand grams of CO_2. Zn(II)-MOP 58 based porous ionic liquid was therefore tested for the encapsulation of chlorofluoro hydrocarbons showing the affinity in the following order $CFCl_3 > CF_2Cl_2 >$ CF_3Cl. Furthermore, empty MOP 58 can also be recovered by releasing the encapsulated guests under a reduced pressure enabling the porous liquid to be recyclable, an important consideration for developing porous industrial materials.
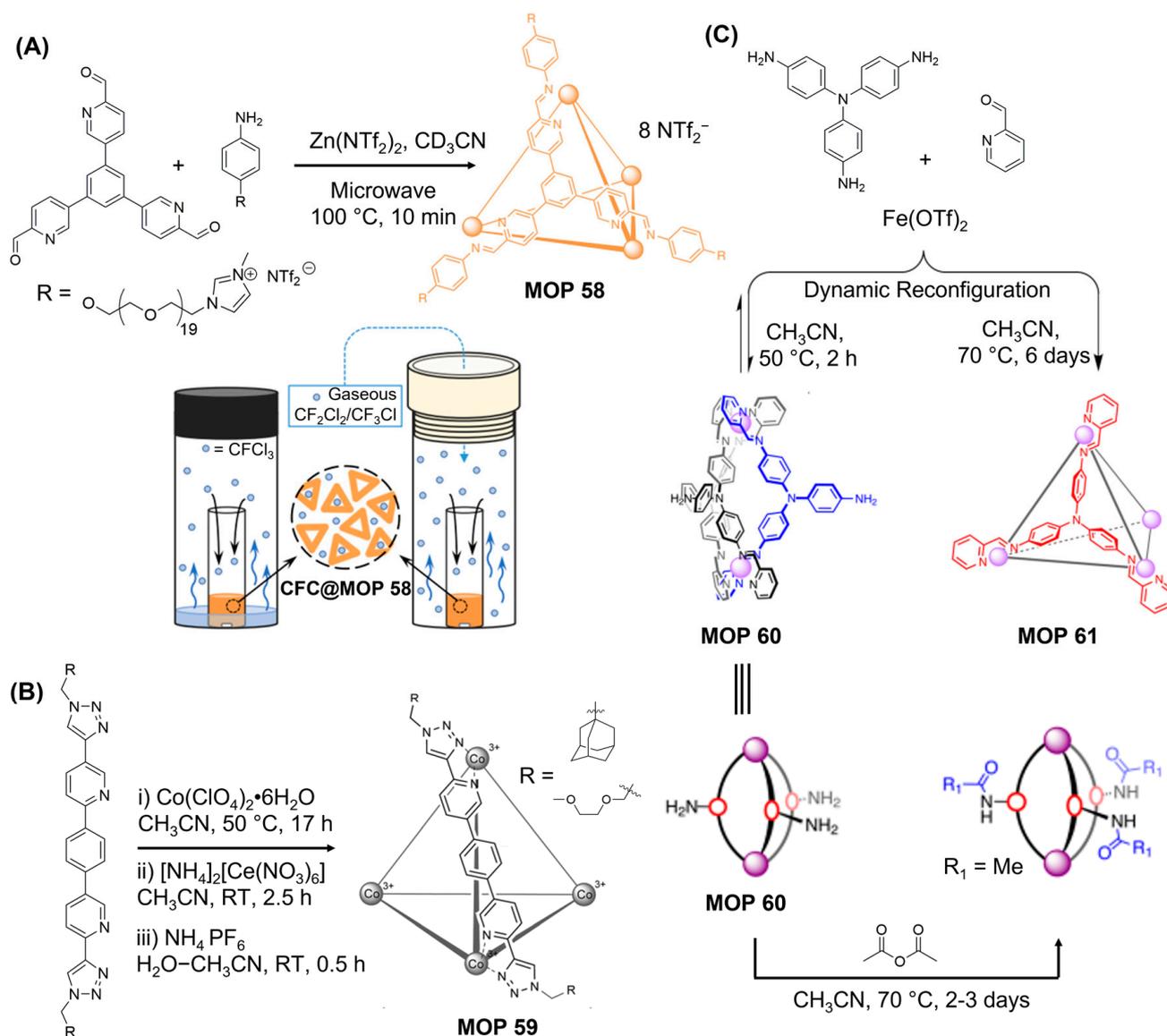
Figure 23. (**A**) Subcomponent self-assembly of MOP 58 from trisaldehyde, aniline and Zn(NTf$_2$)$_2$ in acetonitrile. When neat liquid MOP 58 was stirred under an atmosphere saturated with CFCl$_3$, CF$_2$Cl$_2$ or CF$_3$Cl, the uptake of these gaseous guest molecules was observed. The samples were subsequently analyzed using solution-phase NMR techniques. (**B**) Synthesis of non-equilibrium Co(III) capsules following post-assembly oxidation of Co(II) tetrahedron to kinetically inert Co(III) tetrahedron using ceric ammonium nitrate. (**C**) Subcomponent self-assembly of tris(4-aminophenyl)amine with 2-formylpyridine and iron(II) triflate gave (i) kinetically stable Fe$^{II}_2$L$_3$ helicate MOP 60 and (ii) thermodynamic product Fe$^{II}_4$L$_4$ tetrahedron MOP 61. Covalent functionalization of helicate MOP 60 gave kinetically trapped helicate MOP. Reprinted by permission from Refs. [178–180]. Copyright 2014 from American Chemical Society. Copyright 2015 from Royal Society of Chemistry. Copyright 2020 from Nature Publishing Group.

Combining the inert metal ions with organic linkers has been proven to be a viable route for the preparation of water-soluble and water-stable MOPs, however this approach may not be the straight-forward strategy always. Many self-assembly pathways that use inert metal ions often fall into the kinetic traps leading to the formation of oligomeric intermediates. Methods to overcome the kinetic traps include thermal labilization, use of labilizing competitive ligands and post-assembly modification [181–184]. In a strategy, labile building blocks are assembled to form supramolecular architectures which are then

kinetically locked via subsequent chemical modifications. Taking the benefits of substitutionally non-lability of Co^{III} metal ion compared with Co^{II}, Lusby and coworkers [179] had reported the synthesis of water soluble Co(III)-based tetrahedron MOP 59 from pyridyl-triazole ligand system and $Co(ClO_4)_2$ followed by oxidation of Co^{II} to Co^{III} using ceric ammonium nitrate. d_6 electronic configuration of Co^{II} renders low spin octahedron coordination complex (Figure 23B) at each metal center. $[Co^{II}_4L_6]^{12+}$ tetrahedron MOP 59 was then reacted with ceric ammonium nitrate to form oxidized Co^{III}-based MOP 59 with mixed ClO_4^-/NO_3^- counter-anions. The oxidized MOP 59 becomes more stable and less dynamic due to the enhanced inertness of Co^{III}-N linkages. Counter-anion exchange using $AgNO_3$ gave the water-soluble nitrate (NO_3^-) salt of the corresponding tetrahedron MOP 59 which was found to be stable for indefinite period. In an interesting example, Nitschke and coworkers had demonstrated the PAM locking strategy in order to stabilize meta-stable states that appears in self-assembly pathways [180]. Reaction between tris-amine derivative and 2-formylpyridine in presence of $Fe(NTf_2)_2$ gave the initial metastable kinetic product $Fe^{II}_2L_3$ triple helicate MOP 60 which subsequently rearranges to form thermodynamically favoured $Fe^{II}_4L_4$ face-capped tetrahedron MOP 61 after several days (Figure 23C). Helicate structure MOP 60 only uses two out of three aniline moieties for metal coordination with the third remaining free for subsequent modification. Trapping the third reactive aniline via PAM locking strategy allows the helicate MOP 60 to be trapped at the out-of -equilibrium stage. N-acylation using acid anhydrides or activated esters and subsequent azidation gave PAM-modified kinetically-trapped helicate MOP. Glasson, Lindoy and coworkers had demonstrated that additional covalent buttressing of metallo-supramolecular complexes can render MOPs kinetically more inert and stable [185]. Linear bis(bipyridine) ligand in presence with $Fe(PF_6)_2$ afforded either kinetically favoured $Fe^{II}_2L_3$ or thermodynamically favoured $Fe^{II}_4L_6$ complex from an equilibrium solution depending on the reaction conditions employed. Subsequently, they can be capped by treating the exposed 5-(tert-butyl)benzaldehyde residues with ammonium acetate followed by reduction with sodium cyanoborohydride. Formation of tertiary amine locked each MOPs in their assembled states.

Second row transition metal ions (Pd, Cd, Ag, Rh, Ru) in combination with N-donor ligands have been extensively used to prepare MOPs that show good water solubility and stability to exhibit their potential usefulness for various applications. Early examples of MOPs documented the use of palladium metal ions. Fujita and coworkers have envisaged that square planar geometry of Pd^{II} metal complex would be suitable to combine with multitopic organic linkers to give rise diverse class of MOPs. Hydrophobic 4,4′-bipyridine linker self-assembles with $[(en)Pd]^{2+}$ capping units (en = ethylenediamine) originating from $[(en)Pd](NO_3)_2$ salt to render (Figure 24A) water-soluble MOP 62 $[(en)_4Pd_4(bpy)_4]^{8+}$ in square geometry [60]. Hydrogen-bonding donating ability of the capping unit and the use of hydrophilic nitrate (NO_3^-) counter-anions make the MOP water-soluble. Guest encapsulation ability of the MOP was demonstrated by incorporating hydrophobic molecules such as 1,3,5-trimethoxybenzene within its interior. Later, Fujita group had reported that self-assembly of 1,3,5-tris(4-pyridyl)triazene and $[(en)Pd](NO_3)_2$ salt (in 6:4 ratio) produces the first ever water-soluble octahedron MOP 63, $[Pd_6L_4]^{12+}$ [61]. Four triazine panels are held together by six palladium capping units (Figure 24B) through metal-ligand interactions to form truncated octahedron with alternate closed and open faces. Large interior cavity volume enables guest molecules to occupy the cavity useful for guest recognitions, chemical transformations and transportation [186]. Other variants of palladium(II) capping units including $[(tmeda)Pd]^{2+}$ (tmeda = N,N,N′,N′-tetramethylethylenediamine) [187], chiral $[(EtCyhex)Pd]^{2+}$ (EtCyhex = cis-(1R, 2R)-N,N′-diethyl-1,2-diaminocyclohexane) and $[(bipy)Pd]^{2+}$ (bipy = 2,2′-bipyridine) with two accessible *cis*-oriented coordinated sites were also successfully used to make isostructural MOPs analogous to $[Pd_6L_4]^{12+}$ octahedron.
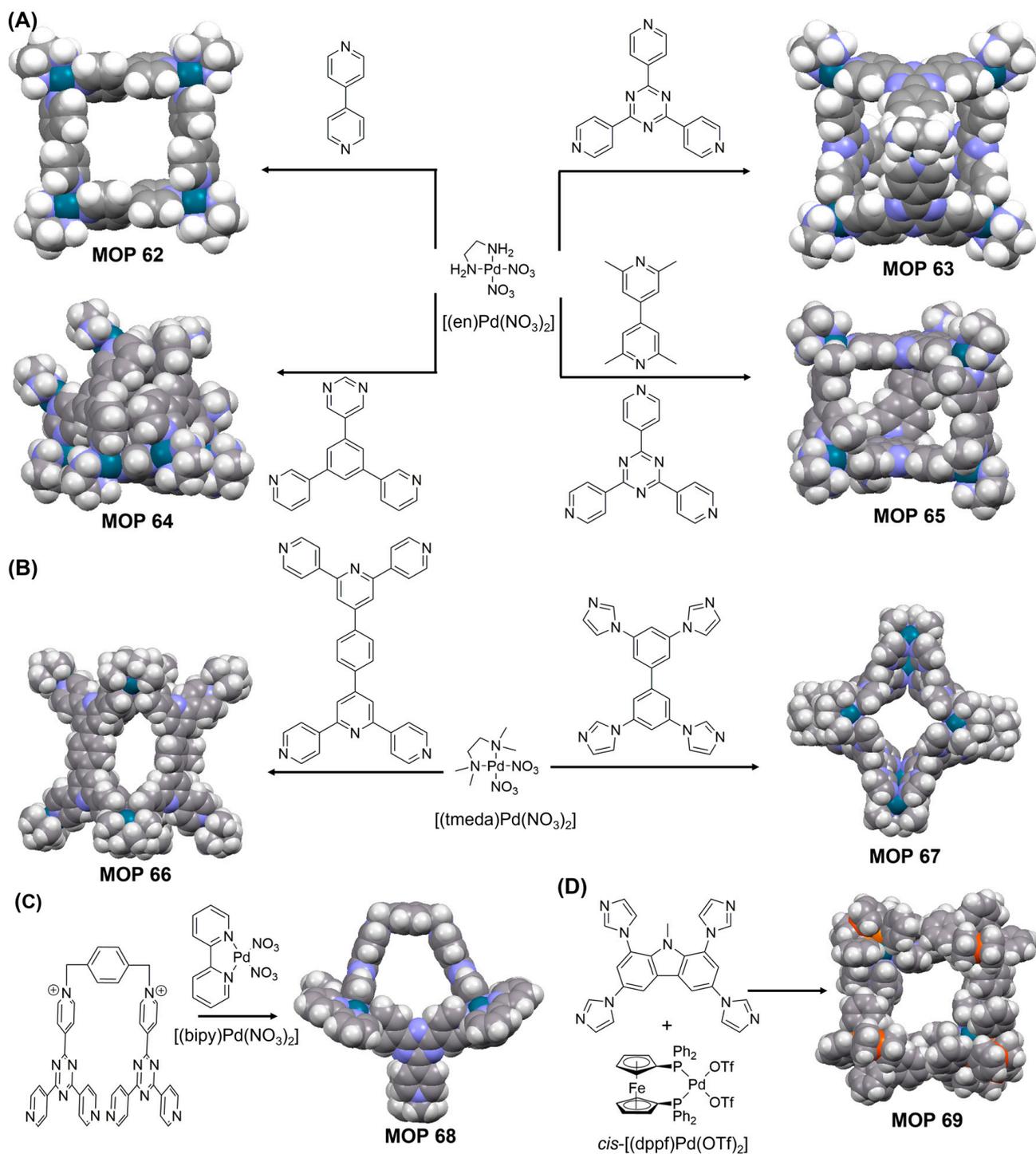
Figure 24. (**A**) Reaction of [(en)Pd(NO$_3$)$_2$]with rigid-oligo pyridines produce N-donor based MOPs 62, 63, 64 and 65. (**B**) Reaction of [(tmeda)Pd(NO$_3$)$_2$] with rigid-oligo pyridines/pyrimidines gave N-donor based MOPs 66 and 67. (**C**) Reaction of [(bipy)Pd(NO$_3$)$_2$] with rigid-oligo pyridine produces N-donor based MOP 68. (**D**) Reaction of *cis*-[(dppf)Pd(OTf)$_2$] with rigid-oligo pyrimidine produces N-donor based MOP 69. Pictures showing the examples of these ligands and the X-ray crystal structures of the corresponding MOPs. Reprinted by permission from Refs. [60,61,63,188–192]. Copyright 1990, 2000, 2005, 218, 2019 from American Chemical Society. Copyright 1995 from Nature Publishing Group. Copyright 2017 from Wiley-VCH.

General strategy to prepare palladium-based water soluble cages demonstrated by Fujita and coworkers was further expanded by the same group using cis-capped [(en)Pd(NO$_3$)$_2$] salt. Pyridine/pyrimidine molecular panels were used to prepare varieties of self-assembled exotic polyhedron architectures [188,193]. Despite having used the hydrophobic organic linkers, the self-assembled MOPs remain water soluble due to the cationic charges associated with palladium(II) metal centers and the corresponding nitrate counter-anions further augmenting the water solubility. The relative lability of palladium(II)-N linkages render thermodynamically favoured MOPs with relatively inert ethylenediamine chelating ligand. The excellent aqueous kinetic stability was ensured by the multitopicity of ligands—use of tri- and tetratopic linkers render MOPs water stable. Other variants of *cis*-capped complex like *cis*-[(tmeda)Pd(NO$_3$)$_2$] and *cis*-[(bpy)Pd(NO$_3$)$_2$] gave water soluble architectures like MOP 66 and MOP 68 (Figure 24) with enhanced stabilities suitable for carrying out applications like guest encapsulation and chemical transformation [63,189]. The generality of this approach was further demonstrated by other groups like Mukherjee [190] and Klajn [194] by using imidazole-containing ligands instead of pyridines/pyrimidines to prepare water soluble MOP 67 and MOP 69. Tri- and tetratopic imidazole-based organic linkers render hydrophobic cages that exhibit water solubility and good stability. Mukherjee and coworkers had reported that palladium(II)-based MOPs (Figure 24) prepared from tetratopic imidazole linker can successfully be used to catalytically enhance the performance of cycloaddition reaction [191].

Mixed-ligand strategy was employed to prepare N-donor coordinated MOP 65 with general formula $M^{II}_6L_2Pillar_3$ (Figure 24A) when triazine panels are mixed with cis-capped [(en)Pd(NO$_3$)$_2$] complex containing chelating ancillary ligands ethylenediamine (en) and ditopic pyridyl-based pillars [195]. By choosing different sized pillars, the height of the MOPs can be adjusted with tunable functionalities for various applications like stabilizing dinucleotide base-pair duplex, stacking of heterometallic clusters containing soft d^{10} metal ions, encapsulating electronically complementary guest molecules etc. [192,196].

Use of [(en)Pd(NO$_3$)$_2$] metal salt enables MOPs which are synthesized from hydrophobic ligands to become water soluble. Naked Pd metal ion originated from Pd(NO$_3$)$_2$ metal salt in combination with hydrophobic organic linkers render diverse class of MOPs which are soluble in organic solvents and often remain water-insoluble unless they are otherwise functionalized to make water-soluble. Additionally, labile Pd-N linkages render MOPs more susceptible to degradation, making extremely challenging for them to be useful for solid and solution state applications. Fujita and coworkers had reported the preparation of series of metal organic polyhedra prepared from Pd(NO$_3$)$_2$ metal salt and bent bipyridyl organic linkers with general formulas M_nL_{2n} and size upto ~8 nm. Four N-donating ligands contributed to form palladium(II) square-planar complexes are self-assembled into various MOP structures including octahedron, cuboctahedron, rhombicuboctahedron, Goldberg polyhedra etc. Nevertheless, water insolubility and instability raise the concern that whether such MOPs can become useful for real-world applications. General strategy to solubilize and stabilize such Pd-based MOPs include attaching water-soluble groups either pre-synthetically or post-synthetically onto the hydrophobic organic linkers. In an interesting study Fujita and coworkers had demonstrated that $M_{12}L_{24}$ cuboctahedron MOP exhibited remarkable stability under cold-spray ionization mass spectrometry condition [72,73]. The molecular ion species of cuboctahedron MOP can be detected from the mass spectrometry owing to the remarkable stabilization of cuboctahedron MOP through the cooperation of 48 Pd(II)-pyridine interactions. Two cuboctahedron MOPs separately prepared from two different bridging linkers didn't undergo ligand exchange when they were mixed together in acetonitrile and allowed to stand overnight at room temperature. Comparative ligand exchange reaction in mononuclear metal complex, [Pd(py)$_4$](OTf)$_2$ is very fast (k_{obs} = 1.9 × 10^{-2} s^{-1}) and the half-life is 105 times lower compared with the ligand exchange reaction in $M_{12}L_{24}$ complex in organic solvents. The reasonable stability of Pd-based MOPs achieved through cooperative interaction encourages to

bring them under aqueous environment to further expand their scopes. Accordingly, the bis-(pyridyl) ligands were successfully functionalized with water-solubilizing groups like sugar molecules, peptides, nucleotides to study their self-assembly in water. Later, Shionoya and coworkers had demonstrated that palladium metal ions in combination with banana-shaped bis-(pyridyl) ligand can be used to prepare M_2L_4-type MOP where two palladium metal ions are attached to four organic linkers in square planar geometry to occupy the top and bottom faces of the MOP, and four organic linkers are aligned across the four edges of the MOP [197]. Clever group did extensive work to prepare palladium-based MOPs and studied their recognition properties in organic solvents [198]. Yoshizawa and coworkers had first demonstrated the preparation of water-soluble version of Pd-based MOP from banana-shaped organic linkers tethered to water-solubilizing groups [199,200]. They had designed a new ligand bearing two anthracene panels and two methoxyethoxy groups on the central *m*-phenylene ring. Mixture of Pd^{II} ions and organic linker in 1:2 ratio led to the exclusive formation of MOP 70 (Figure 25A) which becomes soluble in mixture of water-methanol. Attaching additional methoxyethoxy group onto the ligand renders the water-soluble MOP. Pt-version of the MOP was also prepared and was used for guest encapsulation study in water. The corresponding water-soluble Pd-MOP was able to safely store radical initiators like AIBN which are generally unstable and are kept in dark at low temperature to avoid photochemical and thermal decomposition [201]. Pd-based M_2L_4-type MOP will tend to be less stable in water compared with larger Pd_nL_{2n}-type cages due to the lack of significant number of cooperative interactions responsible for holding the MOP structure. In addition to using inert metal ions and attaching polar functional groups onto the outer surface of the MOP to shield the metal-ligand interactions from water attack, tuning the steric and electronic properties of coordinating ligand would render the cage more kinetically inert. Crowley and coworkers had reported the synthesis of kinetically inert M_2L_4 type MOPs by putting amino group onto the ortho and meta position of the pyridine unit [202]. Three different MOPs, MOP 71: $[Pd_2(tripy)_4](BF_4)_4$, MOP 72: $[Pd_2(2A\text{-}tripy)_4](BF_4)_4$ and MOP 73: $[Pd_2(3A\text{-}tripy)_4](BF_4)_4$ were prepared from three different ligands only varying by substituents (H, *o*-NH_2 and *m*-NH_2) on the pyridine rings (Figure 25B). However, they remain water-insoluble even after performing counter-anion exchange. Water soluble version of MOPs were prepared by functionalizing the organic linker with either hydroxymethyl or sugar molecules [203]. Model palladium(II) N-heterocyclic carbene (NHC) probe complexes allow the determination of relative ranking of the donor abilities of pyridine ligands with the following order 2A-tripy > 3A-tripy > tripy. Enhanced electron-donating property of 3A-tripy ligand ensures that M_2L_4 MOP $[Pd_2(3A\text{-}tripy)_4](BF_4)_4$ is more stable compare with MOP $[Pd_2(tripy)_4](BF_4)_4$ in presence of common biological nucleophiles (Cl^-, histidine and cys). Comparatively, $[Pd_2(2A\text{-}tripy)_4](BF_4)_4$ MOP showed remarkably high stability (Table 2) against all the nucleophiles with half-lives over 2 h whereas corresponding $t_{1/2}$ for the other MOPs were less than 30 min. Modestly stronger donor ability of 2A-tripy ligand can not fully justify the remarkable stability of $[Pd_2(2A\text{-}tripy)_4](BF_4)_4$ MOP, the steric shielding arising from 2-amino group on the *exo*-faces of the $[Pd_2(2A\text{-}tripy)_4](BF_4)_4$ MOP protect the palladium (II) ions from the incoming nucleophiles. It appears from drug binding and cytotoxicity studies that the enhanced stability of MOPs through subtle structural modifications compromises their abilities to bind cisplatin and thus requires more inert metal ion-based MOPs.
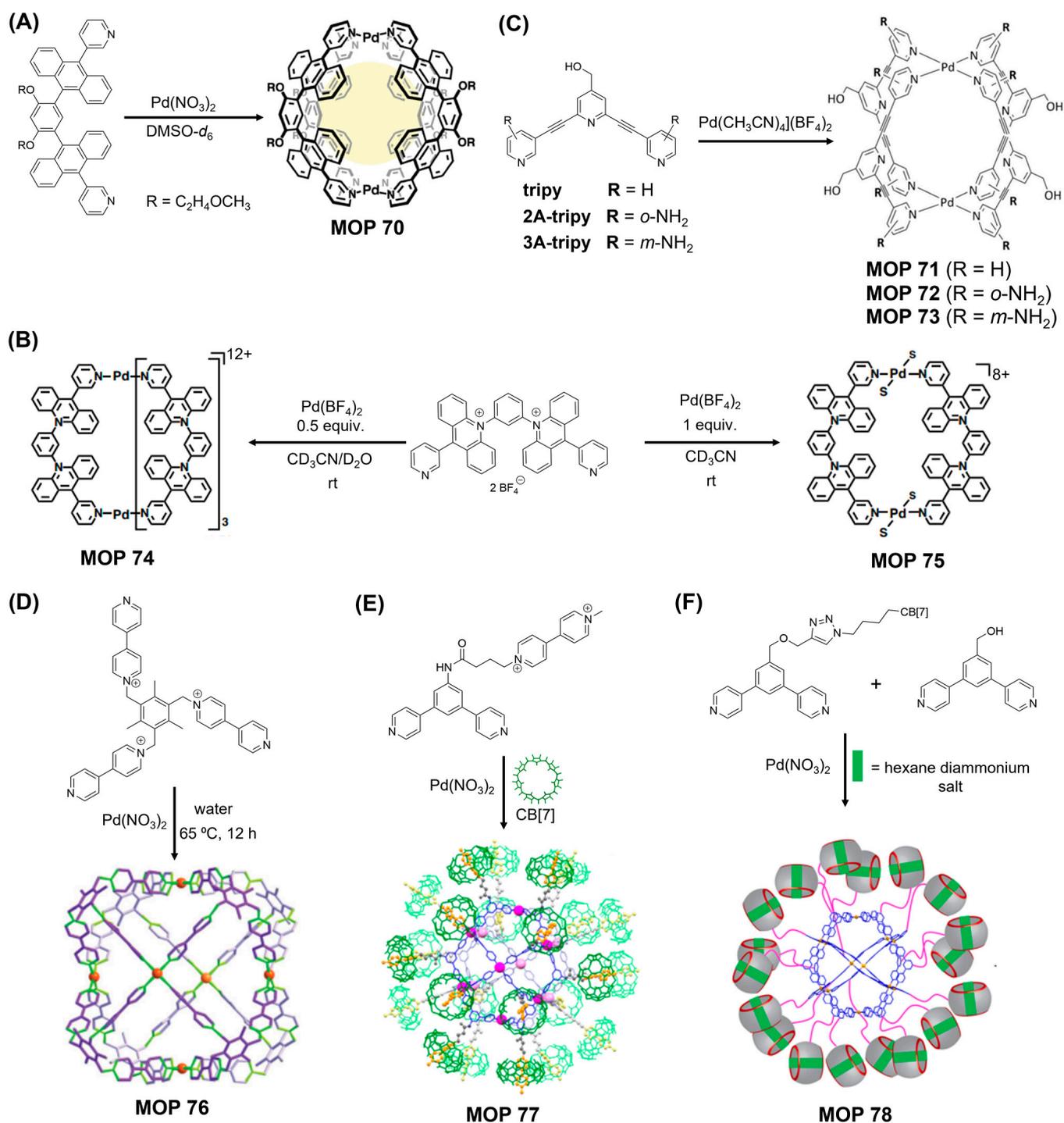
Figure 25. (**A**) Schematic representation of the self-assembly of capsule MOP 70. (**B**) Schematic representation of dodecacationic M_2L_4 capsule MOP 74 and octacationic M_2L_2 cube MOP 75. (**C**) Schematic representation of the synthesis of capsule MOP 71, MOP 72 and MOP 73. (**D**) Preparation of MOP 76 in water via molecular self-assembly. (**E**) Multicomponent self-assembly of CB[7] capped cuboctahedron cage, MOP 73. (**F**) Mixed ligand co-assembly of cuboctahedron cage MOP 78. CB[7] cavity is occupied by hexanediammonium salt. Reprinted by permission from Refs. [199,202,204–207]. Copyright 2011, 2016 and 2017 from American Chemical Society. Copyright 2016 from Royal Society of Chemistry. Copyright 2016 from Wiley-VCH.

Embedding charge on the backbones or on the outer surface of MOPs render water-soluble MOPs. Yoshizawa and coworkers had reported the preparation of polycationic capsular MOPs via self-assembly of Pd^{II} ions and bent bis-acridinium ligands [204]. These architectures showed enhanced solubility in water due to their polycationic shells compared with MOPs containing pendant hydrophilic groups. Reaction of acridinium ligands with Pd(CH$_3$CN)$_4$(BF$_4$)$_2$ at 1:0.5 ratio in solvent mixture (D$_2$O/CD$_3$CN = 5:1) at room temperature afforded cationic M$_2$L$_4$ capsule MOP 74 (Figure 25C). Interestingly, 1:1 reaction mixture in pure CD$_3$CN gave only M$_2$L$_2$ tubular structure MOP 75 indicating the stabilization of the highly charged structure in high dielectric solvent water with sufficient solubility (>5 mM) and stability under ambient conditions. Mukherjee and coworkers had reported the synthesis of water-soluble molecular cube MOP 76 from organic linkers bearing cationic methyl viologen units [205]. Self-assembly of nitrate salt of triscationic organic linker with Pd(NO$_3$)$_2$ in water at 65 °C afforded cubic MOP 76 (Figure 25D) featuring eight organic linker units located at each corner of the cube spanning across the adjacent faces to form six square planar complexes where each palladium(II) metal ion is coordinated by four linkers. Cooperative interplay between multiple weak interactions contributes to the MOP stability in highly dielectric solvent like water even at high temperature upto 90 °C. Interestingly, MOP 76 disintegrates in DMSO-d$_6$ at room temperature which was corroborated by the DFT calculation showing that the free energy gain during the formation of the complex in DMSO-d$_6$ is less than that in water explaining the inherent instability of MOP in DMSO-d$_6$. Large Fujita-type Pd-based cuboctahedron MOP was made and stabilized in water by Isaacs and coworkers [206]. Attaching methyl viologen groups to the bis(pyridine) linkers render the Pd$_{12}$L$_{24}$ type MOP water soluble. Self-assembly of methyl viologen appended bis(pyridyl) ligand and Pd(NO$_3$)$_2$ in DMSO-d$_6$ followed by dialysis in water gave water-soluble version of Pd$_{12}$L$_{24}$ MOP in cuboctahedron geometry (Figure 25E) with 12 square planar palladium(II) complexes linked together by 24 organic linkers. 24 methyl viologen units are attached to the outer surface of MOP (Figure 24E). Post functionalization of MOP with macrocyclic host CB[7] and CB[8] led to the synthesis of CB[n]-capped MOPs (MOP 77 for CB[7]) which was then used to deliver prodrug of doxorubicin to the HeLa cells. CB[n]-loaded MOP was found to be stable in water upto pH slightly lower than physiological pH. Issacs and coworkers further synthesized the covalently linked CB[7]-functionalized Pd$_{12}$L$_{24}$-type MOP 78 (Figure 25F) by self-assembling the CB[7]-appended bispyridyl ligand with Pd(NO$_3$)$_2$ in DMSO [207]. Presence of cationic guests inside CB[7] cavity render the MOP water soluble and stable at physiological pH. Amphiphilic guest molecules bearing hydrophobic tail noncovalently attached to the appended CB[7] molecules backfold and agglomerate inside the MOP-cavity to create nanomicellar sphere which enables hydrophobic guest encapsulation within the cavity. Addition of competitive guest molecules destroys nanomicelles and triggers the stimuli-responsive cargoes delivery to the cancer cells.

Table 2. Describing the stabilities of MOP 71, MOP 72 and MOP 73 in presence of biologically relevant nucleophiles. Half-lives ($t_{1/2}$) for the decomposition of the MOP 71-73 architectures against selected biologically relevant nucleophiles (3:2 DMSO-d$_6$/D$_2$O, 298 K, 500 MHz) as measured through time-course ^{1}H NMR spectroscopy.

Compound	Cl$^-$ (8 Equiv.)	His (4 Equiv.)	Cys (4 Equiv.)
MOP 71	>1 min	18 min	6 min
MOP 72	2 h	46 h	3 h
MOP 73	10 min	25 min	10 min

Other strategy to stabilize Pd-based MOPs includes their encapsulation inside the pores of other supports like metal organic frameworks. Li and coworkers had demonstrated an efficient strategy called as hydrophilicity-directed strategy (Figure 26A) to stabilize Pd-based MOP which is larger in size than the pore apertures of MOFs [208]. As proof of principle chromium-based MOF MIL-101 was used to host M_6L_4-type Pd-based MOP 63. MIL-101 holds two types of mesoporous cavities with internal diameters of 29 and 34 Å, respectively with pore apertures in the range of ~12–16 Å. Palladium based M_6L_4 prepared from $(en)Pd(NO_3)_2$ and tris(pyridyl)triazine ligand is a hollow octahedron structure with diameter of 2.2 nm. As the pore windows are smaller than the diameter of M_6L_4-type MOP 63, the migration and leaching of M_6L_4 can be successfully prohibited to significantly enhance their stability. Hydrophilicity directed strategy (HDA) enables the subcomponents of M_6L_4 MOP to be encapsulated within the more hydrophilic inner surface of MOFs through capillary action. Activated MOF and the ligand L were first introduced into large volume of *n*-hexane followed by the addition of small amount of aqueous solution of $(en)Pd(NO_3)_2$. Capillary force allows the subcomponents to go through the narrow pore apertures to enter within MOF cavities and forms M_6L_4 cage in situ to produce MOP 63 ⊃MIL-101-N (N = 3, 4, 6, or 10), where N denotes the average number of MOF cavities that accommodate one M_6L_4 inside, according to the amount of the precursors added in the reaction solution. Enhanced catalytic efficiency of M_6L_4 cage within the MOF demonstrated the advantages of using HDA strategy to prepare MOP ⊃ MOF compared with other approaches like soaking MOF particles in aqueous M_6L_4 solution or using one solvent instead by soaking MOF in aqueous mixture of the corresponding metal and ligand. Compare with HDA strategy, either approach led to poor loading of Pd-MOPs and they underwent obvious leaching to lose significant amount of palladium metal ions. Encapsulated MOPs quantitatively converted benzyl alcohol to benzaldehyde, which demonstrates the significant enhancement in stability of MOP and its performance compared with free MOP which gave only 60% converted product. Better reusability leading to higher turnover was demonstrated by encapsulated MOP materials as they remain unchanged upto five catalytic cycles compared with pristine MOPs which deactivated significantly. Enhanced catalytic efficacy of encapsulated MOP emphasizes better stability and dispersity of MOPs following their encapsulation within mesoporous MOF cavities.
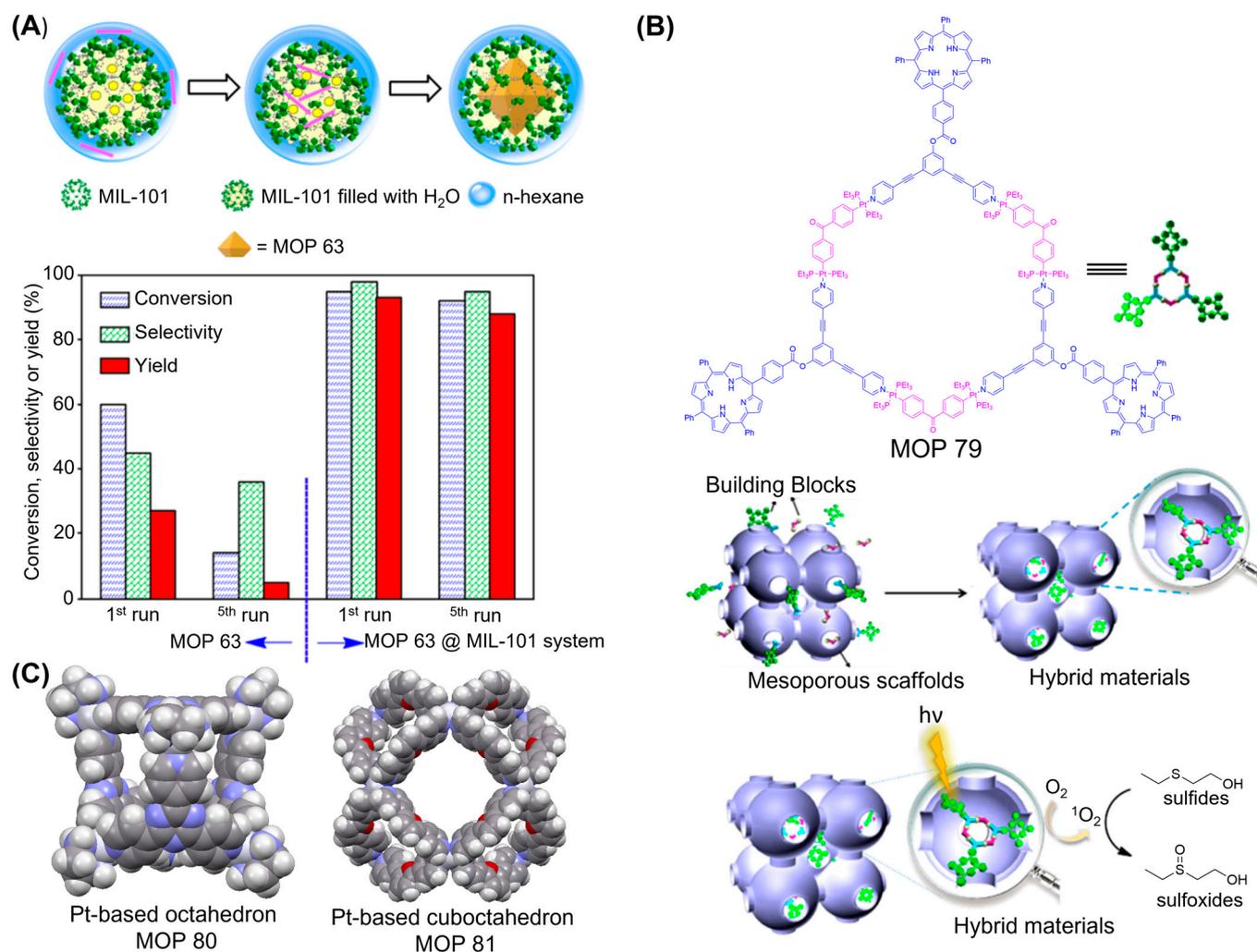
Figure 26. (**A**) Preparation of MOP 63 inside metal organic frameworks, MIL-101 is demonstrated. Catalytic performance and reusability of the MOP 63 and MOP 63⊃MIL-101-4 materials in benzyl alcohol oxidation are reported. (**B**) Chemical and cartoon representation of MOP 79. Schematic presentation of self-assembly of porphyrin metallacycle MOP 79 in cavities of mesoporous carbon FDU-16. Scheme for the oxidation of sulfides (Hybrid materials as catalyst). (**C**) X-ray crystal structures of Pt-based octahedron MOP 80 and Cuboctahedron MOP 81. Reprinted by permission from Refs. [208–211]. Copyright 1998, 2011, 2016 and 2018 from American Chemical Society.

Fujita group had reported the synthesis of N-donor MOPs using kinetically inert metal ions like platinum (Pt). Like palladium, platinum metal ion also forms square-planar complex with N-donor ligands as they belong to the same group in the periodic table. Pitfalls to prepare ordered metal organic structures using kinetically inert metal ions include entrapment of chemicals in undesired architectures not allowing to converge them into ordered desired architectures. Thermal or chemical labilization often become helpful to overcome kinetic barrier to get to the thermodynamic minimum. Triazine tris(pyridyl) ligand with (en)Pt(NO$_3$)$_2$ in D$_2$O afforded kinetically distributed oligomer mixture which eventually converged into thermodynamically stable Pt-based MOP 80 (Figure 26C) upon heating at 100 °C for 24 h in reasonable yield [209]. Addition of suitable guest like sodium adamantane carboxylate to the aqueous mixture followed by stirring at 100 °C for 24 h induces the high-yield conversion of MOP. Both hydrophobic driving force and thermal labilization allow the guest-induced organization of the receptor. Use of inert Pt-N interactions render the cage exceptionally stable in the pH range ~1–11. Strong acid HNO$_3$, base K$_2$CO$_3$ or even strong nucleophile (NEt$_3$) were unable to destroy the framework. Comparatively, palladium(II)

counterpart of the MOP immediately decomposed in presence of acid or nucleophilic base. This work paved the way to prepare stable MOPs using Pt-N interactions. In an interesting example, Fujita and coworkers had reported the preparation of platinum-based larger cuboctahedron MOPs [210]. Reaction of bend bis-pyridine ligand with $Pt(NO_3)_2$ in DMSO was unable to guide the process toward thermodynamic minimum to render $Pt_{12}L_{24}$ type cuboctahedron MOP 81 (Figure 26C). Temporary labilization of inert Pt(II)-pyridine bonds by the addition of strong hydrogen-bond donor 2,2,2-trifluoroethanol (TFE) weakens the pyridine-metal interaction allowing the formation of cuboctahedron cage. Cuboctahedron cage trapped inside thermodynamic minimum remains stable even after removal of solvents. Remarkable stability of cuboctahedron MOP 81 is noteworthy as the Pt-based MOP did not decompose upon addition of excess of nitric acid (480 equiv.). Elongated version of bent bispyridyl ligand unexpectedly gave cubic MOP $Pt(II)_6L_{12}$ when reacted with $Pt(NO_3)_2$, though the same ligand gave the $Pd(II)_{12}L_{24}$ sphere. Presumably $Pt(II)_6L_{12}$ cage is trapped as a metastable local-minimum structure on the potential surface in the self-assembly process, Pt(II)-pyridine interaction remain stronger even in presence of TFE. Mukherjee and coworkers had reported the synthesis of Pt-based MOP from tris-(imidazole) ligand and chiral *cis*-[(1S,2S)-dch]$Pt(NO_3)_2$ [where (1S,2S)-dch = (1S,2S)-1,2-diaminocyclohexane] [212]. 3:1 stoichiometric ratio in H_2O:MeOH yielded a [12 + 4] self-assembled chiral $M_{12}L_4$-type molecular tetrahedron. The $Pt(II)_{12}L_4$ tetrahedron MOP attains thermodynamic stability through positive cooperative effect of 24 Pt(II)-pym coordination bonds. The MOP features an interior cavity which successfully promotes the Michael addition reactions of a series of aromatic nitro-styrenes with indole through supramolecular catalysis.

N-donor based Pt MOP are generally robust by virtue of inert Pt-N interaction. In an interesting example Yang and coworkers [211] had reported the further stabilization of N-donor based Pt MOPs following their inclusion within the pores of other supported materials (Figure 26B). Corresponding starting materials allowed the subcomponent self-assembly to occur to prepare MOP 79 which was then further subjected to the verification of the hypothesis that mesoporous cavities can enhance the stability and activity of MOPs. Accordingly, mesoporous carbon FDU-16 was chosen. Porphyrin containing metallacycle MOP 79 was then successfully prepared within the pores of mesoporous carbon FDU-16 by adding the counterpart of metallacycle into the dipyridyl preloaded mesoporous matrix FDU-16. XRD, TEM and ICP measurements showed enhanced stability and maintenance of ordered structure without obvious aggregation of MOP. The greater stability and activity of MOP 79 within mesoporous cavity was further demonstrated by the enhanced catalytic performance of MOP following the encapsulation within the cavity. Porphyrins are known as photosensitizer to produce singlet oxygen $^1O_2$ upon photoirradiation. Embedding porphyrin macrocycles within metallacycle enables MOP 79 to produce singlet oxygen and improvement of singlet oxygen $^1O_2$ generation efficiency can be ascribed to the better stability and dispersity of MOP 79 in a confined space. Encapsulated MOP 79 was also used as heterogeneous catalyst for the oxidation of sulfide to sulfoxide. Photoirradiation exhibited better catalytic efficiency of MOP 79 to produce sulfoxide when MOP was encapsulated within the pores of mesoporous carbon FDU-16. Control experiment showed that encapsulation of MOP within the confined space has pronounced effect on the catalytic efficiency as the mixture of MOP 79 and mesoporous carbon as heterogenous catalyst is no better than MOP 79 only. Good reusability of mesoporous carbon confined MOP 79 catalyst was observed upto 5 cycles demonstrating the role of solid supports in enhancing the ability, dispersity and activity of MOPs.

Stang and coworkers have done extensive work on the preparation of platinum-based MOPs which showed enhanced kinetic stability due to the involvement of kinetically inert Pt-N interactions. Stang and coworkers have developed the methodology of preparing [*trans*-$Pt(PEt_3)_2NO_3$] unit metathesized organic linkers to self-assemble with multitopic pyridine linkers for the preparation of Pt-based MOPs. Remarkable chemical and solution (including aqueous stability) stabilities render MOP to be useful for various solution-based applications like sensing and biomedical applications, particularly for the development of antitumor agents in the treatment of malignant tumors. Stang and coworkers had

first envisaged that platinum-based self-assembled MOPs can be used to develop novel antitumor agents [213]. Reaction of 2,6-bis(pyrid-4-ylethynyl)aniline and 2,9-bis[trans-Pt(PEt₃)₂(OTf)]phenanthrene afforded tetranuclear platinum-based rhomboidal polygon MOP 82 (Figure 27A). MOP was found to be highly soluble and stable under physiological condition enabling them to be useful for biomedical applications. Remarkable fluorescence property of MOP 82 compared with free ligands allows them to be useful as contrast agent. No significant decrease in metabolism was observed from cytotoxicity studies suggesting low cytotoxicity of MOP 82 within the concentration range of 1 nM to 5 mM. Confocal microscopy showed that MOP 82 remained stable after cellular internalization and did not undergo any photobleaching. Significant tumor volume suppression (64%) was observed from in vivo efficacy study. This pioneering work demonstrated the promise of platinum-based self-assembled MOPs in developing novel antitumor agents. Following this pioneering work large body of research works have been carried out using Pt-based MOPs by Stang and other groups to demonstrate the promise of MOPs in general in biomedical and other potential applications [40,41]. Stang and other groups further extended the scope of using other inert metal ions to prepare stable MOPs containing N-donor ligands. Ruthenium is known to form inert metal complexes with pyridine-based organic ligands [214]. Chi, Stang and coworkers had reported the synthesis of MOPs using multitopic pyridine-based ligands and diruthenium metal clusters [215]. Dimeric ruthenium metal cluster was prepared by reacting bis-benzimidazole with [(*p*-cymene)RuCl₂]₂ complex in presence of sodium acetate. Post-treatment with silver triflate salt in methanol afforded diruthenium molecular clip suitable for use in the self-assembly process in combination with di- and tritopic organic linkers in order to prepare Ru-based MOP 83 and MOP 84 (Figure 27B). Both MOPs were found to be soluble and stable under physiological condition enabling them to demonstrate their antitumor activity toward various cancer cell lines. The antitumor action of these MOPs was evaluated, revealing that bis-benzimidazole-bridged MOPs have the potential to act as potent anticancer agents, particularly in cell lines which are resistant to other Pt-based molecules.
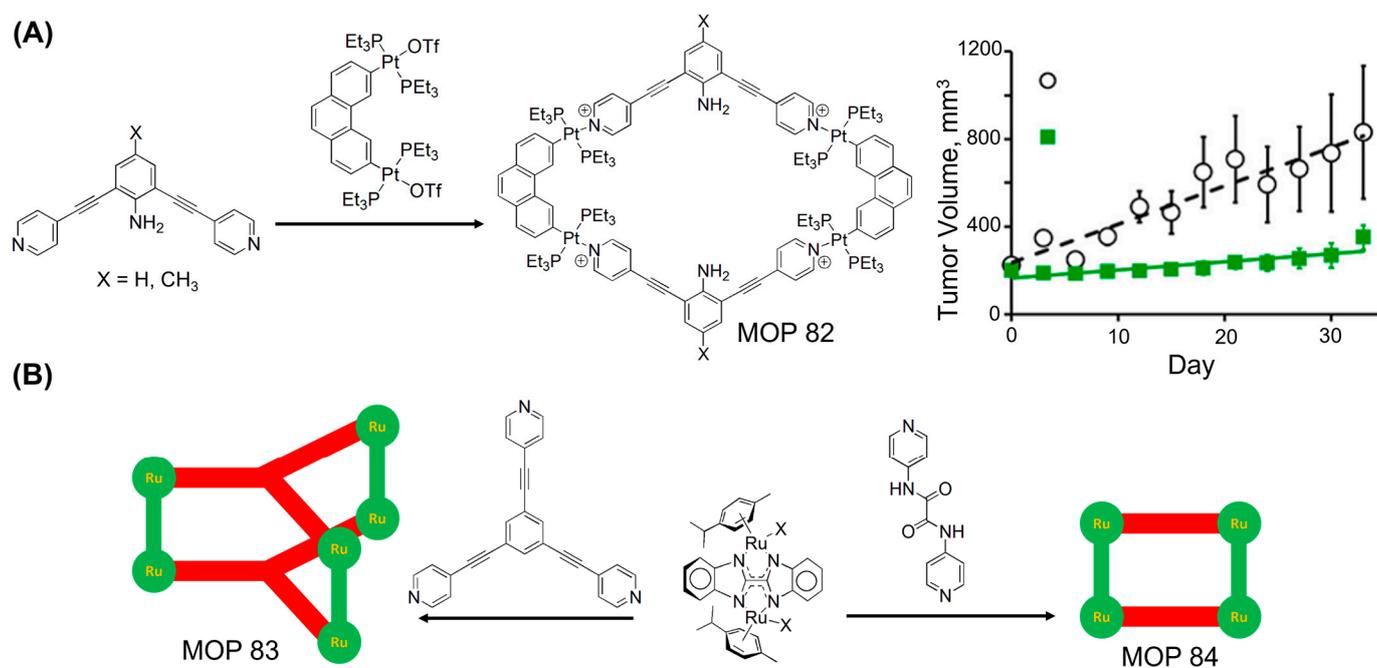

Figure 27. (**A**) Self-assembly of Pt-based supramolecular polygon MOP 82. Antitumor study of xenograft tumor bearing mice of breast cancer MDA-MB-231. (**B**) Use of diruthenium molecular spacer to prepare MOP 83 and MOP 84. Reprinted by permission from Refs. [213,215]. Copyright 2012 from American Chemical Society and copyright 2014 from National Academy of Sciences.

5. MOPs Containing Other Donor Ligands and Mixed Ligands (O- and N-Donor Ligands)

Apart from N-donor and O-donor based MOPs, MOPs containing mixed donor atoms are beginning to appear in literature in recent past. Substantial amount of works have been done to prepare MOPs using mixed ligands mostly containing N-donor, O-donor sites along with other donor atoms including phosphorus, sulfur and different type of metal ions. Generally, N-donor ligands tend to form stable complexes with soft metal ions. Metal complexes using negatively charged O atoms (in case of carboxylate or hydroxide ligand) form strong metal ligand complexes with hard metal ions through strong electrostatic interaction and orbital sharing to pair up electrons. N-donor ligands with neutral N-donor sites form strong complexes with relatively soft metal ions mostly through orbital sharing to pair up electrons and in this process N-donor sites develop partial positive charges on themselves. Although, the use of cooperative interactions renders strong complexes, the development of partial charges on each N-donor atoms attached to single metal center exert electrostatic repulsions to destabilize the M-L interactions. Therefore, MOPs containing mixed donor ligands (Figure 28) featuring both N-donor ligand and negatively charged O-donor ligand would expect to render stable structures as the opposite partial charged developed on both N-donor and O-donor sites contribute to enhance the stability of M-L bond through electrostatic attraction. The effect can further be amplified when inert metal ions are used during the self-assembly. Harrison and coworkers had reported the synthesis of resorcinarene ligand-based water soluble capsule MOP 85 equipped with iminodiacetate chelating groups bearing both N- and O-donor sites [64]. The MOP was readily assembled at pH 6, however the capsule disassembles upon lowering the pH to 1. Cui and coworkers had demonstrated (Figure 14A) the synthesis of chiral heterometallic MOP 30 (HMOP) derived from enantiopure Mn(salen), Cr(salen) and/or Fe(salen) as linear linkers and four Cp_3Zr_3 clusters as three-connected vertices featuring nanoscale hydrophobic cavities and the mixed linker cages bearing Mn(salen) and Cr (salen) species [143]. Heterometallic cage catalysts bearing Mn(salen) and Cr(salen) are shown to be efficient supramolecular catalysts for sequential asymmetric alkene epoxidation/epoxide ring-opening reactions with up to 99.9% *ee* demonstrating improved activity and enantioselectivity over free catalysts owing to the stabilization of catalytically active metallo-salen units and increased concentration of reactants within the cavities. Mukherjee and coworkers had reported the synthesis of triangular MOP 86 from ambivalent ligand bearing both N-donor and O-donor sites [216]. Muller and coworkers had reported the synthesis of octahedron MOP 87 from tris(2-hydroxybenzylidene)triaminoguanidinium chloride, 5,5-diethylbarbiturate (bar^{2-}) and $PdCl_2$ [217]. Palladium(II) metal ions are coordinatively attached to both N-donor and O-donor atoms. Stang and coworkers estimated the energetic gain of heteroleptic coordination environment bearing both N- and O-donor sites around model Pt metal center compared with homoleptic coordination environment bearing two identical-donor sites as $\Delta E = -364.6$ kJ/mol (Figure 28B) which is further manifested in multinuclear complexes to render stable mixed ligand MOP complexes [218]. Self-assembly of pyridyl containing di-, tri- and tetratopic ligands with linear dicarboxylate ligand and *cis*-$Pt(PEt_3)_2(OTf)_2$ linker afforded heteroleptic supramolecular rectangle, trigonal and tetragonal prism (MOP 88), respectively (Figure 28B) where each platinum metal center is heteroleptically coordinated to the ligands, favouring over homoleptic coordination. In an another report Stang and coworkers reported the synthesis of hexagonal prism prepared from amine/N-succinimide functionalized hexakispyridyl ligand, benzene-1,3-dicarboxylate and *cis*-$Pt(PEt_3)_2(OTf)_2$ [219]. MOPs prepared from mixed donor ligands showed excellent stability and therefore can be successfully used in postsynthetic modification. Amine functionalized MOP reacted with isocyanate or maleic anhydride to give post-functionalized MOPs. N-succinimide functionalized MOP undergoes cycloaddition reaction with anthracenyl derivatized ferrocene units.

Other metal ions including ruthenium (Ru) and rhodium (Rh) also known to form kinetically inert MOPs bearing ligands featuring N-donor, O-donor, S-donor, P-donor sites. Mirkin and coworkers had reported the synthesis of tetranuclear heterobimetallic square MOP 89 through cooperative ligand binding [220]. Phosphinothioester-based ligand with mononuclear Rh(I) and Zn(II) assembled in a heterobimetallic square where Rh(I) metal center is attached to phosphorous and sulfur atoms, and Zn(II) metal center is coordinated to nitrogen and oxygen atoms. A homometallic Rh(I) tetranuclear rectangular MOP 90 was isolated and structurally characterized where each Rh(I) metal center is coordinated to nitrogen and phosphorous atoms [221]. In an interesting report, Jin and coworkers had reported the synthesis of multinuclear MOPs prepared from half-sandwich rhodium complex [222]. Half-sandwich Rh(III) metal corners in combination with deprotonated 2,4-diacetyl-5-hydroxy-5-methyl-3-(3-pyridinyl)cyclohexanone (dhmpc) afforded hexagonal MOPs, MOP 91 and MOP 92 (Figure 28). The synthesis of multinuclear MOP was very much dependent on the counter anions used in self-assembly as the anions templated the formation of metalla-macrocycles. When counter anion BF_4^- was used, tetranuclear MOP $[(Cp^*RhL)_4][BF_4]_4$ was formed. Larger counter anions like OTf^-, PF_6^- and SbF_6^- favoured the formation of hexanuclear MOPs $[(Cp^*RhL)_6 \supset 2OTf][OTf]_4$, $[(Cp^*RhL)_6 \supset 2PF_6][PF_6]_4$, and $[(Cp^*RhL)_6 \supset 2SbF_6][SbF_6]_4 \bullet 6CH_3CN$. Interestingly, the MOPs showed excellent air stability and didn't undergo any degradation over months.

Therrien and coworkers had envisaged that use of ruthenium metal ions in combination with mixed donor ligands would give rise to stable MOPs [65]. Combining the ruthenium-based half-sandwich complexes with N-donor and O-donor based ligands enable to synthesize ruthenium based MOP 92, $[Ru_6(p\text{-}^iPrC_6H_4Me)_6(tpt)_2(dhbq\text{-}1)_3]^{6+}$, which incorporates p-cymene ruthenium building blocks bridged together by 2,5-dihydroxy-1,4-benzo-quinonato (dhbq) ligand and two 2,4,6-tris(pyridin-4-yl)-1,3,5-triazine (tpt) panels. The reaction between diruthenium complex $[Ru_2(p\text{-}^iPrC_6H_4Me)_2\text{-}(dhbq)Cl_2]$ and tpt units in the presence of AgO_3SCF_3 afforded water soluble MOP (Figure 29C) which remains water stable. Following this approach Stang, Chi and coworkers had also reported the synthesis of several ruthenium-based MOPs [223,224]. Authors further extended the scope of the synthesis by preparing the diruthenium spacer from several organic ligands like oxalate, tetrahydroxy naphthalene and tetrahydroxy tetracene; and variable multitopic pyridyl-based ligands. Use of four types of diruthenium spacers (oxalate, dhbq, donq and dotq) with trispyridyl ligand led to the preparation of four different MOPs in triangular prism shape (Figure 29A,B) [225]. Use of meta-directed bispyridine linkers gave rectangular MOPs [226]. Incorporating varied functionalities (like azo or amide units) within the linkers allowed to prepare multifunctional ruthenium-based MOPs [227,228]. Use of asymmetric bis(pyridyl) ligands gave Ru-based isomeric MOPs [229]. Stang and coworkers had envisaged to incorporate Pt-based bispyridyl linkers into the Ru-based MOPs to develop mixed-metal MOPs. Self-assembly of diruthenium complexes (oxalate, dhbq, donq and dotq) with bispyridyl ligand embedded with Pt-metal afforded four rectangular MOPs [230]. Exceptional stability of Ru-based MOPs enables them to exhibit their abilities to act as antitumor agents towards various cancer cell lines. Stang and coworkers had observed that Ru-based MOPs exhibited better antitumor activity in comparison with platinum-based drugs like cisplatin. Interestingly, Pt-Ru mixed metal MOPs also showed cytotoxicity towards various cancer cell lines. Comparative study indicated that the mixed-metal MOPs containing Ru and Pt exhibited highest cytotoxicity. The Ru-Pt mixed metal MOPs and Ru-based MOPs showed better activity against some cell lines in comparison with cisplatin which showed poor cytotoxicity. Therrien and coworkers had demonstrated that excellent stability of Ru-based MOP 93 enable them to act as carrier for transporting biomedically relevant cargoes (Figure 29C) [65]. Trigonal prism MOP 93 was able to encapsulate $[(acac)_2M]$ (M = Pd, Pt; acac = acetylacetonato) as guest molecule within its cavity as observed by X-ray crystallography. ^{1}H NMR study showed excellent aque-

ous stability of trigonal prism MOP and its host-guest complexes ([(acac)$_2$M]@MOP 93, M = Pd, Pt). Prolonged aqueous exposure triggered the partial release of guests from the MOP cavity where [(acac)$_2$Pd] guest is released to a greater extent from MOP cavity compared to [(acac)$_2$Pt] guest. The free complexes [(acac)$_2$M] (M = Pd, Pt) which are hydrophobic did not exhibit any cytotoxicities toward ovarian cancer cells, A2780. The host-guest complexes (IC$_{50}$ = 12 mM for [(acac)$_2$Pt@MOP 93]; 1 mM for [(acac)$_2$Pd@MOP]) were found to be significantly more cytotoxic than pristine MOP 93 (IC$_{50}$ = 23 mM). Excellent water solubility and stability endow mixed ligand-based ruthenium MOP 93 to deliver diverse fluorescent agents and antitumor drugs to the cancer cells. Pyrene is well-known for its remarkable fluorescence property and it exhibits affinity towards the Ru-based MOP 93. Ru-MOP was able to bind series of pyrene derivatives with diverse functional groups within its cavity (Figure 29C). Two of the pyrene derivatives—sulfonamide containing pyrene (carbonic anhydrase inhibitor) and ethacrynamide containing pyrene (glutathione transferase inhibitor) form complexes with Ru-MOP 93 and exhibit cytotoxicities similar to cisplatin drug [231]. Subsequently, a prodrug of floxuridine was prepared by attaching pyrene substrate which enables to bind the floxuridine-prodrug within the cavity of Ru-MOP to produce floxuridine-prodrug@MOP 93 complex [232]. Host-guest complex exhibited better cellular uptake of the prodrug and enhanced cytotoxicity (IC$_{50}$ = 0.3 μM) compared to the parent drug floxuridine which suffered poor cellular uptake (Table 3) and bioavailability due to poor water solubility, can be considered as alternative therapeutic approach. Subsequently, Therrien and coworkers had studied the stability of Ru-based MOP 93 inside cancer cells by studying the drug release mechanism [233]. 1-(4,6-dichloro-1,3,5-triazin-2-yl)pyrene (py-tz) derivative was used as a probe for the study. Py-tz undergoes fluorescence quenching inside MOP 93 enabling to visualize the release of guest molecule from the Ru-MOP 93 cavity following cellular internalization using fluorescence microscopy (Figure 29D). Cellular internalization of intrinsically poorly water soluble py-tz was significantly enhanced following their encapsulation within MOP cavity demonstrating the ability of Ru-based MOP to successfully carry cargo molecules inside the cells. Fluorescent microscopy study (Figure 29D) revealed no guest release from the cavity following cellular internalization at pH 2 and pH 7. But at pH 12, the pyrenyl derivative was released from the Ru-MOP cavity due to the destruction of the Ru-MOP structure inside the cell lines as evidenced from enhanced fluorescence intensity observed from the cells following the treatment with host-guest complex. This study demonstrated the potential of water-soluble and water-stable MOPs to be useful as cargo delivery vehicles for potential biomedical applications [38,40,41].

Table 3. Describing the cytotoxicities of cisplatin, MOP 93 and guest encapsulated MOP 93 (guest⊃MOP 93) towards A2780 cells.

Materials	IC$_{50}$
[(acac)$_2$Pd]@MOP 93	1 μM
[(acac)$_2$Pt]@MOP 93	23 μM
[pyrene-sulfonamide]@MOP 93	2 μM
[pyrene-ethacrynamide]@MOP 93	3 μM
[pyrene-floxuridine]@MOP 93	0.3 μM
cisplatin MOP 93	1.6 μM 23 μM
Py-tz@MOP 93	6 μM

(A)

MOP 85   MOP 86   MOP 87

(B)

MOP 88

(C)

MOP 89

MOP 90

(D)

MOP 92

MOP 91

= η5-pentamethylcyclopentadienyl (Cp*)

M = Rh

= HL
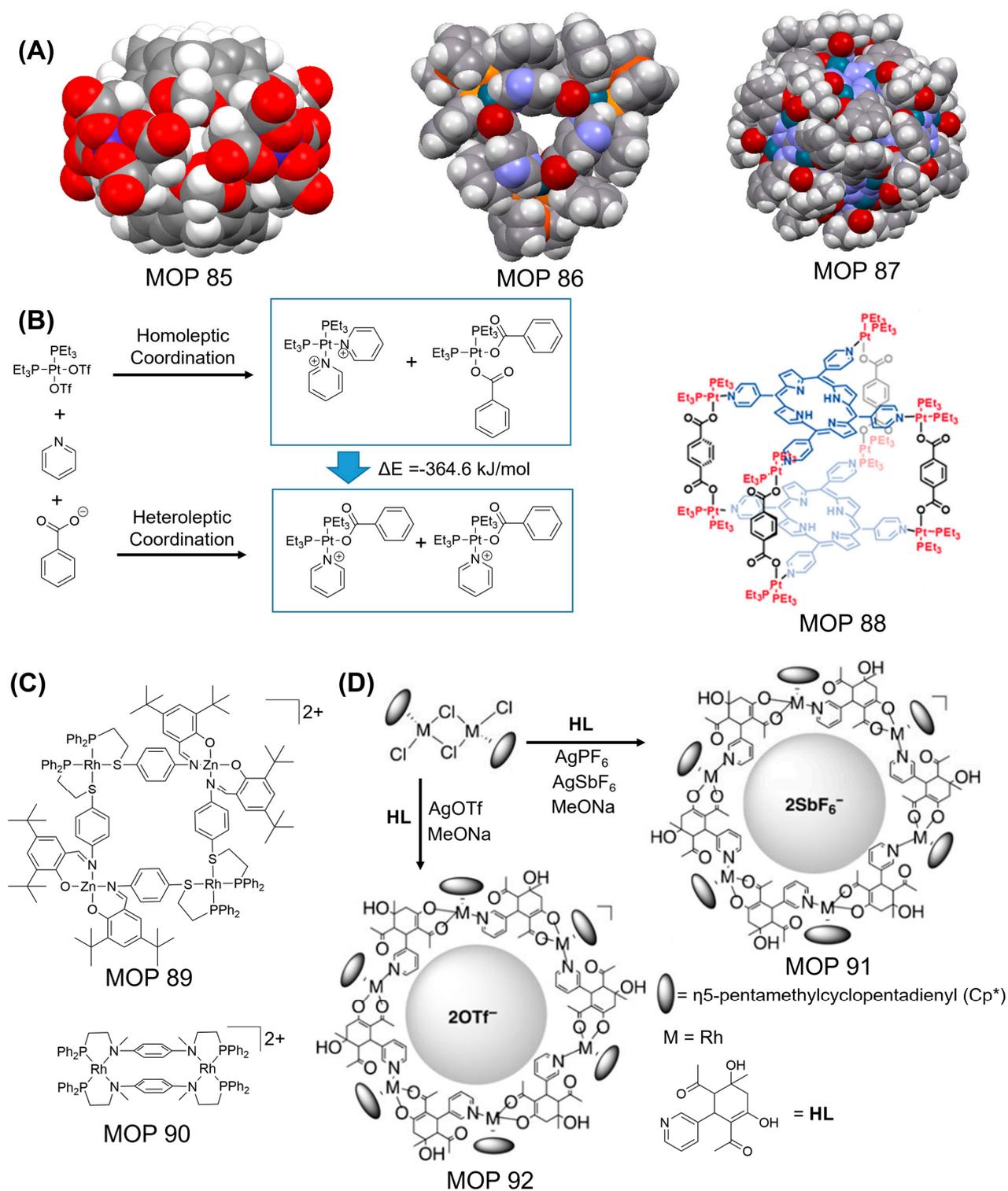
Figure 28. (**A**) Space-filling model of X-ray crystal structures of MOP 85, MOP 86 and MOP 87. (**B**) Selective self-assembly of *cis*-Pt(PEt₃)₂(OTf)₂ with carboxylate and pyridyl moieties due to low energy of the heteroleptic coordination pathway. Chemical structure of tetragonal prism MOP 88. (**C**) Chemical structures of mixed donor atoms containing polygons MOP 89 and MOP 90. (**D**) Templated synthesis of mixed donor atoms bearing polygons MOP 91 and MOP 92. Reprinted by permission form refs. [64,216–218,222]. Copyright 1998 and 2010 from American Chemical Society. Copyright 2009 from Royal Society of Chemistry. Copyright 2004 and 2011 from Wiley-VCH.
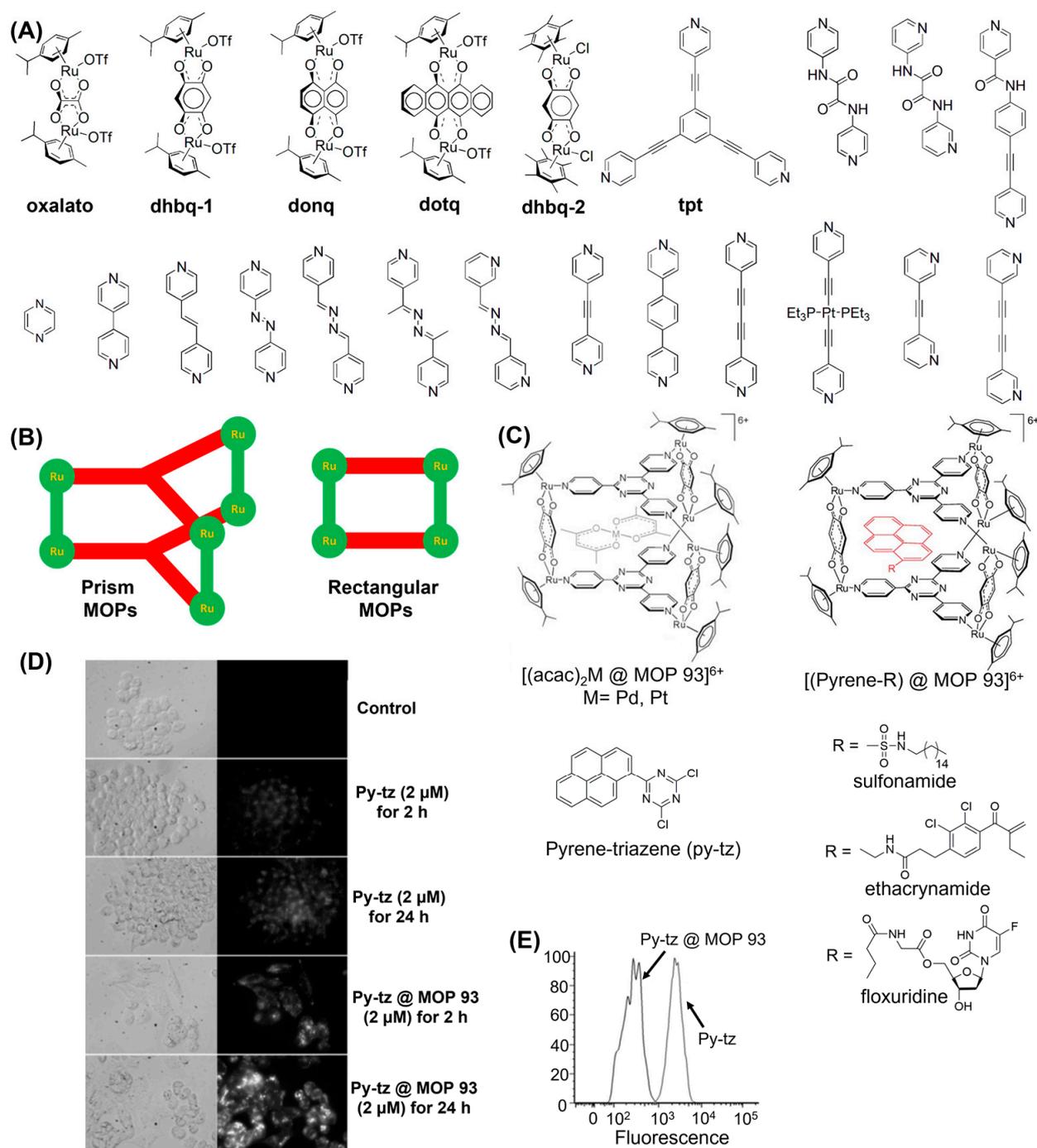
Figure 29. (**A**) Diruthenium molecular spacers (oxalato, dhbq-1, donq, dotq, dhbq-2) undergo self-assembly with ditopic and tritopic pyridyl donors to give metal organic polygons (MOPs). (**B**) Cartoon representation of [2 + 2] and [2 + 3] ruthenium-based MOP. (**C**) Molecular structure of [(acac)$_2$M@MOP 93], M = Pd, Pt is presented. Encapsulation of pyrene derivatives (Pyrene-R) inside MOP 93 give Pyrene-R@MOP 93. (**D**) Microscopy images of cells incubated with py-tz and py-tz@MOP 93, transmitted light (left) and fluorescent (right). (**E**) Flow cytometry study of A2780 cells treated with Py-tz@MOP 93 demonstrated transportation and release of Py-tz inside cancer cell. Reprinted by permission from refs. [65,232,233]. Copyright 2008 and 2010 from Wiley-VCH. Copyright 2012 from American Chemical Society.

6. Summary and Future Outlook

Coordination chemistry is a vibrant discipline in the field of chemistry to study mostly the interaction between organic ligands and metal ions. Over the decades, the field has become matured enough to take its leap from studying simplest building blocks (mostly monometallic complexes) to the preparation of complex metal-ligand structures. Multimetallic coordination structures can be broadly categorized in two sections: discrete structures and network structures. Network structures which can be both nonporous and porous are called as coordination polymers (CPs) and crystalline metal organic frameworks (MOFs). Basic structural units held together by covalent/noncovalent interactions in repetition gave the frameworks. In contrast, discrete structures which generally lack intermolecular interactions between themselves are popularly called as MOPs. By virtue of intrinsic and extrinsic porosities, both MOPs and MOFs were become very useful for various applications. Advancement of crystallographic and computation techniques allows the scientists to design novel structures tailored to guest recognition has tremendously impacted the field of metal coordination chemistry, particularly. Therefore, designing the metal organic structures with appropriate molecular details enable to synthesize functional materials. However, the major remaining challenges are mostly the maintenance of thermal, chemical and mechanical stabilities of metal organic materials. One of the foremost concerns is to render metal organic materials aqueous-stable in order for them to be useful for real-world application. Various approaches include the increase of metal-ligand entanglement can have significant effect on the stability of MOPs as the MOPs prepared from multitopic ligands were found to be more stable compared with MOPs prepared from less-dense linkers. Examples from Fujita [72] and Nitschke [174] show that MOPs prepared from multitopic linkers are significantly stable. MOPs prepared from ligands bearing various donor atoms are mostly remain vulnerable due to weak metal ligand interactions. Systematic works have been carried out to prepare MOPs by using inert metal ions and it was found that MOPs prepared from inert metal ions were stable enough to withstand chemical, thermal and mechanical stress subject to relevant applications. Accordingly, this review article summarizes the instability issues of MOPs and several strategies to prepare stable MOPs [66]. Other approaches are indirect approaches which include trapping the fragile MOPs inside more robust structures (like other solid supports or metal organic frameworks) or transforming them into more robust networks. In general MOPs synthesized from N-donor ligands and soft metal ions were found to be more stable compared MOPs prepared from O-donor ligands. Systematic study showed that robust MOPs can be synthesized by choosing appropriate ligands and metal ions. Nitschke and coworkers had reported the synthesis of water-proof MOPs (with half-life > months) using first row transition metal ions [174]. Fujita and coworkers had reported the synthesis of N-donor based MOPs using platinum metal ions that are known to form inert Pt-N bond. Both octahedron and cuboctahedron MOPs (MOP 80 and MOP 81) were found to be stable under aqueous pH range 1–11 [209,210], demonstrating that exceptional stability can be achieved by tuning metal-ligand interaction. Mixed-ligand strategy was also appeared to be suitable strategy for the preparation of stable MOPs. Stang and coworkers had demonstrated the achievement of overall thermodynamic gain in preparing mixed ligand MOPs [218] compared with the corresponding N-donor and O-donor based homoleptic MOPs. Therrien and coworkers had prepared mixed-donor based Ru-MOPs to deliver cargoes to the cancer cells [65] and to demonstrate that MOPs stability is crucial to investigate the properties of functional materials.

The field of metal organic polygons and polyhedra (MOPs) is a flourishing area of research with far reaching potential applications. Despite these well-developed strategies to prepare MOPs, so far limited number of literature reports are there on thermally and hydrolytically stable MOPs, and thus requires further development of synthetic strategies to prepare stable MOPs tailored to suitable applications. Another challenge includes the advancement of characterization techniques including crystallographic technique as achieving structural characterization often becomes difficult with traditional single crystal

techniques. Therefore, synergistic progress on the development of synthetic methodologies and characterization techniques would offer promising strategies to prepare and characterize stable MOPs for developing practical applications in biological, industrial and chemical synthesis area.

Data Availability Statement: Data sharing not applicable.

Conflicts of Interest: Author declares no conflict of interest.

References

1. Lehn, J.M. *Supramolecular Chemistry: Concepts and Perspectives*; VCH: Weinheim, Germany, 1995.
2. Zaworotko, M.J.; Seddon, K.R. *Crystal Engineering: The Design and Application of Functional Solids*; Kluwer: Dordrecht, The Netherlands, 1999.
3. Perry Iv, J.J.; Perman, J.A.; Zaworotko, M.J. Design and synthesis of metal–organic frameworks using metal–organic polyhedra as supermolecular building blocks. *Chem. Soc. Rev.* **2009**, *38*, 1400–1417. [CrossRef] [PubMed]
4. Chakrabarty, R.; Mukherjee, P.S.; Stang, P.J. Supramolecular Coordination: Self-Assembly of Finite Two- and Three-Dimensional Ensembles. *Chem. Rev.* **2011**, *111*, 6810–6918. [CrossRef] [PubMed]
5. Cook, T.R.; Zheng, Y.-R.; Stang, P.J. Metal–Organic Frameworks and Self-Assembled Supramolecular Coordination Complexes: Comparing and Contrasting the Design, Synthesis, and Functionality of Metal–Organic Materials. *Chem. Rev.* **2013**, *113*, 734–777. [CrossRef] [PubMed]
6. Ding, M.; Flaig, R.W.; Jiang, H.-L.; Yaghi, O.M. Carbon capture and conversion using metal–organic frameworks and MOF-based materials. *Chem. Soc. Rev.* **2019**, *48*, 2783–2828. [CrossRef]
7. Tranchemontagne, D.J.; Mendoza-Cortés, J.L.; O'Keeffe, M.; Yaghi, O.M. Secondary building units, nets and bonding in the chemistry of metal–organic frameworks. *Chem. Soc. Rev.* **2009**, *38*, 1257–1283. [CrossRef]
8. De, S.; Mahata, K.; Schmittel, M. Metal-coordination-driven dynamic heteroleptic architectures. *Chem. Soc. Rev.* **2010**, *39*, 1555–1575. [CrossRef]
9. Brown, C.J.; Toste, F.D.; Bergman, R.G.; Raymond, K.N. Supramolecular Catalysis in Metal–Ligand Cluster Hosts. *Chem. Rev.* **2015**, *115*, 3012–3035. [CrossRef]
10. Xu, L.; Wang, Y.-X.; Chen, L.-J.; Yang, H.-B. Construction of multiferrocenyl metallacycles and metallacages via coordination-driven self-assembly: From structure to functions. *Chem. Soc. Rev.* **2015**, *44*, 2148–2167. [CrossRef]
11. McConnell, A.J.; Wood, C.S.; Neelakandan, P.P.; Nitschke, J.R. Stimuli-Responsive Metal–Ligand Assemblies. *Chem. Rev.* **2015**, *115*, 7729–7793. [CrossRef]
12. Saha, R.; Mondal, B.; Mukherjee, P.S. Molecular Cavity for Catalysis and Formation of Metal Nanoparticles for Use in Catalysis. *Chem. Rev.* **2022**, *122*, 12244–12307. [CrossRef]
13. Leong, W.L.; Vittal, J.J. One-Dimensional Coordination Polymers: Complexity and Diversity in Structures, Properties, and Applications. *Chem. Rev.* **2011**, *111*, 688–764. [CrossRef] [PubMed]
14. Chen, C.-T.; Suslick, K.S. One-dimensional coordination polymers: Applications to material science. *Coord. Chem. Rev.* **1993**, *128*, 293–322. [CrossRef]
15. Khlobystov, A.N.; Blake, A.J.; Champness, N.R.; Lemenovskii, D.A.; Majouga, A.G.; Zyk, N.V.; Schröder, M. Supramolecular design of one-dimensional coordination polymers based on silver(I) complexes of aromatic nitrogen-donor ligands. *Coord. Chem. Rev.* **2001**, *222*, 155–192. [CrossRef]
16. Yaghi, O.M.; Li, H.; Davis, C.; Richardson, D.; Groy, T.L. Synthetic Strategies, Structure Patterns, and Emerging Properties in the Chemistry of Modular Porous Solids. *Acc. Chem. Res.* **1998**, *31*, 474–484. [CrossRef]
17. Wang, Q.; Astruc, D. State of the Art and Prospects in Metal–Organic Framework (MOF)-Based and MOF-Derived Nanocatalysis. *Chem. Rev.* **2020**, *120*, 1438–1511. [CrossRef]
18. Ohtani, R.; Kitagawa, S. Comprehensive Coordination Chemistry III. *Elsevier* **2021**, *7*, 314–327.
19. Zhou, H.-C.; Long, J.R.; Yaghi, O.M. Introduction to Metal–Organic Frameworks. *Chem. Rev.* **2012**, *112*, 673–674. [CrossRef]
20. Zaworotko, M.J. Crystal engineering of diamondoid networks. *Chem. Soc. Rev.* **1994**, *23*, 283–288. [CrossRef]
21. Fujita, M. Metal-directed self-assembly of two- and three-dimensional synthetic receptors. *Chem. Soc. Rev.* **1998**, *27*, 417–425. [CrossRef]
22. Eddaoudi, M.; Kim, J.; Wachter, J.B.; Chae, H.K.; O'Keeffe, M.; Yaghi, O.M. Porous Metal-Organic Polyhedra: 25 Å Cuboctahedron Constructed from 12 Cu2(CO2)4 Paddle-Wheel Building Blocks. *J. Am. Chem. Soc.* **2001**, *123*, 4368–4369. [CrossRef]
23. Moulton, B.; Lu, J.; Mondal, A.; Zaworotko, M.J. Nanoballs: Nanoscale faceted polyhedra with large windows and cavities. *Chem. Commun.* **2001**, *37*, 863–864. [CrossRef]
24. Caulder, D.L.; Raymond, K.N. Supermolecules by Design. *Acc. Chem. Res.* **1999**, *32*, 975–982. [CrossRef]
25. Cook, T.R.; Stang, P.J. Recent Developments in the Preparation and Chemistry of Metallacycles and Metallacages via Coordination. *Chem. Rev.* **2015**, *115*, 7001–7045. [CrossRef] [PubMed]

26. Leininger, S.; Olenyuk, B.; Stang, P.J. Self-Assembly of Discrete Cyclic Nanostructures Mediated by Transition Metals. *Chem. Rev.* **2000**, *100*, 853–908. [CrossRef] [PubMed]

27. Olenyuk, B.; Whiteford, J.A.; Fechtenkötter, A.; Stang, P.J. Self-assembly of nanoscale cuboctahedra by coordination chemistry. *Nature* **1999**, *398*, 796–799. [CrossRef] [PubMed]

28. Percástegui, E.G.; Ronson, T.K.; Nitschke, J.R. Design and Applications of Water-Soluble Coordination Cages. *Chem. Rev.* **2020**, *120*, 13480–13544. [CrossRef]

29. Zhang, D.; Ronson, T.K.; Zou, Y.-Q.; Nitschke, J.R. Metal–organic cages for molecular separations. *Nat Rev Chem.* **2021**, *5*, 168–182. [CrossRef]

30. Ghasempour, H.; Wang, K.-Y.; Powell, J.A.; ZareKarizi, F.; Lv, X.-L.; Morsali, A.; Zhou, H.-C. Metal–organic frameworks based on multicarboxylate linkers. *Coord. Chem. Rev.* **2021**, *426*, 213542. [CrossRef]

31. Lu, W.; Wei, Z.; Gu, Z.-Y.; Liu, T.-F.; Park, J.; Park, J.; Tian, J.; Zhang, M.; Zhang, Q.; Gentle Iii, T.; et al. Tuning the structure and function of metal–organic frameworks via linker design. *Chem. Soc. Rev.* **2014**, *43*, 5561–5593. [CrossRef]

32. Lee, S.; Jeong, H.; Nam, D.; Lah, M.S.; Choe, W. The rise of metal–organic polyhedra. *Chem. Soc. Rev.* **2021**, *50*, 528–555. [CrossRef]

33. Ahmad, N.; Chughtai, A.H.; Younus, H.A.; Verpoort, F. Discrete metal-carboxylate self-assembled cages: Design, synthesis and applications. *Coord. Chem. Rev.* **2014**, *280*, 1–27. [CrossRef]

34. Gianneschi, N.C.; Masar, M.S.; Mirkin, C.A. Development of a Coordination Chemistry-Based Approach for Functional Supramolecular Structures. *Acc. Chem. Res.* **2005**, *38*, 825–837. [CrossRef] [PubMed]

35. Pitt, M.A.; Johnson, D.W. Main group supramolecular chemistry. *Chem. Soc. Rev.* **2007**, *36*, 1441–1453. [CrossRef] [PubMed]

36. Lee, S.J.; Lin, W. Chiral Metallocycles: Rational Synthesis and Novel Applications. *Acc. Chem. Res.* **2008**, *41*, 521–537. [CrossRef] [PubMed]

37. Tidmarsh, I.S.; Faust, T.B.; Adams, H.; Harding, L.P.; Russo, L.; Clegg, W.; Ward, M.D. Octanuclear Cubic Coordination Cages. *J. Am. Chem. Soc.* **2008**, *130*, 15167–15175. [CrossRef]

38. Wang, C.; Wang, W.; Tan, J.; Zhang, X.; Yuan, D.; Zhou, H.-C. Coordination-based molecular nanomaterials for biomedically relevant applications. *Coord. Chem. Rev.* **2021**, *438*, 213752. [CrossRef]

39. Kuppler, R.J.; Timmons, D.J.; Fang, Q.-R.; Li, J.-R.; Makal, T.A.; Young, M.D.; Yuan, D.; Zhao, D.; Zhuang, W.; Zhou, H.-C. Potential applications of metal-organic frameworks. *Coord. Chem. Rev.* **2009**, *253*, 3042–3066. [CrossRef]

40. Samanta, S.K.; Isaacs, L. Biomedical applications of metal organic polygons and polyhedra (MOPs). *Coord. Chem. Rev.* **2020**, *410*, 213181. [CrossRef]

41. Sepehrpour, H.; Fu, W.; Sun, Y.; Stang, P.J. Biomedically relevant self-assembled metallacycles and metallacages. *J. Am. Chem. Soc.* **2019**, *141*, 14005–14020. [CrossRef]

42. Chaemchuen, S.; Kabir, N.A.; Zhou, K.; Verpoort, F. Metal–organic frameworks for upgrading biogas via CO2 adsorption to biogas green energy. *Chem. Soc. Rev.* **2013**, *42*, 9304–9332. [CrossRef]

43. Ahmad, N.; Younus, H.A.; Chughtai, A.H.; Verpoort, F. Metal–organic molecular cages: Applications of biochemical implications. *Chem. Soc. Rev.* **2015**, *44*, 9–25. [CrossRef] [PubMed]

44. Koblenz, T.S.; Wassenaar, J.; Reek, J.N.H. Reactivity within a confined self-assembled nanospace. *Chem. Soc. Rev.* **2008**, *37*, 247–262. [CrossRef] [PubMed]

45. Mason, J.A.; Veenstra, M.; Long, J.R. Evaluating metal–organic frameworks for natural gas storage. *Chem. Sci.* **2014**, *5*, 32–51. [CrossRef]

46. Peng, Y.; Krungleviciute, V.; Eryazici, I.; Hupp, J.T.; Farha, O.K.; Yildirim, T. Methane Storage in Metal–Organic Frameworks: Current Records, Surprise Findings, and Challenges. *J. Am. Chem. Soc.* **2013**, *135*, 11887–11894. [CrossRef] [PubMed]

47. Bolliger, J.L.; Ronson, T.K.; Ogawa, M.; Nitschke, J.R. Solvent Effects upon Guest Binding and Dynamics of a FeII4L4 Cage. *J. Am. Chem. Soc.* **2014**, *136*, 14545–14553. [CrossRef] [PubMed]

48. Plajer, A.J.; Percástegui, E.G.; Santella, M.; Rizzuto, F.J.; Gan, Q.; Laursen, B.W.; Nitschke, J.R. Fluorometric Recognition of Nucleotides within a Water-Soluble Tetrahedral Capsule. *Angew. Chem. Inter. Ed.* **2019**, *58*, 4200–4204. [CrossRef] [PubMed]

49. Park, K.S.; Ni, Z.; Cote, A.P.; Choi, J.Y.; Huang, R.; Uribe-Romo, F.J.; Chae, H.K.; O'Keeffe, M.; Yaghi, O.M. Exceptional chemical and thermal stability of zeolitic imidazolate frameworks. *Proc. Natl. Acad. Sci. USA* **2006**, *103*, 10186–10191. [CrossRef] [PubMed]

50. Canivet, J.; Fateeva, A.; Guo, Y.; Coasne, B.; Farrusseng, D. Water adsorption in MOFs: Fundamentals and applications. *Chem. Soc. Rev.* **2014**, *43*, 5594–5617. [CrossRef]

51. Barea, E.; Montoro, C.; Navarro, J.A.R. Toxic gas removal-metal–organic frameworks for the capture and degradation of toxic gases and vapours. *Chem. Soc. Rev.* **2014**, *43*, 5419–5430. [CrossRef]

52. DeCoste, J.B.; Peterson, G.W. Metal–Organic Frameworks for Air Purification of Toxic Chemicals. *Chem. Rev.* **2014**, *114*, 5695–5727. [CrossRef]

53. Horcajada, P.; Gref, R.; Baati, T.; Allan, P.K.; Maurin, G.; Couvreur, P.; Férey, G.; Morris, R.E.; Serre, C. Metal–Organic Frameworks in Biomedicine. *Chem. Rev.* **2012**, *112*, 1232–1268. [CrossRef] [PubMed]

54. Eddaoudi, M.; Sava, D.F.; Eubank, J.F.; Adil, K.; Guillerm, V. Zeolite-like metal–organic frameworks (ZMOFs): Design, synthesis, and properties. *Chem. Soc. Rev.* **2015**, *44*, 228–249. [CrossRef] [PubMed]

55. Li, J.-R.; Kuppler, R.J.; Zhou, H.-C. Selective gas adsorption and separation in metal–organic frameworks. *Chem. Soc. Rev.* **2009**, *38*, 1477–1504. [CrossRef] [PubMed]

56. Zhao, X.; Bu, X.; Wu, T.; Zheng, S.-T.; Wang, L.; Feng, P. Selective anion exchange with nanogated isoreticular positive metal-organic frameworks. *Nat. Commun.* **2013**, *4*, 2344. [CrossRef] [PubMed]
57. Liu, X.; Demir, N.K.; Wu, Z.; Li, K. Highly Water-Stable Zirconium Metal–Organic Framework UiO-66 Membranes Supported on Alumina Hollow Fibers for Desalination. *J. Am. Chem. Soc.* **2015**, *137*, 6999–7002. [CrossRef] [PubMed]
58. Abourahma, H.; Coleman, A.W.; Moulton, B.; Rather, B.; Shahgaldian, P.; Zaworotko, M.J. Hydroxylated nanoballs: Synthesis, crystal structure, solubility and crystallization on surfaces. *Chem. Commun.* **2001**, *37*, 2380–2381. [CrossRef]
59. Brückner, C.; Powers, R.E.; Raymond, K.N. Symmetry-Driven Rational Design of a Tetrahedral Supramolecular Ti4L4 Cluster. *Angew. Chem. Inter. Ed.* **1998**, *37*, 1837–1839. [CrossRef]
60. Fujita, M.; Yazaki, J.; Ogura, K. Preparation of a macrocyclic polynuclear complex, [(en)Pd(4,4′-bpy)]4(NO3)8 (en = ethylene-diamine, bpy = bipyridine), which recognizes an organic molecule in aqueous media. *J. Am. Chem. Soc.* **1990**, *112*, 5645–5647. [CrossRef]
61. Fujita, M.; Oguro, D.; Miyazawa, M.; Oka, H.; Yamaguchi, K.; Ogura, K. Self-assembly of ten molecules into a nanometer-sized organic host frameworks. *Nature* **1995**, *378*, 469–471. [CrossRef]
62. Mal, P.; Schultz, D.; Beyeh, K.; Rissanen, K.; Nitschke, J.R. An unlockable-relockable iron cage by subcomponent self-assembly. *Angew. Chem. Int. Ed.* **2008**, *47*, 8297–8301. [CrossRef]
63. Howlader, P.; Mondal, B.; Purba, P.C.; Zangrando, E.; Mukherjee, P.S. Self-Assembled Pd(II) Barrels as Containers for Transient Merocyanine Form and Reverse Thermochromism of Spiropyran. *J. Am. Chem. Soc.* **2018**, *140*, 7952–7960. [CrossRef] [PubMed]
64. Fox, O.D.; Dalley, N.K.; Harrison, R.G. A Metal-Assembled, pH-Dependent, Resorcinarene-Based Cage Molecule. *J. Am. Chem. Soc.* **1998**, *120*, 7111–7112. [CrossRef]
65. Therrien, B.; Suess-Fink, G.; Govindaswamy, P.; Renfrew, A.K.; Dyson, P.J. The "complex-in-a-complex" cations [(acac)2M⊂Ru6-(p-iPrC6H4Me)6(tpt)2(dhbq)3]6+: A trojan horse for cancer cells. *Angew. Chem. Int. Ed.* **2008**, *47*, 3773–3776. [CrossRef] [PubMed]
66. Mollick, S.; Fajal, S.; Mukherjee, S.; Ghosh, S.K. Stabilizing Metal–Organic Polyhedra (MOP): Issues and Strategies. *Chem. Asian J.* **2019**, *14*, 3096–3108. [CrossRef] [PubMed]
67. Bistri, O.; Reinaud, O. Supramolecular control of transition metal complexes in water by a hydrophobic cavity: A bio-inspired strategy. *Org. Biomol. Chem.* **2015**, *13*, 2849–2865. [CrossRef]
68. Feng, L.; Wang, K.-Y.; Day, G.S.; Ryder, M.R.; Zhou, H.-C. Destruction of Metal–Organic Frameworks: Positive and Negative Aspects of Stability and Lability. *Chem. Rev.* **2020**, *120*, 13087–13133. [CrossRef]
69. Howarth, A.J.; Liu, Y.; Li, P.; Li, Z.; Wang, T.C.; Hupp, J.T.; Farha, O.K. Chemical, thermal and mechanical stabilities of metal–organic frameworks. *Nat. Rev. Mater.* **2016**, *1*, 15018. [CrossRef]
70. Taube, H. Rates and Mechanisms of Substitution in Inorganic Complexes in Solution. *Chem. Rev.* **1952**, *50*, 69–126. [CrossRef]
71. Richens, D.T. Ligand Substitution Reactions at Inorganic Centers. *Chem. Rev.* **2005**, *105*, 1961–2002. [CrossRef]
72. Sato, S.; Ishido, Y.; Fujita, M. Remarkable Stabilization of M12L24 Spherical Frameworks through the Cooperation of 48 Pd(II)-Pyridine Interactions. *J. Am. Chem. Soc.* **2009**, *131*, 6064–6065. [CrossRef]
73. Sun, B.; Wang, M.; Lou, Z.; Huang, M.; Xu, C.; Li, X.; Chen, L.-J.; Yu, Y.; Davis, G.L.; Xu, B.; et al. From Ring-in-Ring to Sphere-in-Sphere: Self-Assembly of Discrete 2D and 3D Architectures with Increasing Stability. *J. Am. Chem. Soc.* **2015**, *137*, 1556–1564. [CrossRef] [PubMed]
74. Zhao, D.; Tan, S.; Yuan, D.; Lu, W.; Rezenom, Y.H.; Jiang, H.; Wang, L.-Q.; Zhou, H.-C. Surface Functionalization of Porous Coordination Nanocages Via Click Chemistry and Their Application in Drug Delivery. *Adv. Mater.* **2011**, *23*, 90–93. [CrossRef] [PubMed]
75. Mollick, S.; Mukherjee, S.; Kim, D.; Qiao, Z.; Desai, A.V.; Saha, R.; More, Y.D.; Jiang, J.; Lah, M.S.; Ghosh, S.K. Hydrophobic Shielding of Outer Surface: Enhancing the Chemical Stability of Metal–Organic Polyhedra. *Angew. Chem. Inter. Ed.* **2019**, *58*, 1041–1045. [CrossRef] [PubMed]
76. Percastegui, E.G.; Mosquera, J.; Nitschke, J.R. Anion Exchange Renders Hydrophobic Capsules and Cargoes Water-Soluble. *Angew. Chem. Int. Ed.* **2017**, *56*, 9136–9140. [CrossRef] [PubMed]
77. Sun, L.-B.; Li, J.-R.; Lu, W.; Gu, Z.-Y.; Luo, Z.; Zhou, H.-C. Confinement of Metal-Organic Polyhedra in Silica Nanopores. *J. Am. Chem. Soc.* **2012**, *134*, 15923–15928. [CrossRef] [PubMed]
78. Ajami, D.; Liu, L.; Rebek Jr, J. Soft templates in encapsulation complexes. *Chem. Soc. Rev.* **2015**, *44*, 490–499. [CrossRef]
79. Tian, J.; Zhou, T.-Y.; Zhang, S.-C.; Aloni, S.; Altoe, M.V.; Xie, S.-H.; Wang, H.; Zhang, D.-W.; Zhao, X.; Liu, Y.; et al. Three-dimensional periodic supramolecular organic framework ion sponge in water and microcrystals. *Nat Commun.* **2014**, *5*, 5574. [CrossRef]
80. Ke, Y.; Collins, D.J.; Zhou, H.-C. Synthesis and Structure of Cuboctahedral and Anticuboctahedral Cages Containing 12 Quadruply Bonded Dimolybdenum Units. *Inorg. Chem.* **2005**, *44*, 4154–4156. [CrossRef] [PubMed]
81. Li, H.; Eddaoudi, M.; Groy, T.L.; Yaghi, O.M. Establishing Microporosity in Open Metal-Organic Frameworks: Gas Sorption Isotherms for Zn(BDC) (BDC = 1,4-Benzenedicarboxylate). *J. Am. Chem. Soc.* **1998**, *120*, 8571–8572. [CrossRef]
82. Furukawa, H.; Kim, J.; Ockwig, N.W.; O'Keeffe, M.; Yaghi, O.M. Control of Vertex Geometry, Structure Dimensionality, Functionality, and Pore Metrics in the Reticular Synthesis of Crystalline Metal-Organic Frameworks and Polyhedra. *J. Am. Chem. Soc.* **2008**, *130*, 11650–11661. [CrossRef]

83. Tonigold, M.; Hitzbleck, J.; Bahnmüller, S.; Langstein, G.; Volkmer, D. Copper(II) Nanoballs as monomers for polyurethane coatings: Synthesis, urethane derivatization and kinetic stability. *Dalton Trans.* **2009**, *38*, 1363–1371. [CrossRef] [PubMed]

84. Tonigold, M.; Volkmer, D. Comparative solvolytic stabilities of copper(II) nanoballs and dinuclear Cu(II) paddle wheel units. *Inorg. Chim. Acta* **2010**, *363*, 4220–4229. [CrossRef]

85. Furukawa, H.; Kim, J.; Plass, K.E.; Yaghi, O.M. Crystal Structure, Dissolution, and Deposition of a 5 nm Functionalized Metal-Organic Great Rhombicuboctahedron. *J. Am. Chem. Soc.* **2006**, *128*, 8398–8399. [CrossRef]

86. Perry, J.J.; Kravtsov, V.C.; Zaworotko, M.J.; Larsen, R.W. Solid State Structural Characterization and Solution Spectroscopy of a Dodecyloxy Copper Nanoball. *Cryst. Growth Des.* **2011**, *11*, 3183–3189. [CrossRef]

87. Zhu, H.-F.; Fan, J.; Okamura, T.-a.; Zhang, Z.-H.; Liu, G.-X.; Yu, K.-B.; Sun, W.-Y.; Ueyama, N. Metal-Organic Architectures of Silver(I), Cadmium(II), and Copper(II) with a Flexible Tricarboxylate Ligand. *Inorg. Chem.* **2006**, *45*, 3941–3948. [CrossRef]

88. McManus, G.J.; Wang, Z.; Zaworotko, M.J. Suprasupermolecular Chemistry: Infinite Networks from Nanoscale Metal-Organic Building Blocks. *Cryst. Growth Des.* **2004**, *4*, 11–13. [CrossRef]

89. Li, J.-R.; Zhou, H.-C. Bridging-ligand-substitution strategy for the preparation of metal-organic polyhedra. *Nat. Chem.* **2010**, *2*, 893–898. [CrossRef]

90. Jung, H.; Moon, D.; Chun, H. Non-framework coordination polymers with tunable bimodal porosities based on inter-connected metal-organic polyhedra. *Bull. Korean Chem. Soc.* **2011**, *32*, 2489–2492. [CrossRef]

91. Ni, Z.; Yassar, A.; Antoun, T.; Yaghi, O.M. Porous Metal-Organic Truncated Octahedron Constructed from Paddle-Wheel Squares and Terthiophene Links. *J. Am. Chem. Soc.* **2005**, *127*, 12752–12753. [CrossRef]

92. Li, J.-R.; Timmons, D.J.; Zhou, H.-C. Interconversion between Molecular Polyhedra and Metal-Organic Frameworks. *J. Am. Chem. Soc.* **2009**, *131*, 6368–6369. [CrossRef]

93. Li, J.-R.; Yu, J.; Lu, W.; Sun, L.-B.; Sculley, J.; Balbuena, P.B.; Zhou, H.-C. Porous materials with pre-designed single-molecule traps for CO2 selective adsorption. *Nat. Commun.* **2013**, *4*, 1538. [CrossRef] [PubMed]

94. Li, J.-R.; Yakovenko, A.A.; Lu, W.; Timmons, D.J.; Zhuang, W.; Yuan, D.; Zhou, H.-C. Ligand Bridging-Angle-Driven Assembly of Molecular Architectures Based on Quadruply Bonded Mo-Mo Dimers. *J. Am. Chem. Soc.* **2010**, *132*, 17599–17610. [CrossRef] [PubMed]

95. Wang, Z.; Cohen, S.M. Postsynthetic modification of metal–organic frameworks. *Chem. Soc. Rev.* **2009**, *38*, 1315–1329. [CrossRef]

96. Tan, J.C.; Cheetham, A.K. Mechanical properties of hybrid inorganic–organic framework materials: Establishing fundamental structure–property relationships. *Chem. Soc. Rev.* **2011**, *40*, 1059–1080. [CrossRef]

97. Kim, M.; Cahill, J.F.; Fei, H.; Prather, K.A.; Cohen, S.M. Postsynthetic Ligand and Cation Exchange in Robust Metal–Organic Frameworks. *J. Am. Chem. Soc.* **2012**, *134*, 18082–18088. [CrossRef] [PubMed]

98. Deria, P.; Mondloch, J.E.; Karagiaridi, O.; Bury, W.; Hupp, J.T.; Farha, O.K. Beyond post-synthesis modification: Evolution of metal–organic frameworks via building block replacement. *Chem. Soc. Rev.* **2014**, *43*, 5896–5912. [CrossRef] [PubMed]

99. Li, Y.; Zhang, D.; Gai, F.; Zhu, X.; Guo, Y.-n.; Ma, T.; Liu, Y.; Huo, Q. Ionic self-assembly of surface functionalized metal–organic polyhedra nanocages and their ordered honeycomb architecture at the air/water interface. *Chem. Commun.* **2012**, *48*, 7946–7948. [CrossRef]

100. Xie, X.-Y.; Wu, F.; Liu, X.; Tao, W.-Q.; Jiang, Y.; Liu, X.-Q.; Sun, L.-B. Photopolymerization of metal–organic polyhedra: An efficient approach to improve the hydrostability, dispersity, and processability. *Chem. Commun.* **2019**, *55*, 6177–6180. [CrossRef]

101. Makal, T.A.; Wang, X.; Zhou, H.-C. Tuning the Moisture and Thermal Stability of Metal–Organic Frameworks through Incorporation of Pendant Hydrophobic Groups. *Cryst. Growth Des.* **2013**, *13*, 4760–4768. [CrossRef]

102. Jung, M.; Kim, H.; Baek, K.; Kim, K. Synthetic Ion Channel Based on Metal–Organic Polyhedra. *Angew. Chem. Inter. Ed.* **2008**, *47*, 5755–5757. [CrossRef]

103. Luo, Y.-R. *Comprehensive Handbook of Chemical Bond Energies*; CRC Press: Boca Raton, FL, USA, 2007.

104. Park, J.; Perry, Z.; Chen, Y.-P.; Bae, J.; Zhou, H.-C. Chromium(II) Metal–Organic Polyhedra as Highly Porous Materials. *ACS Appl. Mater. Interfaces* **2017**, *9*, 28064–28068. [CrossRef] [PubMed]

105. Stoeck, U.; Krause, S.; Bon, V.; Senkovska, I.; Kaskel, S. A highly porous metal–organic framework, constructed from a cuboctahedral super-molecular building block, with exceptionally high methane uptake. *Chem. Commun.* **2012**, *48*, 10841–10843. [CrossRef] [PubMed]

106. Lu, W.; Yuan, D.; Makal, T.A.; Wei, Z.; Li, J.-R.; Zhou, H.-C. Highly porous metal-organic framework sustained with 12-connected nanoscopic octahedra. *Dalton Trans.* **2013**, *42*, 1708–1714. [CrossRef] [PubMed]

107. Rowland, C.A.; Lorzing, G.R.; Gosselin, A.J.; Trump, B.A.; Yap, G.P.A.; Brown, C.M.; Bloch, E.D. Methane Storage in Paddlewheel-Based Porous Coordination Cages. *J. Am. Chem. Soc.* **2018**, *140*, 11153–11157. [CrossRef] [PubMed]

108. Krause, S.; Bon, V.; Senkovska, I.; Stoeck, U.; Wallacher, D.; Többens, D.M.; Zander, S.; Pillai, R.S.; Maurin, G.; Coudert, F.-X.; et al. A pressure-amplifying framework material with negative gas adsorption transitions. *Nature* **2016**, *532*, 348–352. [CrossRef]

109. Lorzing, G.R.; Gosselin, A.J.; Trump, B.A.; York, A.H.P.; Sturluson, A.; Rowland, C.A.; Yap, G.P.A.; Brown, C.M.; Simon, C.M.; Bloch, E.D. Understanding Gas Storage in Cuboctahedral Porous Coordination Cages. *J. Am. Chem. Soc.* **2019**, *141*, 12128–12138. [CrossRef]

110. Lorzing, G.R.; Trump, B.A.; Brown, C.M.; Bloch, E.D. Selective Gas Adsorption in Highly Porous Chromium(II)-Based Metal–Organic Polyhedra. *Chem. Mater.* **2017**, *29*, 8583–8587. [CrossRef]

111. Gosselin, A.J.; Rowland, C.A.; Balto, K.P.; Yap, G.P.A.; Bloch, E.D. Design and Synthesis of Porous Nickel(II) and Cobalt(II) Cages. *Inorg. Chem.* **2018**, *57*, 11847–11850. [CrossRef]

112. He, Y.-P.; Yuan, L.-B.; Chen, G.-H.; Lin, Q.-P.; Wang, F.; Zhang, L.; Zhang, J. Water-Soluble and Ultrastable Ti4L6 Tetrahedron with Coordination Assembly Function. *J. Am. Chem. Soc.* **2017**, *139*, 16845–16851. [CrossRef]

113. Davis, A.V.; Raymond, K.N. The Big Squeeze: Guest Exchange in an M4L6 Supramolecular Host. *J. Am. Chem. Soc.* **2005**, *127*, 7912–7919. [CrossRef]

114. Hong, C.M.; Morimoto, M.; Kapustin, E.A.; Alzakhem, N.; Bergman, R.G.; Raymond, K.N.; Toste, F.D. Deconvoluting the Role of Charge in a Supramolecular Catalyst. *J. Am. Chem. Soc.* **2018**, *140*, 6591–6595. [CrossRef] [PubMed]

115. Lincoln, S.A.; Mirbach, A.E. Substituted reactions of solvated metal ions. *Adv. Inorg. Chem.* **1995**, *42*, 1–88.

116. Bar, A.K.; Gole, B.; Ghosh, S.; Mukherjee, P.S. Self-assembly of a PdII neutral molecular rectangle via a new organometallic PdII2 molecular clip and oxygen donor linker. *Dalton Trans.* **2009**, *38*, 6701–6704. [CrossRef] [PubMed]

117. Das, N.; Mukherjee, P.S.; Arif, A.M.; Stang, P.J. Facile Self-Assembly of Predesigned Neutral 2D Pt-Macrocycles via a New Class of Rigid Oxygen Donor Linkers. *J. Am. Chem. Soc.* **2003**, *125*, 13950–13951. [CrossRef]

118. Furukawa, S.; Horike, N.; Kondo, M.; Hijikata, Y.; Carné-Sánchez, A.; Larpent, P.; Louvain, N.; Diring, S.; Sato, H.; Matsuda, R.; et al. Rhodium–Organic Cuboctahedra as Porous Solids with Strong Binding Sites. *Inorg. Chem.* **2016**, *55*, 10843–10846. [CrossRef]

119. Young, M.D.; Zhang, Q.; Zhou, H.-C. Metal–organic polyhedra constructed from dinuclear ruthenium paddlewheels. *Inorg. Chimica Acta* **2015**, *424*, 216–220. [CrossRef]

120. Liu, G.; Ju, Z.; Yuan, D.; Hong, M. In Situ Construction of a Coordination Zirconocene Tetrahedron. *Inorg. Chem.* **2013**, *52*, 13815–13817. [CrossRef]

121. Liu, G.; Zeller, M.; Su, K.; Pang, J.; Ju, Z.; Yuan, D.; Hong, M. Controlled Orthogonal Self-Assembly of Heterometal-Decorated Coordination Cages. *Chem. Eur. J.* **2016**, *22*, 17345–17350. [CrossRef]

122. Mukherjee, P.S.; Das, N.; Kryschenko, Y.K.; Arif, A.M.; Stang, P.J. Design, Synthesis, and Crystallographic Studies of Neutral Platinum-Based Macrocycles Formed via Self-Assembly. *J. Am. Chem. Soc.* **2004**, *126*, 2464–2473. [CrossRef]

123. Albalad, J.; Carné-Sánchez, A.; Grancha, T.; Hernández-López, L.; Maspoch, D. Protection strategies for directionally-controlled synthesis of previously inaccessible metal–organic polyhedra (MOPs): The cases of carboxylate- and amino-functionalised Rh(ii)-MOPs. *Chem. Commun.* **2019**, *55*, 12785–12788. [CrossRef]

124. Reiss, P.S.; Little, M.A.; Santolini, V.; Chong, S.Y.; Hasell, T.; Jelfs, K.E.; Briggs, M.E.; Cooper, A.I. Periphery-Functionalized Porous Organic Cages. *Chem. Eur. J.* **2016**, *22*, 16547–16553. [CrossRef] [PubMed]

125. Carné-Sánchez, A.; Craig, G.A.; Larpent, P.; Guillerm, V.; Urayama, K.; Maspoch, D.; Furukawa, S. A Coordinative Solubilizer Method to Fabricate Soft Porous Materials from Insoluble Metal–Organic Polyhedra. *Angew. Chem. Inter. Ed.* **2019**, *58*, 6347–6350. [CrossRef] [PubMed]

126. Liu, X.; Wang, X.; Bavykina, A.V.; Chu, L.; Shan, M.; Sabetghadam, A.; Miro, H.; Kapteijn, F.; Gascon, J. Molecular-Scale Hybrid Membranes Derived from Metal-Organic Polyhedra for Gas Separation. *ACS Appl. Mater. Interfaces* **2018**, *10*, 21381–21389. [CrossRef] [PubMed]

127. Carné-Sánchez, A.; Albalad, J.; Grancha, T.; Imaz, I.; Juanhuix, J.; Larpent, P.; Furukawa, S.; Maspoch, D. Postsynthetic Covalent and Coordination Functionalization of Rhodium(II)-Based Metal–Organic Polyhedra. *J. Am. Chem. Soc.* **2019**, *141*, 4094–4102. [CrossRef] [PubMed]

128. Carné-Sánchez, A.; Craig, G.A.; Larpent, P.; Hirose, T.; Higuchi, M.; Kitagawa, S.; Matsuda, K.; Urayama, K.; Furukawa, S. Self-assembly of metal–organic polyhedra into supramolecular polymers with intrinsic microporosity. *Nat. Commun.* **2018**, *9*, 2506. [CrossRef]

129. Ju, Z.; Liu, G.; Chen, Y.-S.; Yuan, D.; Chen, B. From Coordination Cages to a Stable Crystalline Porous Hydrogen-Bonded Framework. *Chem. Eur. J.* **2017**, *23*, 4774–4777. [CrossRef]

130. Zhou, M.; Liu, G.; Ju, Z.; Su, K.; Du, S.; Tan, Y.; Yuan, D. Hydrogen-Bonded Framework Isomers Based on Zr-Metal Organic Cage: Connectivity, Stability, and Porosity. *Cryst. Growth Des.* **2020**, *20*, 4127–4134. [CrossRef]

131. Lee, S.; Lee, J.H.; Kim, J.C.; Lee, S.; Kwak, S.K.; Choe, W. Porous Zr6L3 Metallocage with Synergetic Binding Centers for CO2. *ACS Appl. Mater. Interfaces* **2018**, *10*, 8685–8691. [CrossRef]

132. Xing, W.-H.; Li, H.-Y.; Dong, X.-Y.; Zang, S.-Q. Robust multifunctional Zr-based metal–organic polyhedra for high proton conductivity and selective CO2 capture. *J. Mater. Chem. A* **2018**, *6*, 7724–7730. [CrossRef]

133. Liu, J.; Duan, W.; Song, J.; Guo, X.; Wang, Z.; Shi, X.; Liang, J.; Wang, J.; Cheng, P.; Chen, Y.; et al. Self-Healing Hyper-Cross-Linked Metal–Organic Polyhedra (HCMOPs) Membranes with Antimicrobial Activity and Highly Selective Separation Properties. *J. Am. Chem. Soc.* **2019**, *141*, 12064–12070. [CrossRef]

134. Nam, D.; Huh, J.; Lee, J.; Kwak, J.H.; Jeong, H.Y.; Choi, K.; Choe, W. Cross-linking Zr-based metal–organic polyhedra via postsynthetic polymerization. *Chem. Sci.* **2017**, *8*, 7765–7771. [CrossRef] [PubMed]

135. Guo, X.; Xu, S.; Sun, Y.; Qiao, Z.; Huang, H.; Zhong, C. Metal-organic polyhedron membranes for molecular separation. *J. Membr. Sci.* **2021**, *632*, 119354. [CrossRef]

136. Liu, G.; Di Yuan, Y.; Wang, J.; Cheng, Y.; Peh, S.B.; Wang, Y.; Qian, Y.; Dong, J.; Yuan, D.; Zhao, D. Process-Tracing Study on the Postassembly Modification of Highly Stable Zirconium Metal–Organic Cages. *J. Am. Chem. Soc.* **2018**, *140*, 6231–6234. [CrossRef] [PubMed]

137. Liu, G.; Yang, Z.; Zhou, M.; Wang, Y.; Yuan, D.; Zhao, D. Heterogeneous postassembly modification of zirconium metal–organic cages in supramolecular frameworks. *Chem. Commun.* **2021**, *57*, 6276–6279. [CrossRef]

138. Li, J.-R.; Zhou, H.-C. Metal-Organic Hendecahedra Assembled from Dinuclear Paddlewheel Nodes and Mixtures of Ditopic Linkers with 120° and 90° Bend Angles. *Angew. Chem. Int. Ed.* **2009**, *48*, 8465–8468. [CrossRef]

139. Gosselin, A.J.; Decker, G.E.; Antonio, A.M.; Lorzing, G.R.; Yap, G.P.A.; Bloch, E.D. A Charged Coordination Cage-Based Porous Salt. *J. Am. Chem. Soc.* **2020**, *142*, 9594–9598. [CrossRef]

140. Teo, J.M.; Coghlan, C.J.; Evans, J.D.; Tsivion, E.; Head-Gordon, M.; Sumby, C.J.; Doonan, C.J. Hetero-bimetallic metal–organic polyhedra. *Chem. Commun.* **2016**, *52*, 276–279. [CrossRef]

141. Su, K.; Jiang, F.; Qian, J.; Chen, L.; Pang, J.; Bawaked, S.M.; Mokhtar, M.; Al-Thabaiti, S.A.; Hong, M. Stepwise Construction of Extra-Large Heterometallic Calixarene-Based Cages. *Inorg. Chem.* **2015**, *54*, 3183–3188. [CrossRef]

142. Xiong, K.; Jiang, F.; Gai, Y.; Yuan, D.; Chen, L.; Wu, M.; Su, K.; Hong, M. Truncated octahedral coordination cage incorporating six tetranuclear-metal building blocks and twelve linear edges. *Chem. Sci.* **2012**, *3*, 2321–2325. [CrossRef]

143. Jiao, J.; Tan, C.; Li, Z.; Liu, Y.; Han, X.; Cui, Y. Design and Assembly of Chiral Coordination Cages for Asymmetric Sequential Reactions. *J. Am. Chem. Soc.* **2018**, *140*, 2251–2259. [CrossRef]

144. Pasquale, S.; Sattin, S.; Escudero-Adan, E.C.; Martinez-Belmonte, M.; de Mendoza, J. Giant regular polyhedra from calixarene carboxylates and uranyl. *Nat. Commun.* **2012**, *3*, 785. [CrossRef] [PubMed]

145. Dai, F.-R.; Wang, Z. Modular Assembly of Metal-Organic Supercontainers Incorporating Sulfonylcalixarenes. *J. Am. Chem. Soc.* **2012**, *134*, 8002–8005. [CrossRef] [PubMed]

146. Liu, M.; Liao, W.; Hu, C.; Du, S.; Zhang, H. Calixarene-Based Nanoscale Coordination Cages. *Angew. Chem. Int. Ed.* **2012**, *51*, 1585–1588. [CrossRef] [PubMed]

147. Du, S.; Hu, C.; Xiao, J.-C.; Tan, H.; Liao, W. A giant coordination cage based on sulfonylcalix[4]arenes. *Chem. Commun.* **2012**, *48*, 9177–9179. [CrossRef]

148. Dai, F.-R.; Sambasivam, U.; Hammerstrom, A.J.; Wang, Z. Synthetic Supercontainers Exhibit Distinct Solution versus Solid State Guest-Binding Behavior. *J. Am. Chem. Soc.* **2014**, *136*, 7480–7491. [CrossRef]

149. Kang, Y.-H.; Liu, X.-D.; Yan, N.; Jiang, Y.; Liu, X.-Q.; Sun, L.-B.; Li, J.-R. Fabrication of Isolated Metal-Organic Polyhedra in Confined Cavities: Adsorbents/Catalysts with Unusual Dispersity and Activity. *J. Am. Chem. Soc.* **2016**, *138*, 6099–6102. [CrossRef]

150. Kumar, R.; Rao, C.N.R. Novel properties of 0D metal-organic polyhedra bonded to the surfaces of 2D graphene and 1D single-walled carbon nanotubes. *Dalton Trans.* **2017**, *46*, 7998–8003. [CrossRef]

151. Lee, J.; Lim, D.-W.; Dekura, S.; Kitagawa, H.; Choe, W. MOP × MOF: Collaborative Combination of Metal-Organic Polyhedra and Metal-Organic Framework for Proton Conductivity. *ACS Appl. Mater. Interfaces* **2019**, *11*, 12639–12646. [CrossRef]

152. Wang, X.-L.; Qin, C.; Wu, S.-X.; Shao, K.-Z.; Lan, Y.-Q.; Wang, S.; Zhu, D.-X.; Su, Z.-M.; Wang, E.-B. Bottom-Up Synthesis of Porous Coordination Frameworks: Apical Substitution of a Pentanuclear Tetrahedral Precursor. *Angew. Chem. Int. Ed.* **2009**, *48*, 5291–5295. [CrossRef]

153. Wang, H.-N.; Meng, X.; Yang, G.-S.; Wang, X.-L.; Shao, K.-Z.; Su, Z.-M.; Wang, C.-G. Stepwise assembly of metal-organic framework based on a metal-organic polyhedron precursor for drug delivery. *Chem. Commun.* **2011**, *47*, 7128–7130. [CrossRef]

154. Wang, H.-N.; Liu, F.-H.; Wang, X.-L.; Shao, K.-Z.; Su, Z.-M. Three neutral metal-organic frameworks with micro- and meso-pores for adsorption and separation of dyes. *J. Mater. Chem. A* **2013**, *1*, 13060–13063. [CrossRef]

155. Brega, V.; Zeller, M.; He, Y.; Peter Lu, H.; Klosterman, J.K. Multi-responsive metal-organic lantern cages in solution. *Chem. Commun.* **2015**, *51*, 5077–5080. [CrossRef] [PubMed]

156. Nouar, F.; Eubank, J.F.; Bousquet, T.; Wojtas, L.; Zaworotko, M.J.; Eddaoudi, M. Supermolecular Building Blocks (SBBs) for the Design and Synthesis of Highly Porous Metal-Organic Frameworks. *J. Am. Chem. Soc.* **2008**, *130*, 1833–1835. [CrossRef]

157. Liu, T.-F.; Chen, Y.-P.; Yakovenko, A.A.; Zhou, H.-C. Interconversion between Discrete and a Chain of Nanocages: Self-Assembly via a Solvent-Driven, Dimension-Augmentation Strategy. *J. Am. Chem. Soc.* **2012**, *134*, 17358–17361. [CrossRef] [PubMed]

158. Pfeil, A.; Lehn, J.M. Helicate self-organization: Positive cooperativity in the self-assembly of double-helical metal complexes. *J. Chem. Soc. Chem. Commun.* **1992**, *28*, 838–840. [CrossRef]

159. Lehn, J.M.; Rigault, A.; Siegel, J.; Harrowfield, J.; Chevrier, B.; Moras, D. Spontaneous assembly of double-stranded helicates from oligobipyridine ligands and copper(I) cations: Structure of an inorganic double helix. *Proc. Natl. Acad. Sci. USA* **1987**, *84*, 2565–2569. [CrossRef]

160. Lehn, J.-M.; Rigault, A. Helicates: Tetra- and Pentanuclear Double Helix Complexes of CuI and Poly(bipyridine) Strands. *Angew. Chem. Inter. Ed.* **1988**, *27*, 1095–1097. [CrossRef]

161. Garrett, T.M.; Koert, U.; Lehn, J.-M.; Rigault, A.; Meyer, D.; Fischer, J. Self-assembly of silver(I) helicates. *J. Chem. Soc. Chem. Commun.* **1990**, *26*, 557–558. [CrossRef]

162. Baxter, P.; Lehn, J.-M.; DeCian, A.; Fischer, J. Multicomponent Self-Assembly: Spontaneous Formation of a Cylindrical Complex from Five Ligands and Six Metal Ions. *Angew. Chem. Inter. Ed.* **1993**, *32*, 69–72. [CrossRef]

163. Coronado, E.; Galan-Mascaros, J.R.; Gavina, P.; Marti-Gastaldo, C.; Romero, F.M.; Tatay, S. Self-Assembly of a Copper(II)-Based Metallosupramolecular Hexagon. *Inorg. Chem.* **2008**, *47*, 5197–5203. [CrossRef]

164. Mamula, O.; Von Zelewsky, A.; Bernardinelli, G. Completely stereospecific self-assembly of a circular helicate. *Angew. Chem. Int. Ed.* **1998**, *37*, 290–293. [CrossRef]

165. Beauchamp, D.A.; Loeb, S.J. Molecular squares, rectangles and infinite helical chains utilising the simple corner' ligand 4-(2-pyridyl)pyrimidine. *Chem. Commun.* **2002**, *38*, 2484–2485. [CrossRef]

166. Campos-Fernández, C.S.; Schottel, B.L.; Chifotides, H.T.; Bera, J.K.; Bacsa, J.; Koomen, J.M.; Russell, D.H.; Dunbar, K.R. Anion Template Effect on the Self-Assembly and Interconversion of Metallacyclophanes. *J. Am. Chem. Soc.* **2005**, *127*, 12909–12923. [CrossRef] [PubMed]

167. Campos-Fernández, C.S.; Clérac, R.; Koomen, J.M.; Russell, D.H.; Dunbar, K.R. Fine-Tuning the Ring-Size of Metallacyclophanes: A Rational Approach to Molecular Pentagons. *J. Am. Chem. Soc.* **2001**, *123*, 773–774. [CrossRef]

168. Meng, W.; Breiner, B.; Rissanen, K.; Thoburn, J.D.; Clegg, J.K.; Nitschke, J.R. A Self-Assembled M8L6 Cubic Cage that Selectively Encapsulates Large Aromatic Guests. *Angew. Chem. Inter. Ed.* **2011**, *50*, 3479–3483. [CrossRef] [PubMed]

169. Bolliger, J.L.; Belenguer, A.M.; Nitschke, J.R. Enantiopure Water-Soluble [Fe4L6] Cages: Host-Guest Chemistry and Catalytic Activity. *Angew. Chem. Int. Ed.* **2013**, *52*, 7958–7962. [CrossRef]

170. Whitehead, M.; Turega, S.; Stephenson, A.; Hunter, C.A.; Ward, M.D. Quantification of solvent effects on molecular recognition in polyhedral coordination cage hosts. *Chem. Sci.* **2013**, *4*, 2744–2751. [CrossRef]

171. Zarra, S.; Clegg, J.K.; Nitschke, J.R. Selective Assembly and Disassembly of a Water-Soluble Fe10L15 Prism. *Angew. Chem. Int. Ed.* **2013**, *52*, 4837–4840. [CrossRef] [PubMed]

172. Xi, S.-F.; Bao, L.-Y.; Lin, J.-G.; Liu, Q.-Z.; Qiu, L.; Zhang, F.-L.; Wang, Y.-X.; Ding, Z.-D.; Li, K.; Gu, Z.-G. Enantiomers of tetrahedral metal-organic cages: A new class of highly efficient G-quadruplex ligands with potential anticancer activities. *Chem. Commun.* **2016**, *52*, 10261–10264. [CrossRef] [PubMed]

173. Ren, D.-H.; Qiu, D.; Pang, C.-Y.; Li, Z.; Gu, Z.-G. Chiral tetrahedral iron(II) cages: Diastereoselective subcomponent self-assembly, structure interconversion and spin-crossover properties. *Chem. Commun.* **2015**, *51*, 788–791. [CrossRef] [PubMed]

174. Percastegui, E.G.; Mosquera, J.; Ronson, T.K.; Plajer, A.J.; Kieffer, M.; Nitschke, J.R. Waterproof architectures through subcomponent self-assembly. *Chem. Sci.* **2019**, *10*, 2006–2018. [CrossRef] [PubMed]

175. Irving, H.; Williams, R.J.P. The stability of transition-metal complexes. *J. Chem. Soc.* **1953**, 3192–3210. [CrossRef]

176. O'Reilly, N.; Giri, N.; James, S.L. Porous liquids. *Chem. A Eur. J.* **2007**, *13*, 3020–3025. [CrossRef] [PubMed]

177. Zhang, J.; Chai, S.-H.; Qiao, Z.-A.; Mahurin, S.M.; Chen, J.; Fang, Y.; Wan, S.; Nelson, K.; Zhang, P.; Dai, S. Porous Liquids: A Promising Class of Media for Gas Separation. *Angew. Chem. Int. Ed.* **2015**, *54*, 932–936. [CrossRef]

178. Ma, L.; Haynes, C.J.E.; Grommet, A.B.; Walczak, A.; Parkins, C.C.; Doherty, C.M.; Longley, L.; Tron, A.; Stefankiewicz, A.R.; Bennett, T.D.; et al. Coordination cages as permanently porous ionic liquids. *Nat. Chem.* **2020**, *12*, 270–275. [CrossRef]

179. Symmers, P.R.; Burke, M.J.; August, D.P.; Thomson, P.I.T.; Nichol, G.S.; Warren, M.R.; Campbell, C.J.; Lusby, P.J. Non-equilibrium cobalt(iii) "click" capsules. *Chem. Sci.* **2015**, *6*, 756–760. [CrossRef]

180. Roberts, D.A.; Castilla, A.M.; Ronson, T.K.; Nitschke, J.R. Post-assembly Modification of Kinetically Metastable FeII2L3 Triple Helicates. *J. Am. Chem. Soc.* **2014**, *136*, 8201–8204. [CrossRef]

181. Roberts, D.A.; Pilgrim, B.S.; Nitschke, J.R. Covalent post-assembly modification in metallosupramolecular chemistry. *Chem. Soc. Rev.* **2018**, *47*, 626–644. [CrossRef]

182. Zeng, H.; Stewart-Yates, L.; Casey, L.M.; Bampos, N.; Roberts, D.A. Covalent Post-Assembly Modification: A Synthetic Multipurpose Tool in Supramolecular Chemistry. *ChemPlusChem* **2020**, *85*, 1249–1269. [CrossRef]

183. Samanta, S.K.; Moncelet, D.; Vinciguerra, B.; Briken, V.; Isaacs, L. Metal Organic Polyhedra: A Click-and-Clack Approach Toward Targeted Delivery. *Helv. Chim. Acta* **2018**, *101*, e1800057. [CrossRef]

184. Zheng, W.; Chen, L.-J.; Yang, G.; Sun, B.; Wang, X.; Jiang, B.; Yin, G.-Q.; Zhang, L.; Li, X.; Liu, M.; et al. Construction of Smart Supramolecular Polymeric Hydrogels Cross-linked by Discrete Organoplatinum(II) Metallacycles via Post-Assembly Polymerization. *J. Am. Chem. Soc.* **2016**, *138*, 4927–4937. [CrossRef] [PubMed]

185. Glasson, C.R.K.; Meehan, G.V.; Davies, M.; Motti, C.A.; Clegg, J.K.; Lindoy, L.F. Post-Assembly Covalent Di- and Tetracapping of a Dinuclear [Fe2L3]4+ Triple Helicate and Two [Fe4L6]8+ Tetrahedra Using Sequential Reductive Aminations. *Inorg. Chem.* **2015**, *54*, 6986–6992. [CrossRef] [PubMed]

186. Zheng, Y.-R.; Suntharalingam, K.; Johnstone, T.C.; Lippard, S.J. Encapsulation of Pt(IV) prodrugs within a Pt(II) cage for drug delivery. *Chem. Sci.* **2015**, *6*, 1189–1193. [CrossRef] [PubMed]

187. Nishioka, Y.; Yamaguchi, T.; Kawano, M.; Fujita, M. Asymmetric [2 + 2] Olefin Cross Photoaddition in a Self-Assembled Host with Remote Chiral Auxiliaries. *J. Am. Chem. Soc.* **2008**, *130*, 8160–8161. [CrossRef] [PubMed]

188. Umemoto, K.; Yamaguchi, K.; Fujita, M. Molecular Paneling via Coordination: Guest-Controlled Assembly of Open Cone and Tetrahedron Structures from Eight Metals and Four Ligands. *J. Am. Chem. Soc.* **2000**, *122*, 7150–7151. [CrossRef]

189. Cai, L.-X.; Li, S.-C.; Yan, D.-N.; Zhou, L.-P.; Guo, F.; Sun, Q.-F. Water-Soluble Redox-Active Cage Hosting Polyoxometalates for Selective Desulfurization Catalysis. *J. Am. Chem. Soc.* **2018**, *140*, 4869–4876. [CrossRef] [PubMed]

190. Saha, R.; Devaraj, A.; Bhattacharyya, S.; Das, S.; Zangrando, E.; Mukherjee, P.S. Unusual Behavior of Donor-Acceptor Stenhouse Adducts in Confined Space of a Water-Soluble PdII8 Molecular Vessel. *J. Am. Chem. Soc.* **2019**, *141*, 8638–8645. [CrossRef]

191. Roy, B.; Devaraj, A.; Saha, R.; Jharimune, S.; Chi, K.-W.; Mukherjee, P.S. Catalytic Intramolecular Cycloaddition Reactions by Using a Discrete Molecular Architecture. *Chem.A Eur. J.* **2017**, *23*, 15704–15712. [CrossRef]

192. Yoshizawa, M.; Ono, K.; Kumazawa, K.; Kato, T.; Fujita, M. Metal-Metal d-d Interaction through the Discrete Stacking of Mononuclear M(II) Complexes (M = Pt, Pd, and Cu) within an Organic-Pillared Coordination Cage. *J. Am. Chem. Soc.* **2005**, *127*, 10800–10801. [CrossRef]

193. Fujita, M.; Tominaga, M.; Hori, A.; Therrien, B. Coordination Assemblies from a Pd(II)-Cornered Square Complex. *Acc. Chem. Res.* **2005**, *38*, 369–378. [CrossRef]

194. Hanopolskyi, A.I.; De, S.; Bialek, M.J.; Diskin-Posner, Y.; Avram, L.; Feller, M.; Klajn, R. Reversible switching of arylazopyrazole within a metal-organic cage. *Beilstein J. Org. Chem.* **2019**, *15*, 2398–2407. [CrossRef] [PubMed]

195. Klosterman, J.K.; Yamauchi, Y.; Fujita, M. Engineering discrete stacks of aromatic molecules. *Chem. Soc. Rev.* **2009**, *38*, 1714–1725. [CrossRef] [PubMed]

196. Yoshizawa, M.; Kumazawa, K.; Fujita, M. Room-Temperature and Solution-State Observation of the Mixed-Valence Cation Radical Dimer of Tetrathiafulvalene, [(TTF)2]+•, within a Self-Assembled Cage. *J. Am. Chem. Soc.* **2005**, *127*, 13456–13457. [CrossRef] [PubMed]

197. Clever, G.H.; Tashiro, S.; Shionoya, M. Inclusion of Anionic Guests inside a Molecular Cage with Palladium(II) Centers as Electrostatic Anchors. *Angew. Chem. Inter. Ed.* **2009**, *48*, 7010–7012. [CrossRef]

198. Pullen, S.; Clever, G.H. Mixed-Ligand Metal–Organic Frameworks and Heteroleptic Coordination Cages as Multifunctional Scaffolds—A Comparison. *Acc. Chem. Res.* **2018**, *51*, 3052–3064. [CrossRef]

199. Kishi, N.; Li, Z.; Yoza, K.; Akita, M.; Yoshizawa, M. An M2L4 Molecular Capsule with an Anthracene Shell: Encapsulation of Large Guests up to 1 nm. *J. Am. Chem. Soc.* **2011**, *133*, 11438–11441. [CrossRef]

200. Yoshizawa, M.; Catti, L. Bent Anthracene Dimers as Versatile Building Blocks for Supramolecular Capsules. *Acc. Chem. Res.* **2019**, *52*, 2392–2404. [CrossRef]

201. Yamashina, M.; Sei, Y.; Akita, M.; Yoshizawa, M. Safe storage of radical initiators within a polyaromatic nanocapsule. *Nat. Commun.* **2014**, *5*, 4662. [CrossRef]

202. Preston, D.; McNeill, S.M.; Lewis, J.E.M.; Giles, G.I.; Crowley, J.D. Enhanced kinetic stability of [Pd2L4]4+ cages through ligand substitution. *Dalton Trans.* **2016**, *45*, 8050–8060. [CrossRef]

203. Lewis, J.E.M.; Elliott, A.B.S.; McAdam, C.J.; Gordon, K.C.; Crowley, J.D. 'Click' to functionalise: Synthesis, characterisation and enhancement of the physical properties of a series of exo- and endo-functionalised Pd2L4 nanocages. *Chem. Sci.* **2014**, *5*, 1833–1843. [CrossRef]

204. Yazaki, K.; Sei, Y.; Akita, M.; Yoshizawa, M. Polycationic-shelled capsular and tubular nanostructures and anionic-guest binding properties. *Chem.A Eur. J.* **2016**, *22*, 17557–17561. [CrossRef] [PubMed]

205. Roy, B.; Zangrando, E.; Mukherjee, P.S. Self-assembly of a redox active water soluble Pd6L8 'molecular dice'. *Chem. Commun.* **2016**, *52*, 4489–4492. [CrossRef] [PubMed]

206. Samanta, S.K.; Moncelet, D.; Briken, V.; Isaacs, L. Metal-Organic Polyhedron Capped with Cucurbit[8]uril Delivers Doxorubicin to Cancer Cells. *J. Am. Chem. Soc.* **2016**, *138*, 14488–14496. [CrossRef] [PubMed]

207. Samanta, S.K.; Quigley, J.; Vinciguerra, B.; Briken, V.; Isaacs, L. Cucurbit[7]uril Enables Multi-Stimuli-Responsive Release from the Self-Assembled Hydrophobic Phase of a Metal Organic Polyhedron. *J. Am. Chem. Soc.* **2017**, *139*, 9066–9074. [CrossRef] [PubMed]

208. Qiu, X.; Zhong, W.; Bai, C.; Li, Y. Encapsulation of a Metal-Organic Polyhedral in the Pores of a Metal-Organic Framework. *J. Am. Chem. Soc.* **2016**, *138*, 1138–1141. [CrossRef] [PubMed]

209. Ibukuro, F.; Kusukawa, T.; Fujita, M. A Thermally Switchable Molecular Lock. Guest-Templated Synthesis of a Kinetically Stable Nanosized Cage. *J. Am. Chem. Soc.* **1998**, *120*, 8561–8562. [CrossRef]

210. Fujita, D.; Takahashi, A.; Sato, S.; Fujita, M. Self-Assembly of Pt(II) Spherical Complexes via Temporary Labilization of the Metal-Ligand Association in 2,2,2-Trifluoroethanol. *J. Am. Chem. Soc.* **2011**, *133*, 13317–13319. [CrossRef]

211. Chen, L.-J.; Chen, S.; Qin, Y.; Xu, L.; Yin, G.-Q.; Zhu, J.-L.; Zhu, F.-F.; Zheng, W.; Li, X.; Yang, H.-B. Construction of Porphyrin-Containing Metallacycle with Improved Stability and Activity within Mesoporous Carbon. *J. Am. Chem. Soc.* **2018**, *140*, 5049–5052. [CrossRef]

212. Bhat, I.A.; Devaraj, A.; Howlader, P.; Chi, K.-W.; Mukherjee, P.S. Preparation of a chiral Pt12 tetrahedral cage and its use in catalytic Michael addition reaction. *Chem. Commun.* **2018**, *54*, 4814–4817. [CrossRef]

213. Grishagin, I.V.; Pollock, J.B.; Kushal, S.; Cook, T.R.; Stang, P.J.; Olenyuk, B.Z. In vivo anticancer activity of rhomboidal Pt(II) metallacycles. *Proc. Natl. Acad. Sci. USA* **2014**, *111*, 18448–18453. [CrossRef]

214. Morris, R.E.; Aird, R.E.; del Socorro Murdoch, P.; Chen, H.; Cummings, J.; Hughes, N.D.; Parsons, S.; Parkin, A.; Boyd, G.; Jodrell, D.I.; et al. Inhibition of Cancer Cell Growth by Ruthenium(II) Arene Complexes. *J. Med. Chem.* **2001**, *44*, 3616–3621. [CrossRef] [PubMed]

215. Vajpayee, V.; Lee, S.M.; Park, J.W.; Dubey, A.; Kim, H.; Cook, T.R.; Stang, P.J.; Chi, K.-W. Growth Inhibitory Activity of a Bis-Benzimidazole-Bridged Arene Ruthenium Metalla-Rectangle and -Prism. *Organometallics* **2013**, *32*, 1563–1566. [CrossRef] [PubMed]

216. Bar, A.K.; Chakrabarty, R.; Chi, K.-W.; Batten, S.R.; Mukherjee, P.S. Synthesis and characterisation of heterometallic molecular triangles using ambidentate linker: Self-selection of a single linkage isomer. *Dalton Trans.* **2009**, *38*, 3222–3229. [CrossRef] [PubMed]

217. Mueller, I.M.; Spillmann, S.; Franck, H.; Pietschnig, R. Rational design of the first closed coordination capsule with octahedral outer shape. *Chem. A Eur. J.* **2004**, *10*, 2207–2213. [CrossRef]

218. Zheng, Y.-R.; Zhao, Z.-G.; Wang, M.; Ghosh, K.; Pollock, J.B.; Cook, T.R.; Stang, P.J. A Facile Approach toward Multicomponent Supramolecular Structures: Selective Self-Assembly via Charge Separation. *J. Am. Chem. Soc.* **2010**, *132*, 16873–16882. [CrossRef]

219. Wang, M.; Lan, W.-J.; Zheng, Y.-R.; Cook, T.R.; White, H.S.; Stang, P.J. Post-Self-Assembly Covalent Chemistry of Discrete Multicomponent Metallosupramolecular Hexagonal Prisms. *J. Am. Chem. Soc.* **2011**, *133*, 10752–10755. [CrossRef]

220. Gianneschi, N.C.; Mirkin, C.A.; Zakharov, L.N.; Rheingold, A.L. A Tetranuclear Heterobimetallic Square Formed from the Cooperative Ligand Binding Properties of Square Planar and Tetrahedral Metal Centers. *Inorg. Chem.* **2002**, *41*, 5326–5328. [CrossRef]

221. Liu, X.; Stern, C.L.; Mirkin, C.A. Chemical Origami: Formation of Flexible 52-Membered Tetranuclear Metallacycles via a Molecular Square Formed from a Hemilabile Ligand. *Organometallics* **2002**, *21*, 1017–1019. [CrossRef]

222. Wang, G.-L.; Lin, Y.-J.; Jin, G.-X. Anion-Templated Assembly of Half-Sandwich Rhodium-Based Multinuclear Metallamacrocycles. *Chem. A Eur. J.* **2011**, *17*, 5578–5587. [CrossRef]

223. Linares, F.; Galindo, M.A.; Galli, S.; Angustias Romero, M.; Navarro, J.A.R.; Barea, E. Tetranuclear Coordination Assemblies Based on Half-Sandwich Ruthenium(II) Complexes: Noncovalent Binding to DNA and Cytotoxicity. *Inorg. Chem.* **2009**, *48*, 7413–7420. [CrossRef]

224. Mattsson, J.; Govindaswamy, P.; Renfrew, A.K.; Dyson, P.J.; Stepnicka, P.; Suss-Fink, G.; Therrien, B. Synthesis, Molecular Structure, and Anticancer Activity of Cationic Arene Ruthenium Metallarectangles. *Organometallics* **2009**, *28*, 4350–4357. [CrossRef]

225. Vajpayee, V.; Yang, Y.J.; Kang, S.C.; Kim, H.; Kim, I.S.; Wang, M.; Stang, P.J.; Chi, K.-W. Hexanuclear self-assembled arene-ruthenium nano-prismatic cages: Potential anticancer agents. *Chem. Commun.* **2011**, *47*, 5184–5186. [CrossRef] [PubMed]

226. Vajpayee, V.; Song, Y.H.; Jung, Y.J.; Kang, S.C.; Kim, H.; Kim, I.S.; Wang, M.; Cook, T.R.; Stang, P.J.; Chi, K.-W. Coordination-driven self-assembly of ruthenium-based molecular-rectangles: Synthesis, characterization, photo-physical and anticancer potency studies. *Dalton Trans.* **2012**, *41*, 3046–3052. [CrossRef] [PubMed]

227. Vajpayee, V.; Lee, S.; Kim, S.-H.; Kang, S.C.; Cook, T.R.; Kim, H.; Kim, D.W.; Verma, S.; Lah, M.S.; Kim, I.S.; et al. Self-assembled metalla-rectangles bearing azodipyridyl ligands: Synthesis, characterization and antitumor activity. *Dalton Trans.* **2013**, *42*, 466–475. [CrossRef] [PubMed]

228. Vajpayee, V.; Song, Y.H.; Yang, Y.J.; Kang, S.C.; Kim, H.; Kim, I.S.; Wang, M.; Stang, P.J.; Chi, K.-W. Coordination-Driven Self-Assembly and Anticancer Activity of Molecular Rectangles Containing Octahedral Ruthenium Metal Centers. *Organometallics* **2011**, *30*, 3242–3245. [CrossRef] [PubMed]

229. Mishra, A.; Jung, H.; Park, J.W.; Kim, H.K.; Kim, H.; Stang, P.J.; Chi, K.-W. Anticancer Activity of Self-Assembled Molecular Rectangles via Arene-Ruthenium Acceptors and a New Unsymmetrical Amide Ligand. *Organometallics* **2012**, *31*, 3519–3526. [CrossRef] [PubMed]

230. Vajpayee, V.; Song, Y.H.; Yang, Y.J.; Kang, S.C.; Cook, T.R.; Kim, D.W.; Lah, M.S.; Kim, I.S.; Wang, M.; Stang, P.J.; et al. Self-Assembly of Cationic, Hetero- or Homonuclear Ruthenium(II) Macrocyclic Rectangles and Their Photophysical, Electrochemical, and Biological Studies. *Organometallics* **2011**, *30*, 6482–6489. [CrossRef]

231. Mattsson, J.; Zava, O.; Renfrew, A.K.; Sei, Y.; Yamaguchi, K.; Dyson, P.J.; Therrien, B. Drug delivery of lipophilic pyrenyl derivatives by encapsulation in a water soluble metalla-cage. *Dalton Trans.* **2010**, *39*, 8248–8255. [CrossRef]

232. Yi, J.W.; Barry, N.P.E.; Furrer, M.A.; Zava, O.; Dyson, P.J.; Therrien, B.; Kim, B.H. Delivery of Floxuridine derivatives to cancer cells by water-soluble organometallic cages. *Bioconj. Chem.* **2012**, *23*, 461–471. [CrossRef]

233. Zava, O.; Mattsson, J.; Therrien, B.; Dyson, P.J. Evidence for Drug Release from a Metalla-Cage Delivery Vector Following Cellular Internalisation. *Chem. A Eur. J.* **2010**, *16*, 1428–1431. [CrossRef]